THE ROLE OF COPPER IN HOMOGENEOUS CATALYSIS: SINGLE ELECTRON TRANSFER AND BEYOND

Shaofei Ni

UNIVERSITAT ROVIRA i VIRGILI

The Role of Copper in Homogeneous Catalysis: Single Electron Transfer and Beyond

---

Shaofei Ni

DOCTORAL THESIS
2019

UNIVERSITAT ROVIRA I VIRGILI
THE ROLE OF COPPER IN HOMOGENEOUS CATALYSIS: SINGLE ELECTRON TRANSFER AND BEYOND.
Shaofei Ni

UNIVERSITAT ROVIRA I VIRGILI
THE ROLE OF COPPER IN HOMOGENEOUS CATALYSIS: SINGLE ELECTRON TRANSFER AND BEYOND.
Shaofei Ni

Shaofei Ni

The Role of Copper in Homogeneous Catalysis: Single Electron Transfer and Beyond

DOCTORAL THESIS

Supervised by

Prof. Feliu Maseras

Institute of Chemical Research of Catalonia

(ICIQ)

Tarragona, Spain
2019

UNIVERSITAT ROVIRA I VIRGILI
THE ROLE OF COPPER IN HOMOGENEOUS CATALYSIS: SINGLE ELECTRON TRANSFER AND BEYOND.
Shaofei Ni

ICIQ- Institut Català d'Investigació Química
Avda. Països Catalans, 16,
43007 Tarragona(Spain)

Prof. Feliu Maseras, Group Leader at the Institute of Chemical Research of Catalonia,

I STATE that the present study, entitled "The Role of Copper in Homogeneous Catalysis: Single Electron Transfer and Beyond", presented by Shaofei Ni for the award of the degree of Doctor, has been carried out under my supervision in my group at the Institute of Chemical Research of Catalonia and that it fulfills all the requirements to be eligible for the International Doctor Distinction.

Tarragona, September, 2019

Doctoral Thesis Supervisor

Prof. Feliu Maseras

UNIVERSITAT ROVIRA I VIRGILI
THE ROLE OF COPPER IN HOMOGENEOUS CATALYSIS: SINGLE ELECTRON TRANSFER AND BEYOND.
Shaofei Ni

Acknowledgement

In the past years of my stay in ICIQ and Tarragona is really a great experience in my life. Here, I would like to express my very great appreciation to the following persons for their help.

Foremost, I would like to express my deep gratitude to my advisor Prof. Feliu Maseras for the continuous support, valuable and constructive suggestions for my Ph.D study and research, for his patience, motivation, enthusiasm, and immense knowledge. His guidance helped me in all the time of research and writing of this thesis. His willingness to give his time so generously has been very much appreciated. I could not have imagined having a better advisor and mentor for my Ph.D study. I also would like to acknowledge ICIQ for providing such excellent research environment and fellowship for me. Also, I would like to extend my thanks to Prof. Carles Bo, Prof. Nuria Lopez, Martin Gumbau and Moises Alvares for their kind advice and support. My special thanks are extended to Nuria Vendrell for her administrative support, this made my life in Tarragona much easier. I wish to thank various people in the group, Dr. Maria Besora, Dr. Mauro, Ignacio, Angel, Adiran, Rositha, Victor, Bruna, Raul, Sara, Lucia, and all the members in the theoretical groups, you all helped me a lot during these years.

My great appreciation also goes to Prof. Fahmi Himo, my short stay supervisor in Stockholm University. I would like to thank him for his patient guidance, enthusiastic encouragement for my research work, also for his endless joking. I would also like to thank Xiang, Man, Binh, Masound, Oriana, Henrik, Akinobu, Ferran for their help during my stay in Stockholm. Many thanks to Erasmus and URV for supporting me to go to Sweden.

I will be always grateful for Prof. Elena Fernández, Prof. Sergio

Castillón Miranda and Prof. María Yolanda Díaz Giménez for their awesome collaboration work.

My special thanks are extended to my friends and Chinese communities in Tarragona, Stockholm, and everywhere, you all make my life full of love.

Last but not the least, I would like to thank my parents for supporting me throughout my life.

Funding Agencies

ICIQ
Institut Català d'Investigació Química

Generalitat de Catalunya
Departament d'Innovació, Universitats i Empresa

GOBIERNO DE ESPAÑA
MINISTERIO DE EDUCACIÓN, CULTURA Y DEPORTE

UNIVERSITAT ROVIRA I VIRGILI
THE ROLE OF COPPER IN HOMOGENEOUS CATALYSIS: SINGLE ELECTRON TRANSFER AND BEYOND.
Shaofei Ni

List of publications

Related with the thesis (ICIQ) :

[1] J. Royes, **S.-F. Ni,** A. Farré, E. La Cascia, J.-J. Carbó, A.-B. Cuenca,* F. Maseras,* E. Fernández,* *ACS Catalysis* **2018**, *8*, 2833.

[2] Copper-Catalyzed Cyanotrifluoromethylation of Alkene: Uncovering a General Manifold for Enantioselective Cu-catalyzed Difunctionalization of Alkenes via Radical Process. Manuscript in Preparation.

[3] On the Mechanism of α- and β-C-H Activation in Iridium/Copper Co-catalyzed Aerobic α,β-Dehydrogenation: A DFT Study. Manuscript in Preparation.

[4] Mechanistic Understanding of the Synthesis of Indazoles through N-N Bond Formation Promoted by the Rh(III)/Cu(II)-cocatalyst System. Manuscript in Preparation.

Not related with the thesis (ICIQ or Stockholm University) :

[1] First Mechanism Study of Chiral Diaminophosphine Oxide Involved Asymmetric Transformations: Hydrocarbamoylation of Homoallylic Formamide. Manuscript in Preparation.

[2] Mechanism Study of the Synthesis of β-fluoroamines by RIng-opening of Aziridines. Manuscript in Preparation.

Previous publications (SUSTech & STU) :

[1] L.-B. Zhang, M.-H. Zhu, **S.-F. Ni,*** L.-R. Wen,* M. Li,* *ACS Catalysis* **2019**, *9*, 1680. *(Corresponding Author)*

[2] Z. Zhong, Z.-Y. Wang, **S.-F. Ni,** L. Dang,* H.-K. Lee, X.-S. Peng,* H.-N.-C. Wong,* *Organic Letters* **2019**, *21*, 700.

[3] W.-C. Chen, B. Huang, **S.-F. Ni,** Y. Xiong, A.-L. Rogach, Y.-P. Wan, D. L.-S. Liao,* F.-L. Wong, C.-S. Lee,* Advanced Functional Materials **2019**, Accepted.

[4] C.-F. Wang, **S.-F. Ni,** S. Braun, M. Fahlman,* X.-J. Liu, *Journal of Materials Chemistry C* **2019**, *7*, 879.

[5] Y.-S. Zheng, S.-S. Sun, L. Xu,* **S.-F. Ni,** W.-J. Liu, B.-J. Huang, Q.-X. Huang, Q.-C.

Zhang,* F.-X. Lu,; M.-D. Li,* *Dyes and Pigments* **2019**, *165*, 301.

[6] M.-M. Zhou, B.-L. Jiang, **S.-F. Ni,** L. Dang,* The *Journal of Organic Chemistry* **2019**, *84*, 9454.

[7] **S.-F. Ni,** P. Zhang, C.-Q. Chu, P. Qin, L. Dang,* *European Journal of Organic Chemistry* **2018**, *6*, 806.

[8] S. Chen,[+] **S.-F. Ni,**[+] P.-N. Liu,* L. Dang,* *Journal of Organometallic Chemistry* **2018**, *877*, 59. *(co-first Authors)*

[9] T.-L.Yang, **S.-F. Ni,** P. Qin, L. Dang,* *Chemical Communications* **2018**, *54*, 1113.

[10] W.-C. Chen, Y. Yuan, Z.-L. Zhu, **S.-F. Ni,** Z.-Q. Jiang, L.-S. Liao,* F.-L. Wong, C.-S. Lee,* *Chemical Communications* **2018**, *54*, 4541.

[11] Z.-L. Zhu, **S.-F. Ni,** W.-C. Chen, M. Chen, J.-J. Zhu, Y. Yuan, Q.-X. Tong,* F.-L.

Wong, C.-S. Lee,* *Journal of Materials Chemistry C* **2018**, *6*, 3584.

[12] L. Li,[+] L. Ye,[+] **S.-F. Ni,**[+] Z.-L. Li, S. Chen, L. Dang,* X.-Y. Liu,* *Organic Chemistry Frontiers* **2017**, *4*, 2139. *(co-first Authors)*

[13] **S.-F. Ni,** T.-L.Yang, L. Dang,* *Organometallics* **2017**, *36*, 2746.

[14] W.-C. Chen, Y. Yuan, **S.-F. Ni,** Q.-X. Tong,* F.-L. Wong, C.-S. Lee,* *Chemical science* **2017**, *8*, 3599.

[15] W.-C. Chen, Y. Yuan, **S.-F. Ni,** Z.-L. Zhu, J. Zhang, Z.-Q. Jiang, L.-S. Liao,* F.-L.

Wong, C.-S. Lee,* *ACS applied materials & interfaces* **2017**, *9*, 7331.

[16] Z.-L. Zhu, **S.-F. Ni,** W.-C. Chen, Y. Yuan, Q.-X. Tong,* C.-S. Lee,* *Dyes and Pigments* **2017**, *146*, 219.

[17] **S.-F. Ni,** L. Dang,* *Physical Chemistry Chemical Physics* **2016**, *18*, 4860.

[18] P. Zhang,[+] **S.-F. Ni,**[+] L. Dang,* *Chemistry–An Asian Journal* **2016**, *11*, 2528. *(co-first Authors)*

[19] X. Deng, **S.-F. Ni,** Z.-Y. Han, Y.-Q. Guan, H. Lv, L. Dang,* X.-M. Zhang,* *Angewandte Chemie* **2016**, *128*, 6403.

[20] T.-L.Yang, **S.-F. Ni,** P. Zhang, L. Dang,* *Journal of Organometallic Chemistry* **2016**, *806*, 60.

[21] Z.-L. Zhu, M. Chen, W.-C. Chen, **S.-F. Ni,** Y.-Y. Peng, C. Zhang, Q.-X. Tong,* Lu,

F.; C.-S. Lee,* *Organic Electronics* **2016**, *38*, 323.

[22] Y. Yuan, J.-X. Chen, W.-C. Chen, **S.-F. Ni,** H.-X. Wei, J. Ye, F.-L. Wong, Z.-W. Zhou, Q.-X. Tong,* C.-S. Lee,* *Organic Electronics* **2015**, *18*, 61.

[23] L. Dang,* **S.-F. Ni,** M.-B. Hall, E.-N. Brothers, *Inorganic chemistry* **2014**, *53*,

9692.

[24] H.-X. Lin, H.-L. Liang, G.-H. Chen,* F.-L. Gu,* W.-G. Liu, **S.-F. Ni**, *The Journal of*

Physical Chemistry A **2012**, *116*, 11656.

UNIVERSITAT ROVIRA I VIRGILI
THE ROLE OF COPPER IN HOMOGENEOUS CATALYSIS: SINGLE ELECTRON TRANSFER AND BEYOND.
Shaofei Ni

Abstract

In general, the mechanism of organic reactions is believed to undergo the two-electron transfer pathways. However, the one-electron transfer could also exist in some biology and radical chemistry. Copper has surfaced as omnipresent catalysts in organic reactions because of their easily accessible Cu(0), Cu(I), Cu(II), and Cu(III) oxidation states. Thus, the mechanism of the Cu-catalyzed reactions could be quite complex with the change of the oxidation states of the metal centers in different reaction conditions and ligand spheres. Both the one-electron (radical) and two-electron processes could occur for the bond-breakage and bond-formation processes. In addition, the Cu(II), which could act both the promoter and terminal oxidant, capable of promoting a wide range of reactions initiated with the single-electron transfer (SET) process. Molecular oxygen is often used as a sink for the electrons to regenerate the copper(II) or to achieve the higher Cu(III) oxidation state for the two electron reductive elimination.

With the development of new synthetic methods, the need for mechanistic understanding of the reaction details is urgent. Thus, computational chemistry has been proved as the powerful tool to gain mechanistic information of these reactions. In this thesis, we have applied density functional theory (DFT) to perform a comprehensive computational study on the mechanism of the Cu catalyzed or co-catalyzed reactions. In particularly, we pay our attention on the single electron process, together with the reactivity and selectivity.

The first chapter will give an overview on the copper chemistry and the single electron transfer process, whereas Chapter 2 will give some introduction on the theoretical methods used in this thesis.

Chapter 3 presents the mechanism Cu-catalyzed borylative ring closing C-C coupling reaction. Our computational results give reasonable explanation on the reactivity by varying the nature of the organic reactant R, the leaving group **X**, the counter cation **C** in the base as well as the number of explicit THF molecules around the cation. The key steps for all the catalytic cycles are the halogen abstraction and C-C coupling processes via a concerted or stepwise manner, which determining the reactivity.

In Chapter 4, the mechanism of enantioselective intermolecular cyanotrifluoromethylation of styrenes by using chiral bis(oxazoline)/Cu(I) catalyst was elucidated. Our results indicate that the rate determining step is the release of CF_3 radical and the enantioselectivity determining step is the reductive elimination process from the Cu(III) center. The NCI plot and the energy decomposition analysis indicate that the small steric repulsion between the ligand and the benzylic cation makes the formation of the R-products more favorable.

Chapter 5 covers the mechanism study of Iridium catalyzed aerobic α,β-dehydrogenation of γ,δ-unsaturated amides and acids under the presence of $Cu(OAc)_2 \cdot H_2O$ and O_2 as oxidant. An alternative mechanism was proposed from our theoretical calculations. An Ir-enolate intermediate is confirmed to be involved instead of the Ir-allyl species. The rate determining transition state is the α-C-H bond activation, where both the Cu and Ir play an important role in this process. The $AgBF_4$ and $[Cu(OAc)_2 \cdot H_2O]_2$ are proved to be important in this new mechanism; the first one activates the initial Ir(III) catalyst by Cl abstraction and the latest one cooperated in the C-H activation and facilitating the catalyst recovery by Ir(I) oxidation.

At the last Chapter 6, we calculated the mechanism for the synthesis of 1H-indazole through C-H amidation and N-N bond formation by a Rh(III)/Cu(II)-

cocatalyst system. The mechanism shows that the key step is the N-N bond reductive formation from the Cu(III) center. The interactions between the Cu and Rh that connected by the acetate ligand and the coordination of substrate to the Rh(III) center are quite important for this N-N bond formation process.

Table of contents

List of figures

List of tables

Chapter 1

Introduction

1.1 Cu catalysts

Organic synthesis is the transformative science that focuses on the intentional construction of new organic compounds with wide applications in a variety of fields including modern materials, biochemistry, and pharmaceutical industries. During the past decades, organic synthesis has confirmed its role as a key tool in molecular sciences.[1]

A number of very significant advances in transformative organic synthesis have been accomplished through the application of the catalytic ability of 4d and 5d transition metal complexes. For example, palladium,[2–9] iridium,[10–16] rhodium,[17–23] and ruthenium[24–32] are present in many of the most widely used transition metal complexes used as catalysts. Unfortunately, as shown in Figure 1.1, these 4d and 5d transition metals are quite expensive and most of them are rather toxic, which will limit their wide applications in the organic synthesis of the future.[1]

The more earth-abundant (Figure 1.2) 3d-transition metals are usually more cost-effective than 4d and 5d metals. 3d-transition metal complexes are increasing becoming alternative catalysts. They have been proven as powerful options for the development of novel synthetic methods.[33–45] Moreover,

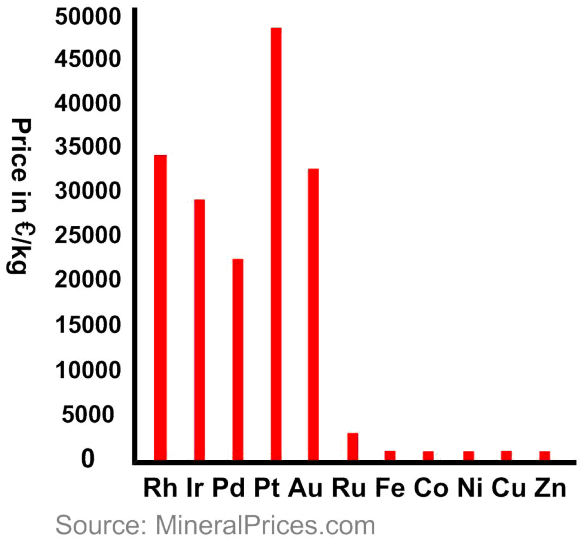

Fig. 1.1 Price of transition metals (TMs) that are widely used in organic synthesis.[1]

the prominent involvement of 3d metals in enzymatic processes indicates they are usually less toxic than their 4d and 5d counterparts.[1]

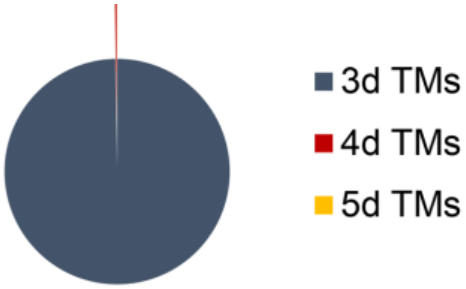

Fig. 1.2 Natural abundance of 3d, 4d, and 5d transition metals. This figure is from *Chem. Rev.* **2019**, *119*, 2192-2452.

As a representative member of the group of 3d transition metals, copper has surfaced as an omnipresent catalysts in organic reactions thanks in part to its easy access to the Cu(0), Cu(I), Cu(II), and Cu(III) oxidation states.[46] The mechanism of the Cu-catalyzed reactions can thus be especially com-

plicated. Both one-electron (radical) and two-electron steps can participate in bond cleavage and bond formation processes.[47] The diversity of oxidation states also provides high versatility and tolerance to a lot of different functional groups.[48] A number of reviews have been published by different groups on Cu-catalyzed[46, 49–56] and Cu-mediated[57–59] organic reactions.

1.2 Aerobic Cu-catalyzed organic reactions

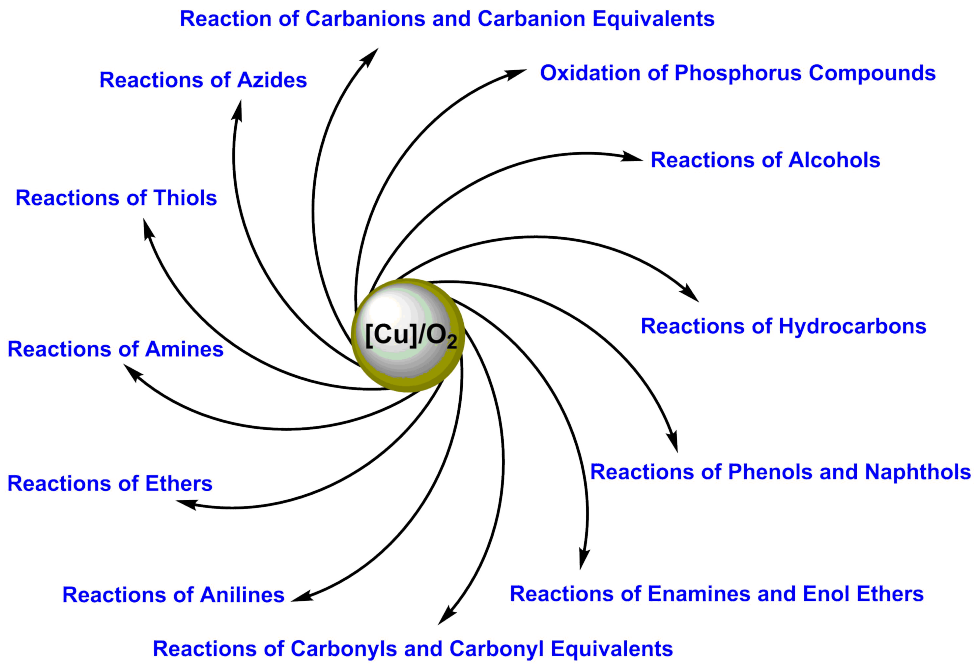

Fig. 1.3 Aerobic Copper-Catalyzed Organic Reactions.

Molecular oxygen attracts academic and industrial interest as an ideal oxidant for green and sustainable chemistry. It is easily available in nature, has low cost and is environmentally friendly.[51, 52] During the past decades, significant advances in transition-metal catalyzed reactions employing molecular

oxygen as the sole oxidant have been achieved as shown in Figure 1.3. Punniyamurthy and co-workers published indeed a review on the transition-metal catalyzed oxidation of organic substrates with molecular oxygen. Molecular oxygen has also found an active role in C–H functionalization (Figure 1.4), oxidative Heck reactions, oxidative dehydrogenative coupling reactions, and free radical reactions.[51]

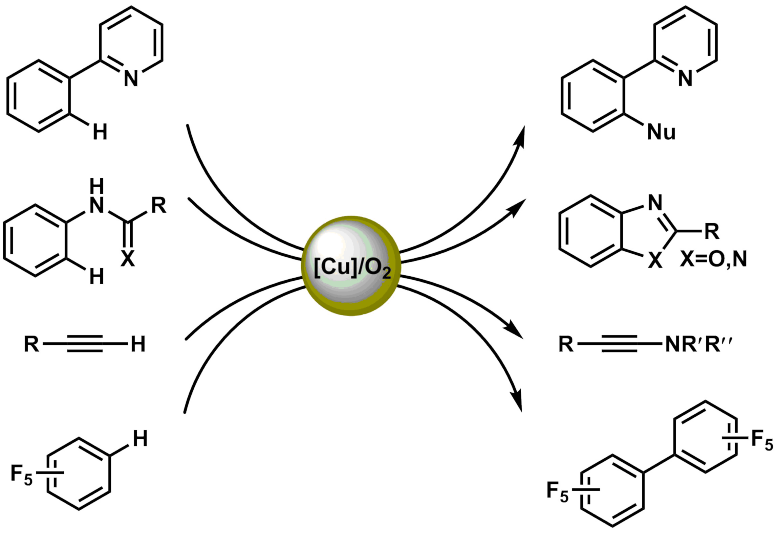

Fig. 1.4 Copper-Catalyzed Aerobic Oxidative C-H Functionalizations.

However, there are also many reactions involving oxidation which cannot operate with O_2 as the sole oxidant. Other oxidants, such as $PhI(OAc)_2$, benzoquinone, Cu(II) or Ag(I), are essential for these transformations to achieve catalytic turnover. These oxidants are usually proposed to participate in the formation of high-valent intermediates promoting reductive elimination steps.[52, 60–62] Among these alternative oxidants, the combination of Cu(II) with molecular O_2 has been particularly successful in recent years.[63] Copper(II) is a versatile oxidant, able to act either as promoter or terminal oxidant, in particular because of this ability to participate in single-electron transfer (SET) processes. Molecular oxygen acts in these cases as a sink

for the electrons, and it allows the copper species to regenerate its catalytic active form. H_2O, occasionally H_2O_2, is usually the by-product of these transformations.[46, 52, 64] The field has been reviewed by a number of authors. Stahl and co-workers summarized the mechanistic knowledge on Cu-catalyzed aerobic oxidative C-H functionalizations (Figure 1.4).[52] Kozlowski and co-workers published a comprehensive review of Cu-catalyzed aerobic organic reactions.[46] Additional reviews on the copper-catalyzed aerobic oxidations of organic molecules have been also reported by Stahl's group.[65, 66]

1.3 Single electron transfer processes

In the industrial field, the traditional way to obtain radicals is the homolytic bond cleavage at high temperature, an approach which may also be used by synthetic chemists in academia.[67]

Most organic reactions take place through two-electron transfer processes. However, one-electron transfer steps also exist in a number of cases. They are usually known as single electron transfers (SET).

The obtention of radical cations and radical anions through electrochemistry is well known since the 19th century. The SET process in organic synthesis was firstly characterized by Faraday in 1834. He observed formation of new organic compounds in electrodes as shown in Figure 1.5. Following this pioneering work, similar treatments for organic synthesis were used by the groups of Wurtz,[68] Barbier, and Sandmeyer[69]

One well-known example of application of SET in organic chemistry is the combination of a colorless electron-donor (D) and a colorless electron-acceptor (A) to form a colored electron donor-acceptor (EDA) complex. A total (or partial) transfer of one electron is involved in these charge transfer complex (CTC). The study of this type of compounds was one of the first examples of application of quantum chemistry. The ground state of this

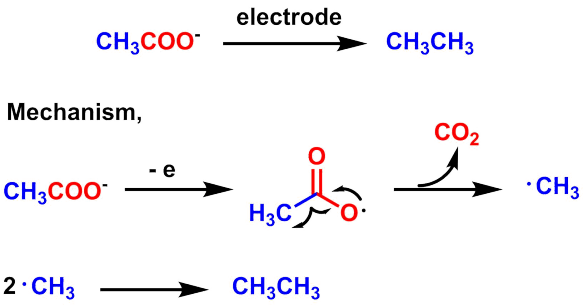

Fig. 1.5 Faraday's synthesis of ethane by SET.

EDA complex was confirmed to be stabilized by donor-acceptor interactions with the quantum mechanical theory developed by Mulliken in 1952.[70] As shown in Figure 1.6, the mixture of the colorless species D and A produced the encounter complex [D, A]. And the encounter species was colored because of the charge transfer between the two fragments.

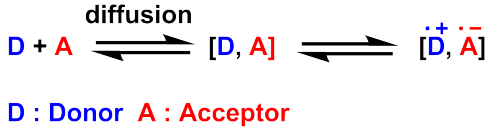

Fig. 1.6 Mulliken Definition of ET.

Single electron transfer(SET) processes became widely recognized only especially after the publication of the Taube[71–73] classification and the Marcus[74] theory. In 1953, Taube studied the SET process from organic compounds to metal complexes and introduced the original definition of ISET (inner-sphere electron transfer) and OSET (outer-sphere electron transfer). He postulated that the ISET should exist between two metals that were connected by a bridging ligand, while the OSTE should happen in absence of the bridging ligand. These ISET and OSET models were further adapted to organic chemistry by Eberson, Chanon, and Kochi in the early 1980s.[75] They are shown in Figure 1.7. According to the commission of physical organic chemistry from the organic division of the IUPAC, the ISET is associated

to strong D-A enthalpic interactions (H_{DA} > 5 kcal/mol) while the OSET is associated to weak interactions (H_{DA} < 4 kcal/mol).[76]

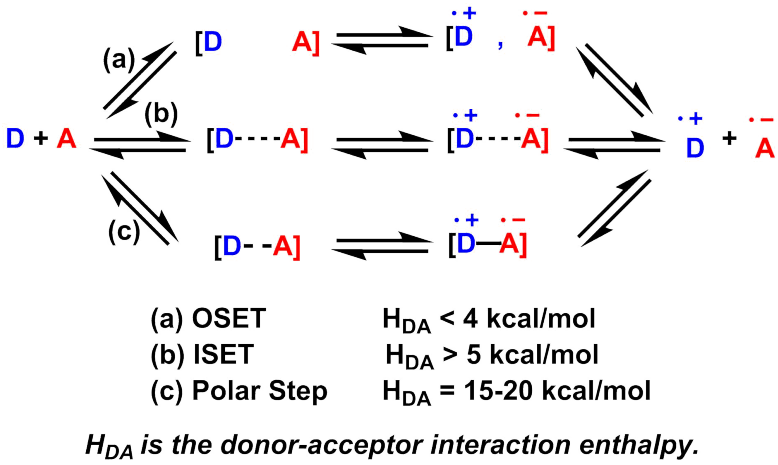

Fig. 1.7 OSET, ISET, and Polar Step

Another significant development was the publication of the Marcus theory for the description of the rate of OSET processes. The key ideas are shown in Figure 1.8.[74] The validity of the Marcus equation was confirmed experimentally by the measure of the rates of electron transfer by Sutin and Bennett.

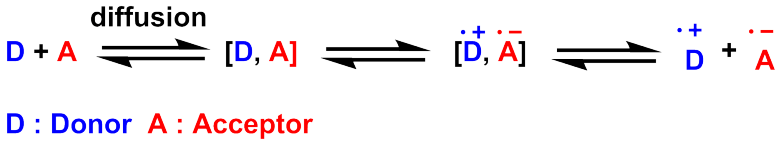

Fig. 1.8 Marcus Conception of OSET.

Nowadays, the commission of physical organic chemistry from the organic division of the IUPAC defined the SET reaction as “a reaction mechanism characterized by the transfer of a single electron between the species occurring on the reaction coordinate of one of the elementary steps.”[67, 76] The process of bond formation and cleavage *via* SET is well established in

organic chemistry. A classification of SET processes and radical processes is presented in Figure 1.9. Different reactivity patterns are possible, such as radical-radical coupling, single electron transfer, atom or group transfer, radical addition and elimination reactions.

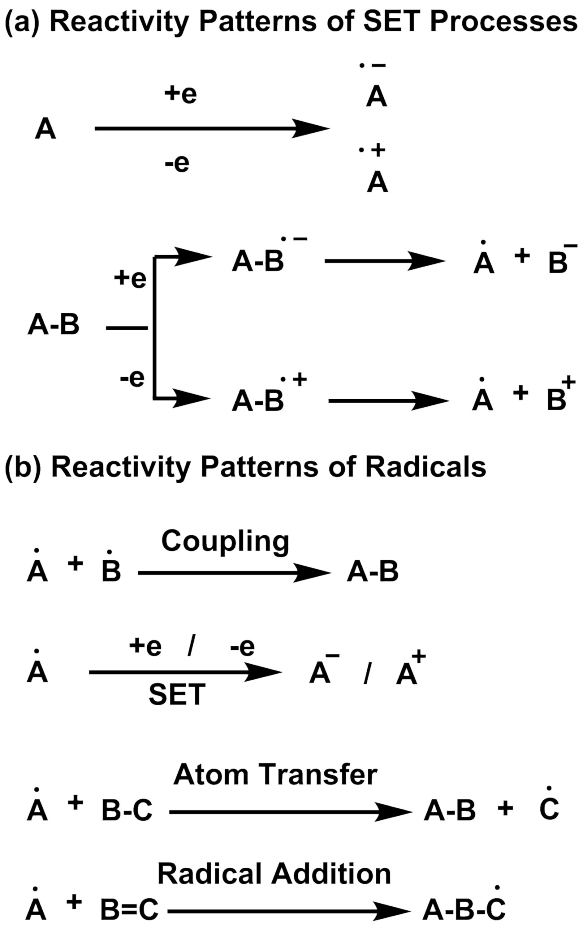

Fig. 1.9 Reactivity Patterns of SET(a) and Radicals(b).

Among these reactivity patterns, the atom-transfer radical addition (ATRA) has attracted a lot of attention since the seminal work by Kharasch, Engelmann, and Mayo in 1973. The general reaction and the mechanistic scheme of ATRA is summarized in Figure 4.2. The reaction initiates with the abstraction

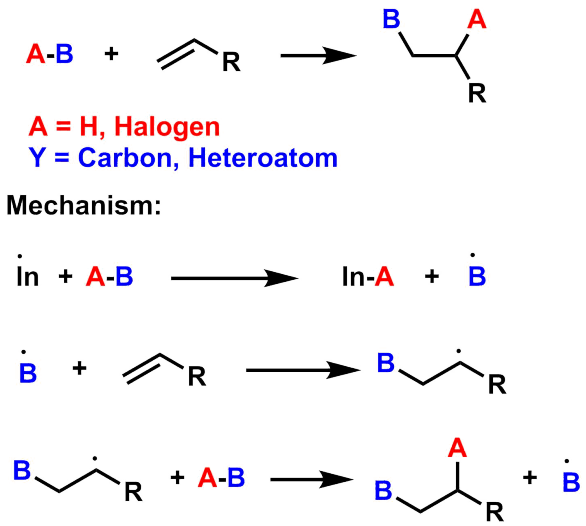

Fig. 1.10 The ATRA Reaction and its mechanistic scheme.

of an X atom from X-Y by an inductor In·, which produces the radical Y·. In the propagation step Y· is added to the C=C double bond of the alkene and the further abstraction of X· from X-Y occurs successively. The whole process is rapid and exothermic.

The transition metal version of ATRA reaction was first published by Minisci in 1961 by using $FeCl_2$ as shown in Figure 1.11 The field of transition metal-catalyzed ATRA reaction has been further developed by various research groups, including those of Asscher and Vofsi, Barton, and Curran.[77] Different transition metals, such as Cu, Fe, Ru, and Ni can be used in the radical generation process.

1.4 Objectives

Cu-catalyzed organic synthesis are abundant and important, and a better mechanistic understanding is highly desirable, especially in cases involving single electron transfer (SET).

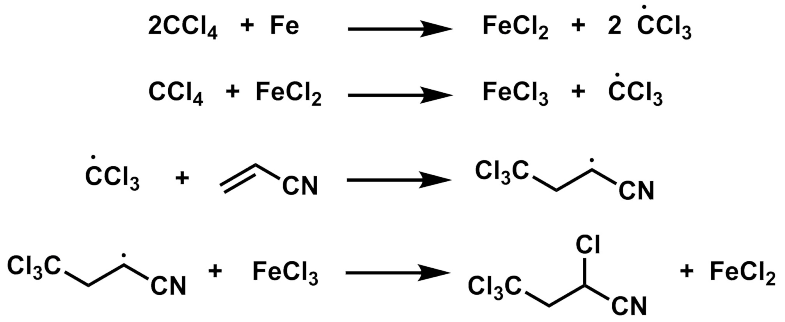

Fig. 1.11 The transition metal-catalyzed ATRA Reaction.

In this thesis, we carry out DFT calculations on the mechanism of four different representative Cu-catalyzed or co-catalyzed organic reactions.

-In Chapter 3, we will try to rationalize the mechanism of a C-C coupling process *via* Cu-catalyzed borylative ring closing. The role of different factors, such as the nature of the organic reactant R, the leaving group **X**, and the counter cation **C** in the base, will be considered.

-In Chapter 4, we aim to elucidate the role of the single electron transfer process in the mechanism of the enantioselective intermolecular cyanotrifluoromethylation of styrenes using chiral bis(oxazoline)/Cu(I) catalyst. The origin of enatioselectivity will be an important target for our study.

-In Chapter 5, we will try to understand the mechanism and the role of Cu(II) and Ag(I) on the iridium catalyzed aerobic α,β-dehydrogenation of γ,δ-unsaturated amides and acids.

-In Chapter 6, we will attempt to clarify the mechanism of the oxidative synthesis of 1H-indazole through C-H amidation and N-N bond formation with azides as amino sources in the presence of a Rh(III)/Cu(II)-cocatalyst system. The cooperative role of the Rh(III) and Cu(II) in the catalytic cycle, especially in the N-N bond formation, are especially puzzling.

We expect that the study of these diverse processes will bring a better general understanding on the role of copper complexes in catalysis.

Chapter 2

Theoretical Background

2.1 Open-shell systems in DFT

Single electron, or the unpaired electrons, are always exist in the intermediates and transition states along the reaction pathways of the single electron transfer process or the Cu(II) related reactions. DFT methods are not multiconfigurational, it cannot be used to describe the unpaired electrons. In these cases, only the multiconfigurational approach can be used to describe the wavefunctions. However, the high level multiconfigurational methods are quite computationally demanding and not suitable for our systems.

The unrestricted Kohn-Sham (UKS) formalism is the alternative way to obtain accurate energies of these systems. Here, the α orbital is not forced to be identical with the β orbital. Unfortunately , this approach provides the formally incorrect spin densities, as the KS orbitals produced from this unrestricted calculation are not eigenfunctions of the spin operator. The break of the spin symmetry could be contaminated with higher multiplicity spin states. However, this provides a better description of the energies than that obtained with restricted approach, even though the restricted approach shows better realistic densities. Therefor, the unrestricted version is used here for the calculation of the unpaired electron systems.

2.2 Implicit solvation model

For most of the cases, the reactivities of the chemical species are strongly related and effected by the medium. The choose of proper solvent is always the key factors during the optimization of the reaction conditions. The reaction results could be largely affected by the stabilization or distabilization of the reactants, intermediates, transition states, and products with different solvent. Therefore, adequate description of the solvent is quite important for the computational chemistry. However, the use of explicit solvent models is quite computationally demanding due to the large systems. In addition, the optimization of the intermediates and transition states become more and more difficult because it is not easy to find the minimum with different spatial configurations.

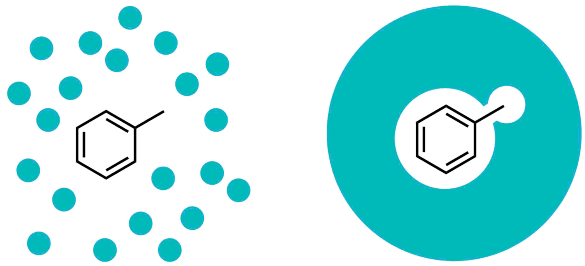

Fig. 2.1 Left: explicit solvent; Right: continuum solvent model.

These problems could be avoided by using the widely applied continuum solvation methods, where the molecular is placed in the cavity of the field with the dielectric constant of the real solvent as shown in Figure 2.1 Several continuum models have been developed and the Solvent Model based on Dispersion (SMD) will be used in this thesis. The SMD model divide the free energy of the solvent into two terms. The first term is the bulk electrostatic contribution, which is based on the traditional Polarized Continuum Model. The second term is the cavity dispersion, which takes the short-range effects of the solvent and the molecule into consideration.

2.3 Marcus theory of electron transfer

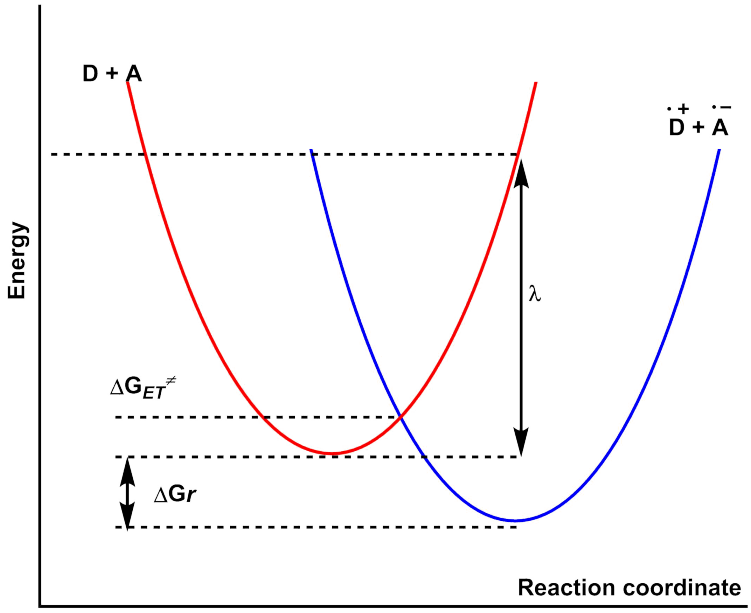

Fig. 2.2 Marcus diagram for OSET.

As for the OSET (outer-sphere electron transfer) mentioned in Chapter 1, the electron donor (D) and the electron acceptor (A) interact with each other through the single electron transfer process, this is quite different from other elementary steps containing bond broken or formation process. To estimate this electron transfer barrier, the Marcus theory is widely used (Figure 1.8). [74] The activation energy of the SET process of the donor-acceptor pair can be estimated by locating the crossing point of the two intersecting parabolas of the reactants and products as shown in Figure 2.2

According to the Marcus equation, the solvent reorganization energy λ_0 may be calculated from equation 2.1 :

$$\lambda_0 = (332kcal/mol)\left(\frac{1}{2a_1}+\frac{1}{2a_2}-\frac{1}{R}\right)\left(\frac{1}{\varepsilon_{op}}-\frac{1}{\varepsilon}\right) \qquad (2.1)$$

$$D + A = D^{\cdot +} + A^{\cdot -} \tag{2.2}$$

a1 and a2 are the radii of the molecules D and A, R = a1 + a2, ε_{op} is the optical dielectric constant (ε_{op} = 2.05), ε is the static dielectric constant for the solvent.

According to Marcus theory, the barrier can be calculated by equation 2.3:

$$\Delta G_{ET}^{\neq} = \Delta G_0^{\neq} \left(1 + \frac{\Delta G_r}{4\Delta G_0^{\neq}} \right)^2 \tag{2.3}$$

where ΔG_r is the reaction energy, and $\Delta G_0{}^{\neq}$ is the intrinsic barrier.

$$\Delta G_0^{\neq} = \frac{\lambda}{4} \tag{2.4}$$

We estimate the inner reorganization energy for the reactants $\lambda_i = 0$. Thus, the total reorganization energy $\lambda = \lambda_0 + \lambda_i$.

Then,

$$\Delta G_{ET}^{\neq} = \frac{(\Delta G_r + \lambda)^2}{4\lambda} \tag{2.5}$$

2.4 Selectivity calculation

In organic chemistry, the development of novel synthetic methodology for specific products is always the goal for organic chemists. This is related to the selectivity, such as the regioselectivity, chemoselectivity, and enantioselectivity. It will be quite helpful for the further development of the organic chemistry with the understanding of the origin of selectivity. For the experimental investigations, the deeply understanding of the reaction mechanism and the further analysis of the selectivity is not that easy. Computational chemistry could provide reasonable solution for this. By calculating the mechanism of the reactions, the different pathways leading to different products could be

figured out. In addition, the reaction barriers of each elementary steps of the mechanism could be estimated from computational chemistry. The selectivity determining transition states could also be identified, which could be used to analysis where the selectivity come from and how the selectivity of the process works.

In principal, the reaction will follow a Boltzmann distribution of the energy barriers when the different pathways have similar activation barriers and the reaction steps are irreversible. The difference of the barrier could be used to express the reaction ratios γ by equation 2.6, where the ΔG$_1$ and ΔG$_2$ represents the activation free energy barriers of the different pathways.

$$\gamma = \frac{\sum_i e^{-\Delta G_{1i}/(RT))}}{\sum_i e^{-\Delta G_{2i}/(RT))}} \tag{2.6}$$

2.5 Standard state for free energy calculation

In this thesis, all the calculations are carried out under the ideal gas (1 atm.) conditions. According to the Ideal Gas Law, this corresponds to a concentration of 1/24.5 M. So a correction of 1.89 kcal/mol has to be added to all the calculations for the transfer of 1 atom. to 1M. This term can be easily obtained from the following equation 2.7:

$$\Delta G_{1M} = -RT \ln\left(\frac{1/24.5M}{1M}\right) \tag{2.7}$$

Here, R is the ideal gas constant and T is the temperature.

This correction is self-compensating when the numbers of the reactants and products are the same. But this is not the case when numbers change. Here, all the calculations in this thesis include this correction.

Chapter 3

C-C Coupling through Cu-Catalyzed Borylative Ring Closing

3.1 Background

The synthesis of spirocyclic scaffolds has witnessed exponential growth recently due to the exclusive properties of these compounds due to their dense and rigid structures with high application in modern medicinal chemistry. If we take the 4-membered rings as an example, more than 2 millions of structures of the spirocyclic 4-membered rings have been reported.[78]

In general, spirocyclic compounds have a high sp^3/sp^2 ratio thus facilitating the design of new classes of biologically active molecules with improved properties. Spirocyclic compounds have the added appeal of a reduced lipophilicity compared to analogous cyclic molecules because of their compactness, which can be even increased by introducing heteroatoms in the spirocycles. These spiroheterocycles are also superior to traditional saturated heterocycles in their unique structural advantages both in physicochemical properties and pharmacokinetic effects.[79, 80]

Because of this, organic chemists have been attracted to discover new strategies for the synthesis of these compounds, and they have been also incorporated into other complex structures.[78]

Some representative examples of construction of spirocycles are depicted in Figure 3.1. In 2013, Ito and co-workers explored the Cu-catalyzed borylative exocyclization process to build spirocyclobutane rings onto saturated carbocycles. Later on, the reaction leading to a spirocyclobutylpiperidine-based skeleton was also explored by the same group in 2017.[81–83] Fernández and co-workers focused on the synthesis of [m,n]-spiroheterocyclic structures (m,n = 3-5) with a methylene boronate substituent bound to a cyclic backbone, aiming to expand the chemical space of multifunctional cores. For the preparation of this target spiroheterocyclic structures, they employed a synthetic strategy whereby an O- or N-containing heterocycle is already present in the starting material as shown in Figure 3.2. The spiroheterocylce structures with a pendant methylene boronate substituent were then formed through Cu-catalyzed borylative ring closing C-C coupling.[80] This could be further used as a handle for functionalization toward primary alcohols, aldehydes, acids and esters, or olefination using gem-bisborylsilyl methane species. Furthermore, attempts to synthesize dispirocyclic compounds by assembly of three different cyclic systems were also explored in her group.

The experimental investigation by Fernández shows that the reactivity depends non-trivially on a variety of factors.[80] The C-C coupling reactions towards the 5-membered rings is observed to be more challenging hat to the 4-membered rings, but is faster than for the 6-membered rings. In addition, the use of iodinated substrates is shown to accelerate the transformation when compared with the corresponding Br substrates. Also, as far as the base is concerned, KOtBu is found to be optimal, as the related NaOtBu is proved to be less efficient. These observations prompted us to colaborate with Fernández's group carrying out density functional theory studies to shed light on the mechanism of this reaction.[84–86]

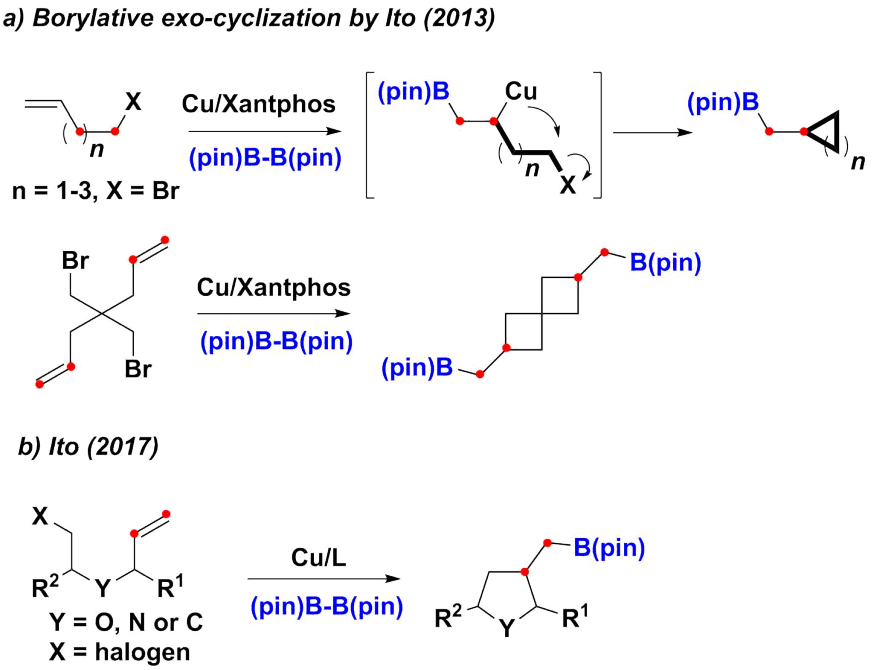

Fig. 3.1 Cu-catalyzed borylative cyclization process.

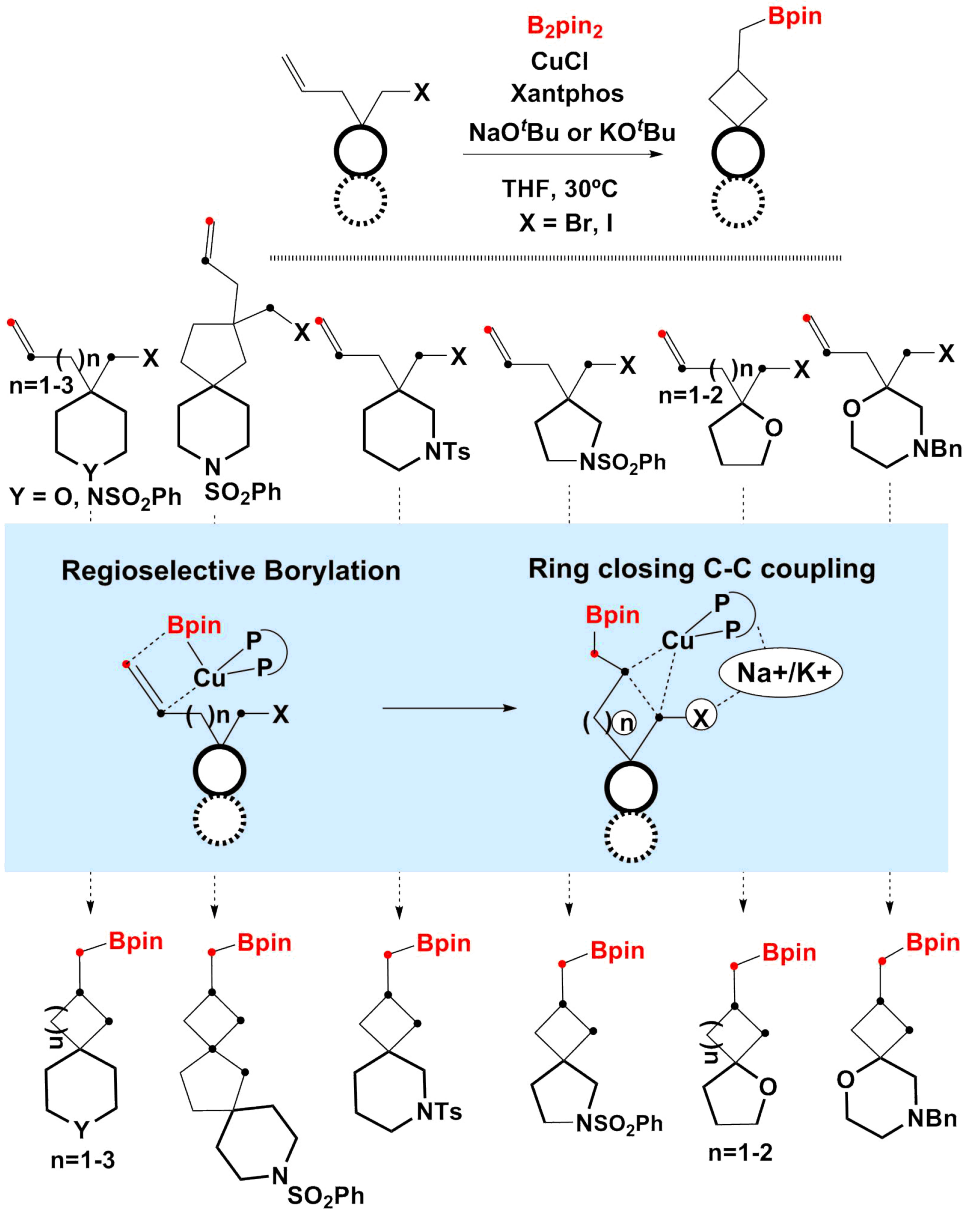

Fig. 3.2 Cu-catalyzed borylative ring closing C-C coupling toward spiro- and dispiroheterocycles.

3.2 Computational details

The ωB97X-D[87] functional was used for all calculations, which were carried out with the Gaussian 09 program.[88] Two different basis sets were used. Basis set I was used for geometry optimizations and frequency calculations. The effective core potentials (ECPs) of Hay and Wadt with a double-ζ valence basis set (LANL2DZ) were employed for Cu, P, Br, I, and K,[89–92] supplemented with polarization shells with the following exponents: Cu (f = 3.525), P (d = 0.387), Br (d = 0.428), I (d = 0.289), and K (d = 1.000);[93] and the all-electron 6-31G(d) basis set was used in describing all other atoms.[94] All calculations, including geometry optimizations were carried out within a solvent (THF) represented via the SMD model. All stationary points were confirmed as minima (no imaginary frequency) or transition state structures (only one imaginary frequency). The latter were confirmed to connect appropriate intermediates, reactants, or products by intrinsic reaction coordinate (IRC) calculations. Potential energies were refined through single point calculations with a larger basis set II, which consisted of LANL2TZ(f) for Cu, LANL08(d) for P, Br and I, LANL08 for K, and 6-311++G(d,p) for other atoms.[95–97] Free energy corrections were considered at a concentration of 1 M and a temperature of 298.15 K. The 3D structures were drawn by CYLview program.

3.3 Results

A total of 28 different free energy profiles were calculated varying the nature of the organic reactant R, the leaving group X, the counter cation C in the base as well as the number of explicit THF molecules. In the following sections, we will analyze the mechanism and the roles of these factors one by one.

3.3.1 General mechanism

As a preliminary calculation, we evaluated the stability of KOtBu and NaOtBu with the coordination of different numbers of THF molecules. The results shown in Figure 3.3 indicate that the coordination of one molecule of THF on the cation center gives the most stable structures for both KOtBu and NaOtBu.

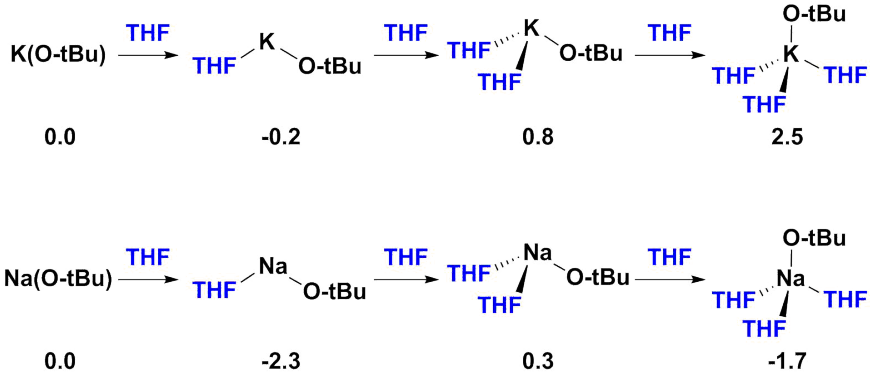

Fig. 3.3 Stability of KOtBu and NaOtBu with different numbers of THF molecules (Gibbs energies in solvent in kcal/mol).

We carried out our first set of calculations on the mechanism proper on the experimental system leading to the formation of 5-membered spirocyclic product with Br as the leaving group and KOtBu as base. The calculated free energy profile is shown in Figure 3.4. The starting point is intermediate **I1**, the diphosphine copper(I) alkoxide complex that could be readily obtained upon mixing CuCl, the Xantphos ligand and the base. The corresponding Cu-B species **I2** would then form readily through the exothermic reaction of **I1** with B_2pin_2. The substrate **Br-spiro-R5** approaches the Cu(I) center by coordination of the C=C double bond, and the C=C bond inserts into the Cu-B bond *via* transition state **Br-spiroC5-TS1**. This process needs to overcome a barrier of 14.6 kcal/mol, leading to a stable intermediate **Br-spiro-I4**. From **Br-spiro-I4**, halogen abstraction occurs with the assistance

of cationic K^+ *via* transition state **K-Br-spiroC5-2THF-TS2**. As shown in the 3D presentation of **K-Br-spiroC5-2THF-TS2** in Figure 3.5, the C-Br bond is elongated to 2.502 Å, while the Cu-C bond (2.808Å) is starting to form. The free energy barrier for this step has a respectable value of 25.7 kcal/mol. Remarkably, the Cu(III) intermediate **K-Br-spiroC5-2THF-I6**, which had been postulated by Ito and co-workers, appears in this mechanism. This Cu(III) intermediate does not seem however kinetically significant, as it sits in a shallow well, and undergoes a rapid reductive elimination process *via* transition state **spiroC5-TS3** to give the spirocyclic product. The Cu-C bonds in the Cu(III) intermediate in Figure 3.5 are 1.986 and 1.965 Å, and they are elongated to 2.052 and 2.000 Å in the reductive elimination transition state **spiroC5-TS3**. The new C-C bond starts to emerge in **spiroC5-TS3**, although with a quite long bond length of 2.345 Å. The highest barrier in the catalytic cycle is associated to the conversion from **Br-spiro-I4** to **K-Br-spiroC5-2THF-TS2**, with a value of 25.7 kcal/mol, and decides the overall efficiency of the process. This value is in line with the experimental observation that the reaction producing a 45% yield after 4 h at 30 °C.

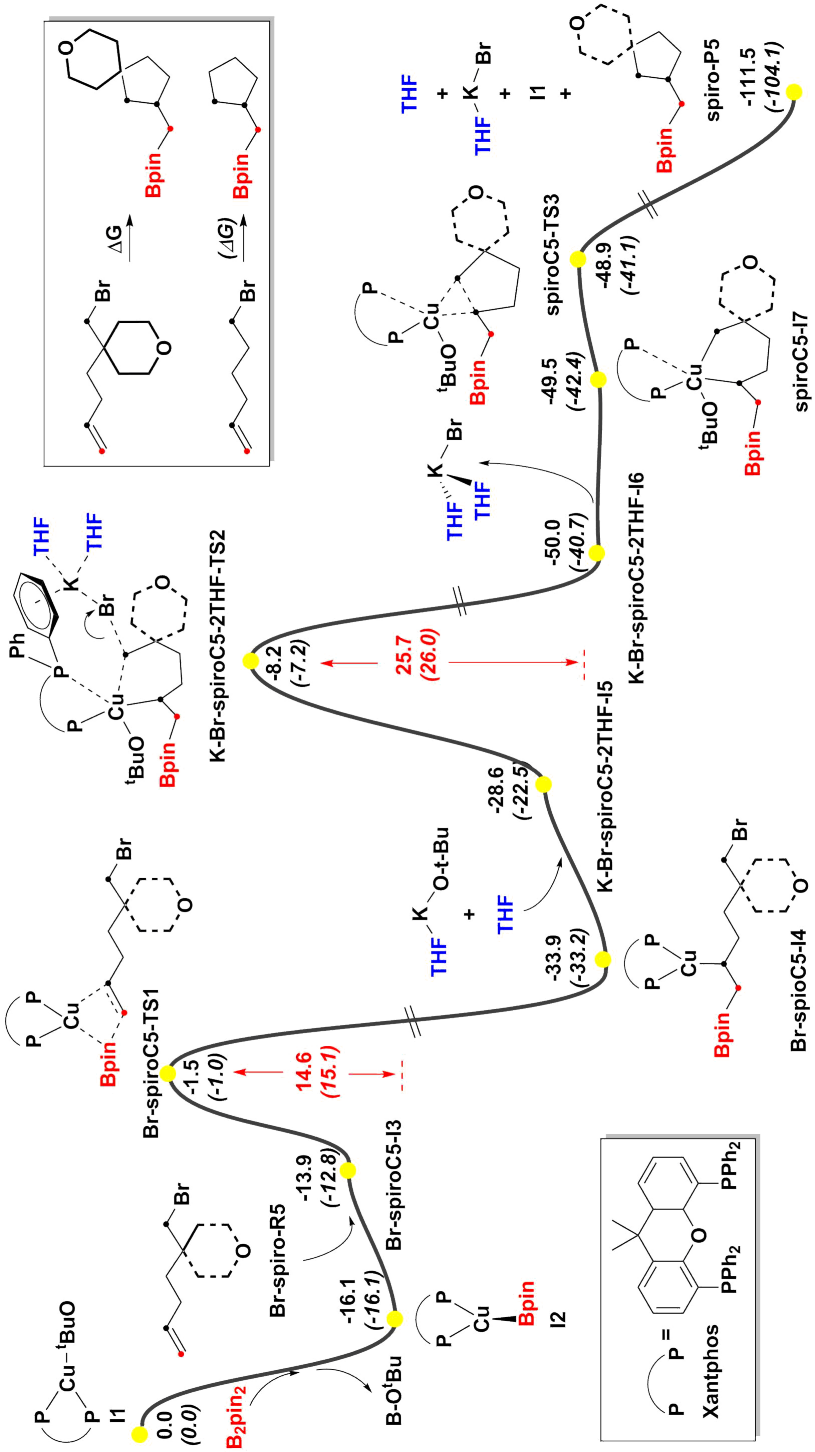

Fig. 3.4 Computed free energy profile (in kcal/mol) for the formation of the 5-membered spiro-ring product with Br as the leaving group and KOtBu as base (with the coordination of two THF)(The energies in brackets are the model molecular in our calculations by removing the spirocycles).

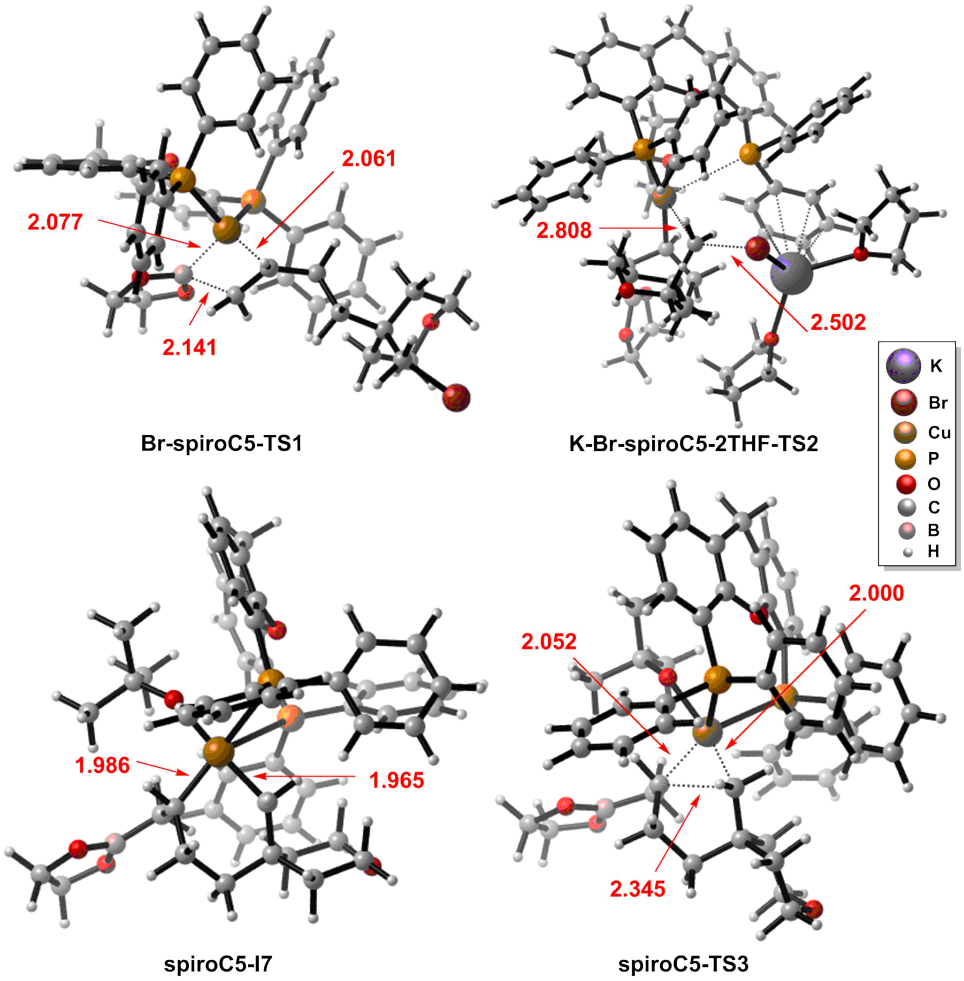

Fig. 3.5 3D structures of the key intermediates and transition states for the formation of the 5-membered spiro-ring product.

We next evaluated the effect on this mechanism of the number of THF molecules coordinating the K cation. We recomputed the barrier associated to the key transition state by changing the number of THF molecules from 0 to 3. The results are collected in the first column of Table 3.1. The barriers cover a range from 25.7 to 29.8 kcal/mol. This indicates that the description

Table 3.1 Summary of the free energy barriers (kcal/mol) for the rate determining transition states(m: numbers of THF).

	K(O-tBu)						Na(O-tBu)
	Br				I		Br
	spiroC5	C4	C5	C6	C5	C6	C5
m=0	29.8	23.5	29.5	33.1	26.4	33.6	36.2
m=1	28.7	19.3	28.2	34.9	22.1	30.8	32.5
m=2	25.7	17.5	26.0	34.5	19.3	26.6	28.7
m=3	28.3	21.6	26.0	31.5	20.0	29.6	28.6

of the $K(THF)_m$ species is quite critical for the computational reproduction of the system.

Alternative mechanisms without the involvement of the cation were also studied and were found to have significantly higher barriers (see Figure 3.6).

Our next test concerned the computational model. We evaluated the role of the connected spiro ring by replacing it with two hydrogen atoms. The corresponding energy values for this model have been already included in parentheses in the free energy profile of Figure 3.4 reported above. A minor effect is observed in the barrier of the rate determining transition state, which increased only by 0.3 kcal/mol to 26.0 kcal/mol. We consider that this error is sufficiently small to justify the use of this simplified model lacking the spiro connection in out later calculations.

We concluded this study on the general mechanism by considering the possibility of a Heck-type mechanism.[98, 99] The calculated results are shown in Figure 3.7. The key feature of this mechanism is that initial activation of the substrate occurs through the C-X bond rather than from the C=C double bond. The free energy barrier corresponding to the activation of the C-Br bond in **Br-spiro-R5** is as high as 34.5 kcal/mol *via* **Br-spiroC5-TS4a**, much higher than that for the mechanism in Figure 3.4. Other possible transition

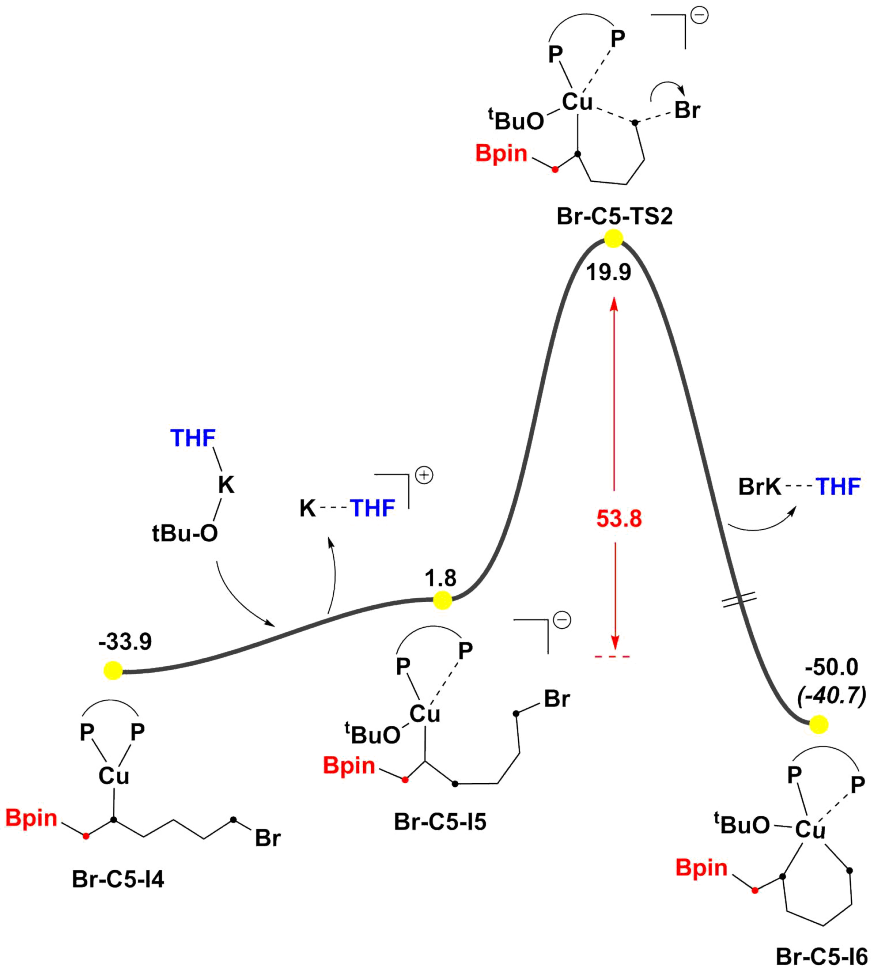

Fig. 3.6 Computed free energy profile (in kcal/mol) for the formation of the 5-membered ring product without the cation K.

states for the activation of C-Br bond were also located and found to have high free energy barriers incompatible with the reported experimental conditions.

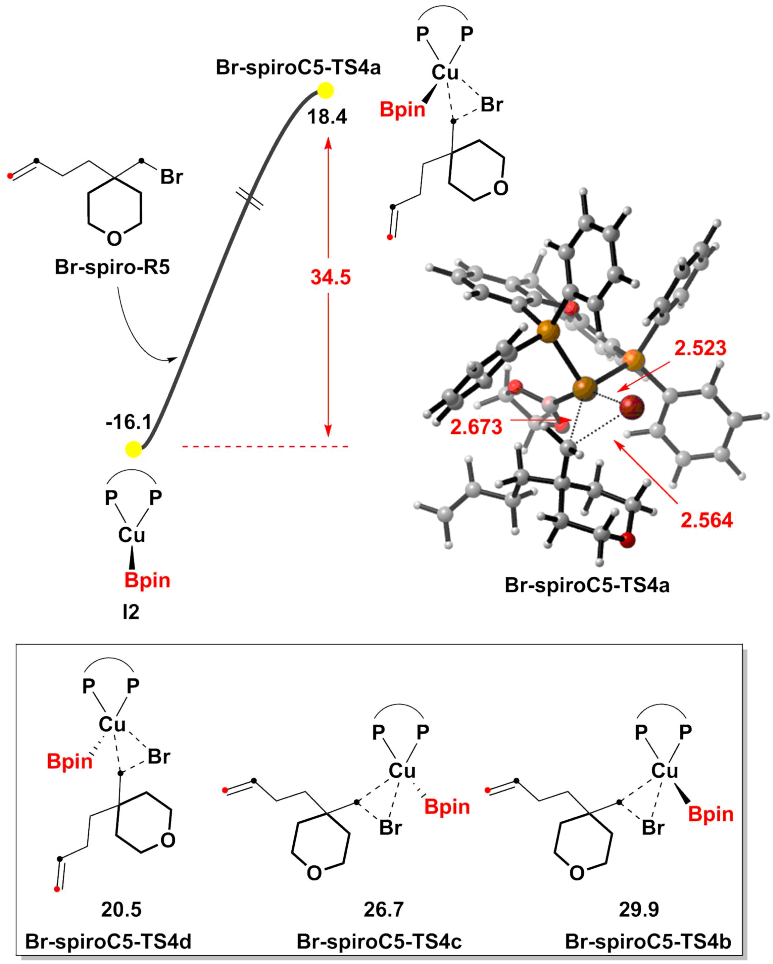

Fig. 3.7 Computed free energy profile (in kcal/mol) of the possible transition states starting with Heck-type C-Br activation.

3.3.2 Role of the ring size

Experimental results indicate a strong dependence of the reaction efficiency on the size of the rings being formed. So we repeated the study reported

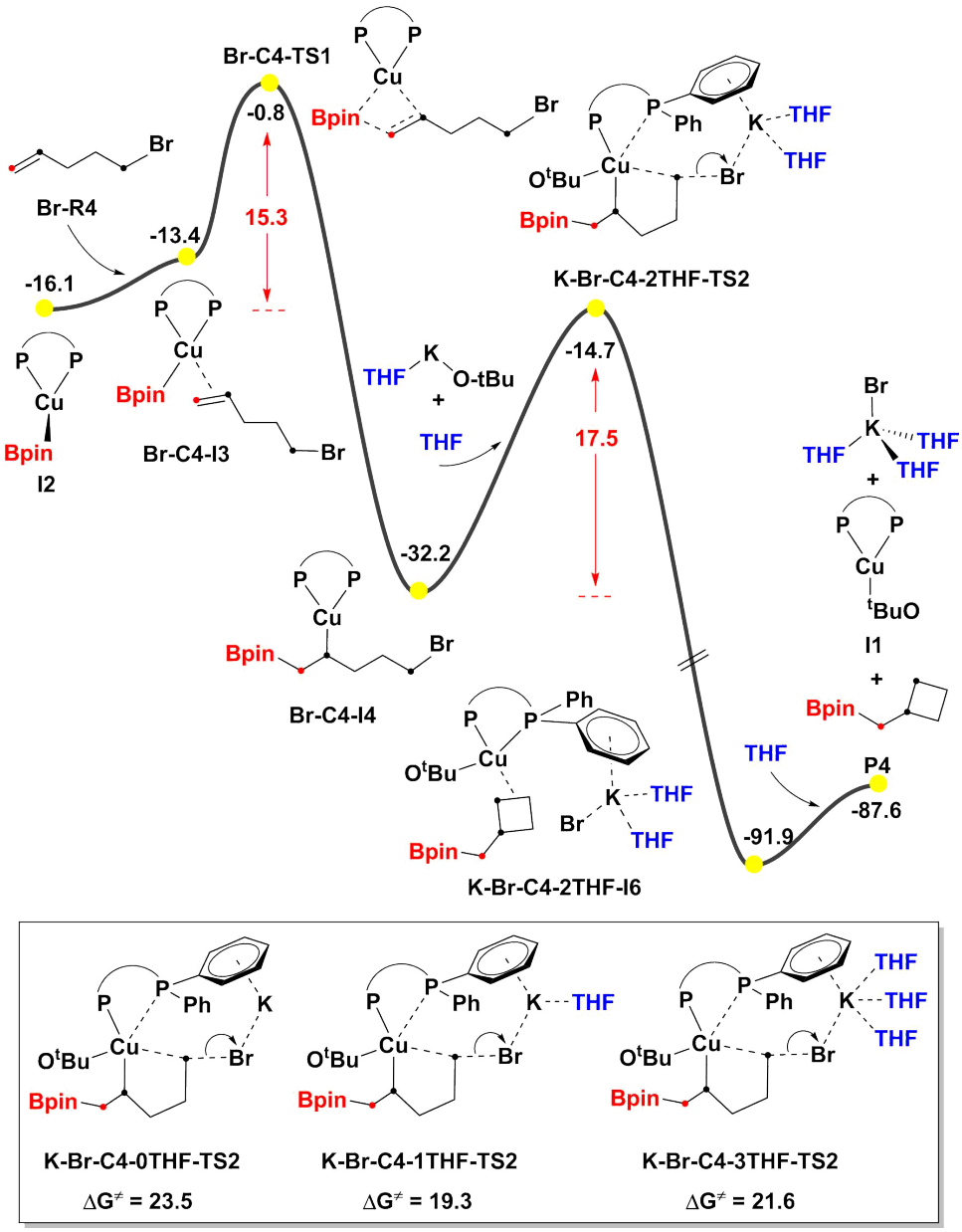

Fig. 3.8 Computed free energy profile (in kcal/mol) for the formation of the 4-membered ring product by using the model reactant with Br as the leaving group and KOtBu as base.

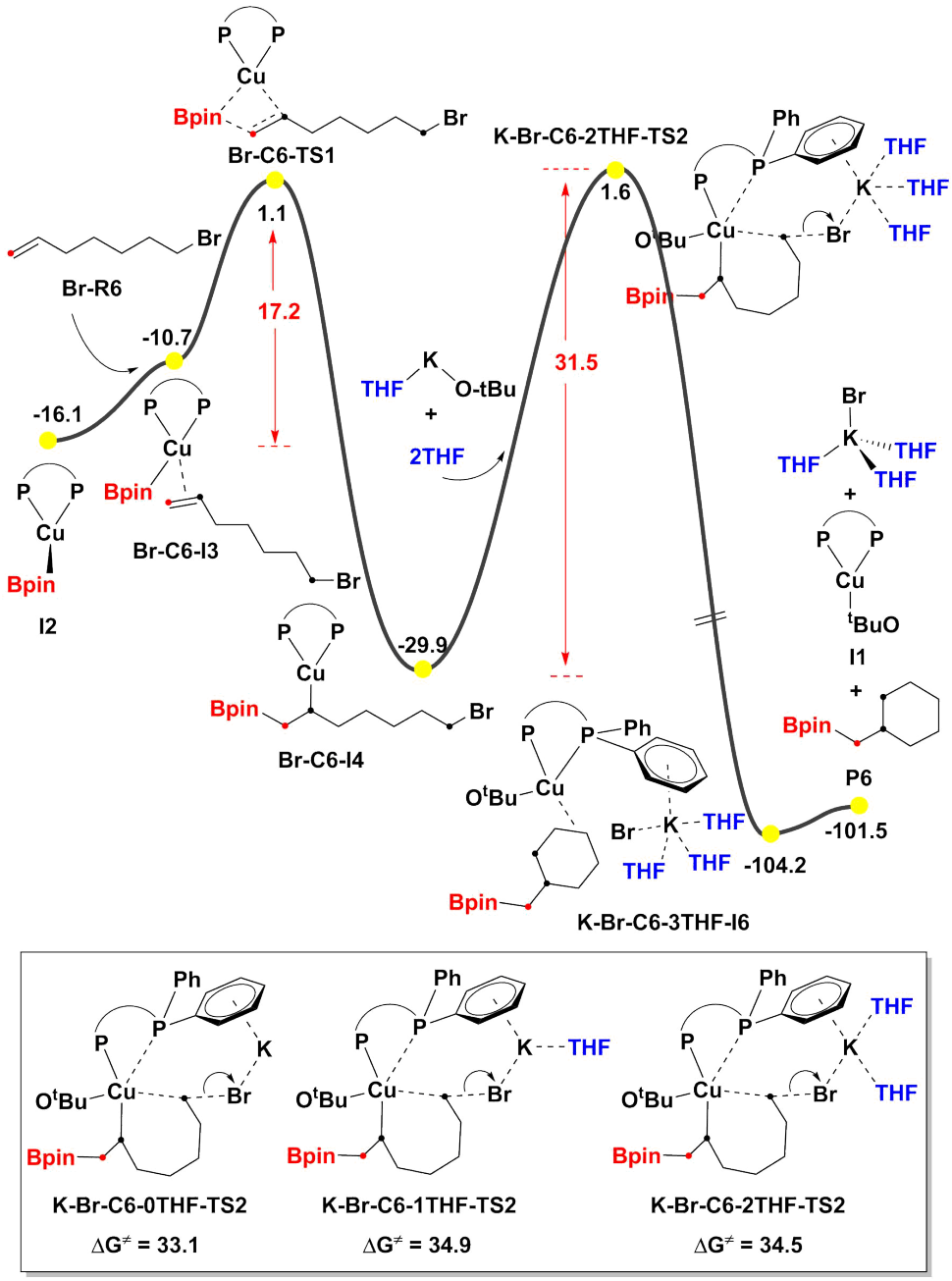

Fig. 3.9 Computed free energy profile (in kcal/mol) for the formation of the 6-membered ring product by using the model reactant with Br as the leaving group and KOtBu as base.

above for the process leading to the 5-membered ring products, now with reactions starting from different organic chains that would lead to 4- and 6-membered ring products. Free energy profiles of the mechanism leading to the 4 and 6-membered ring products are shown in Figure 3.8 and 3.9. The main qualitative features of the mechanism for the formation of the 4 and 6-membered ring products were identical to those for the 5-membered rings. The only minor difference is that the Cu(III) intermediates are not located for either the 4 or 6-membered ring systems. Instead of the stepwise halogen abstraction and ring closure process *via* Cu(III) in Figure 3.4, a concerted step consisting of the halogen abstraction and C-C bond coupling transition state was observed for both the 4 and 6-membered ring systems. This further indicates that this intermediate is not kinetically relevant. The transition states with different numbers of THF were also located and the barriers of the rate determining transition states are summarized in Table 3.1.

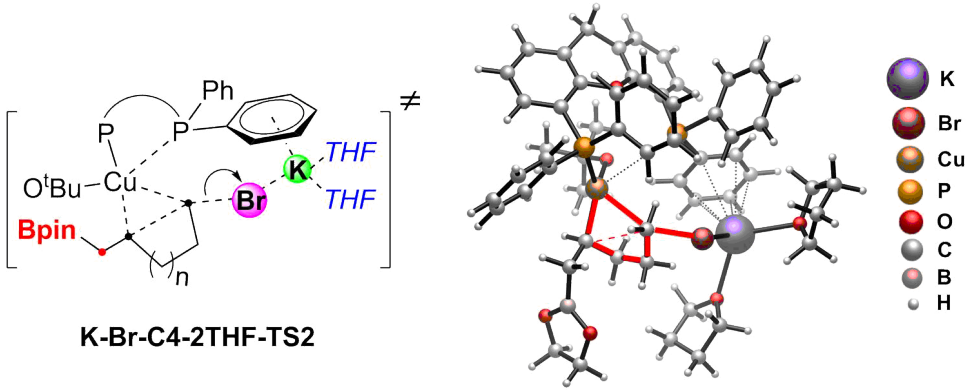

Fig. 3.10 3D structure of **K-Br-C4-2THF-TS2**.

The overall barriers corresponding to the formation of 4- and 6-membered ring products with the same leaving group and base are 17.5, and 31.5 kcal/mol, respectively. Our calculated barriers of 17.5, 26.0 and 31.5 kcal/mol for the 4,5,and 6-membered rings clearly reproduced the experimental trend in favor of smaller rings (93%, 45%, and 20% yields for 4-, 5-, 6-membered

rings). Differences in barriers are certainly larger than expected, but we must mention that the isolated yield of 93% for the 4-member ring corresponds in practice to quantitative conversion, and the 20% observed for the 6-membered ring may come from a different reaction path. A simple qualitative explanation on the preference for the more strained small rings can be made from inspection of the 3-D drawing in Figure 3.10. The increasing negative charge of the leaving bromide group is stabilized by the nearby presence of the potassium cation, which is also interacting with phenyl rings attached to the phosphines. The formation of the 4-membered ring brings naturally the bromide in the vicinity of potassium. This is not the case for the transition states leading to the 5- and 6-membered rings. The organic chains in these systems have to distort, with the subsequent energy penalty, to keep the attractive interactions.

3.3.3 Role of the leaving group X

Next, we analyzed the influence of the leaving group **X** by replacing bromide with iodide. The barriers of the rate determining transition states for the formation of the 5- and 6-membered ring products are summarized in Figure 3.11 and 3.12. The lowest barrier for the formation of 5- and 6-membered ring products are 19.3 and 26.6 kcal/ mol, respectively. These two barriers are lower than those reported above using Br as the leaving group (26.0 and 31.5 kcal/mol, respectively), which correlates well with the increased experimental reactivity of the iodinated systems. We attribute this result to the lower strength of the C-I bond compared to the C-Br bond, which makes the halogen abstraction process much easier for the iodinated structures.

3.3.4 Role of the counter cation C

Finally, we studied computationally the role of the alkaline ion by changing the base from KOtBu to NaOtBu. For the system leading to the formation of

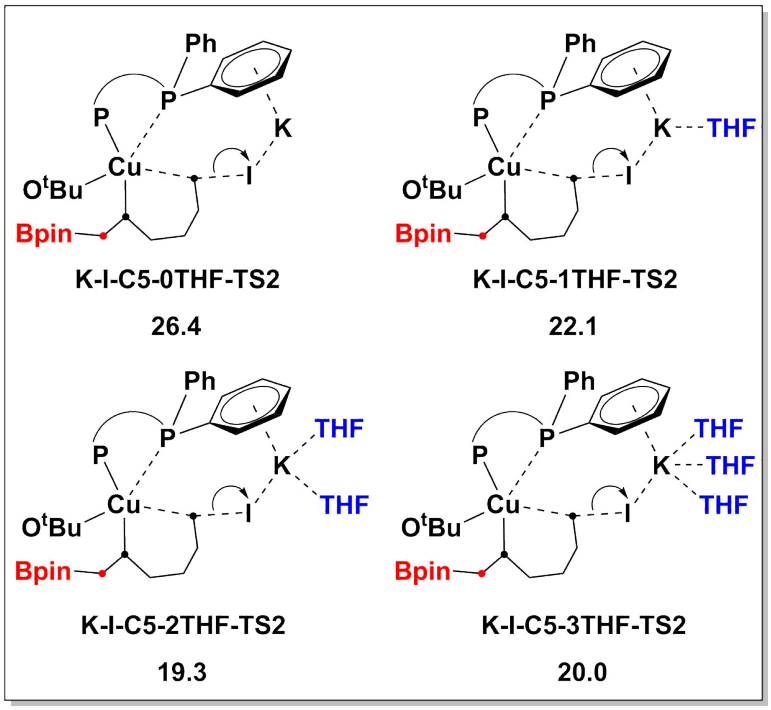

Fig. 3.11 Role of the leaving group: Key rate-determining transition states by replacing bromide with iodide.

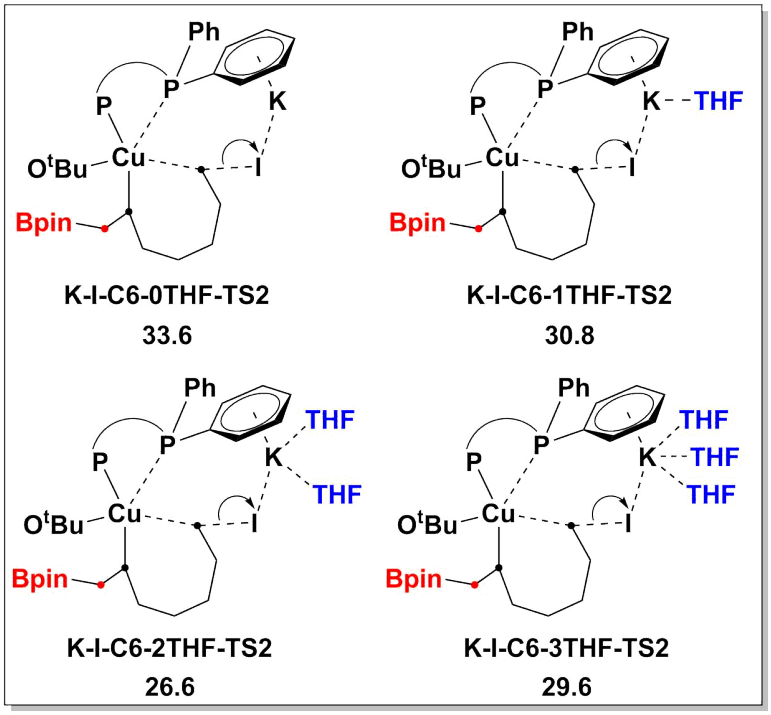

Fig. 3.12 Role of the leaving group: Key rate-determining transition states by replacing bromide with iodide.

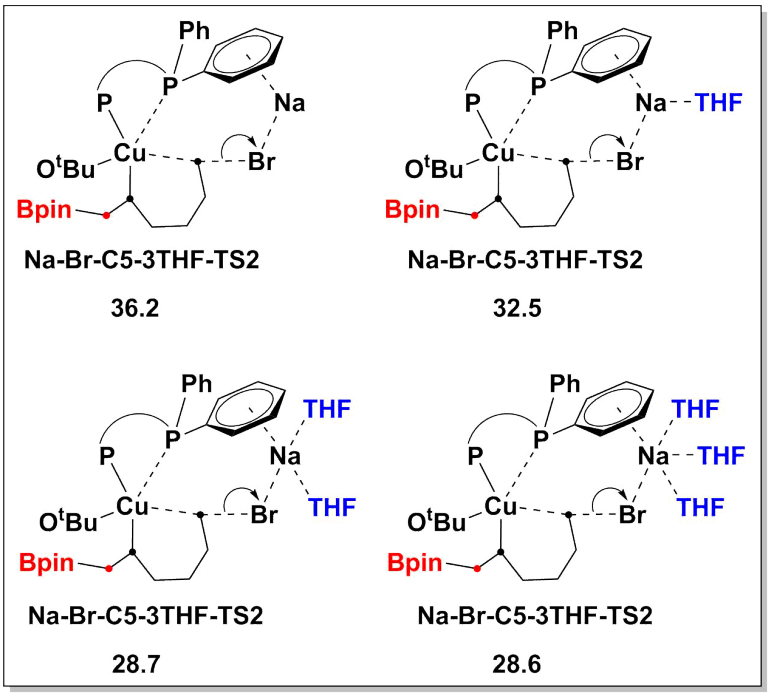

Fig. 3.13 Role of the counter cation: Key rate-determining transition states by using NaOtBu.

a 5-membered ring, the barrier increases by 2.6 kcal/mol, going from 26.0 to 28.6 kcal/mol. This reproduces the experimental sluggishness of the reaction conducted using NaOtBu as base, and confirms the relevance of the cation in the key transition state **TS2** corresponding to the halogen abstraction and ring closing. The 3-D drawing in Figure 3.10 also indicates that the size of the cation is important for the interactions between the leaving group X, the cation C, and the phenyl group on the ligand, highlighting that potassium seems more adequate for these particular systems.

3.4 Conclusions

Density functional theory calculations (DFT) were used to shed light on the reaction mechanism of the synthesis of spiro- and dispiroheterocycles *via* copper-catalyzed C-C coupling through borylative ring closing. A total of 28 different free energy profiles were computed by varying the nature of the organic reactant R, the leaving group **X** and, the counter cation **C** in the base as well as the number of explicit THF molecules around the cation. Our computational results shows that the key steps for all the catalytic cycles are the halogen abstraction and C-C coupling processes *via* a concerted or stepwise manner, which determining the reactivity.

The computed barriers for the formation of 4-, 5- and 6-membered ring products correlate well with the experimental observation that the reaction trend in favor of smaller rings. This can be explained by inspecting the key transition states of halogen abstraction. When the 4-membered rings are formed, the short organic chain brings naturally the leaving group in the vicinity of cation. In contrast, the longer organic chains in the case of 5- and 6-membered rings have to distort to keep the attractive interactions, and this has a free energy penalty.

The influence of the leaving group **X** was explored through replacement of bromide by iodide and we found that the higher yield can be attributed to the lower strength of the C-I bond when compared with the C-Br bond.

Finally, the investigation of the role of the alkaline ion through the replacement of potassium by sodium shows that the size of the cation is important for the interactions between the leaving group, the cation and the phenyl group.

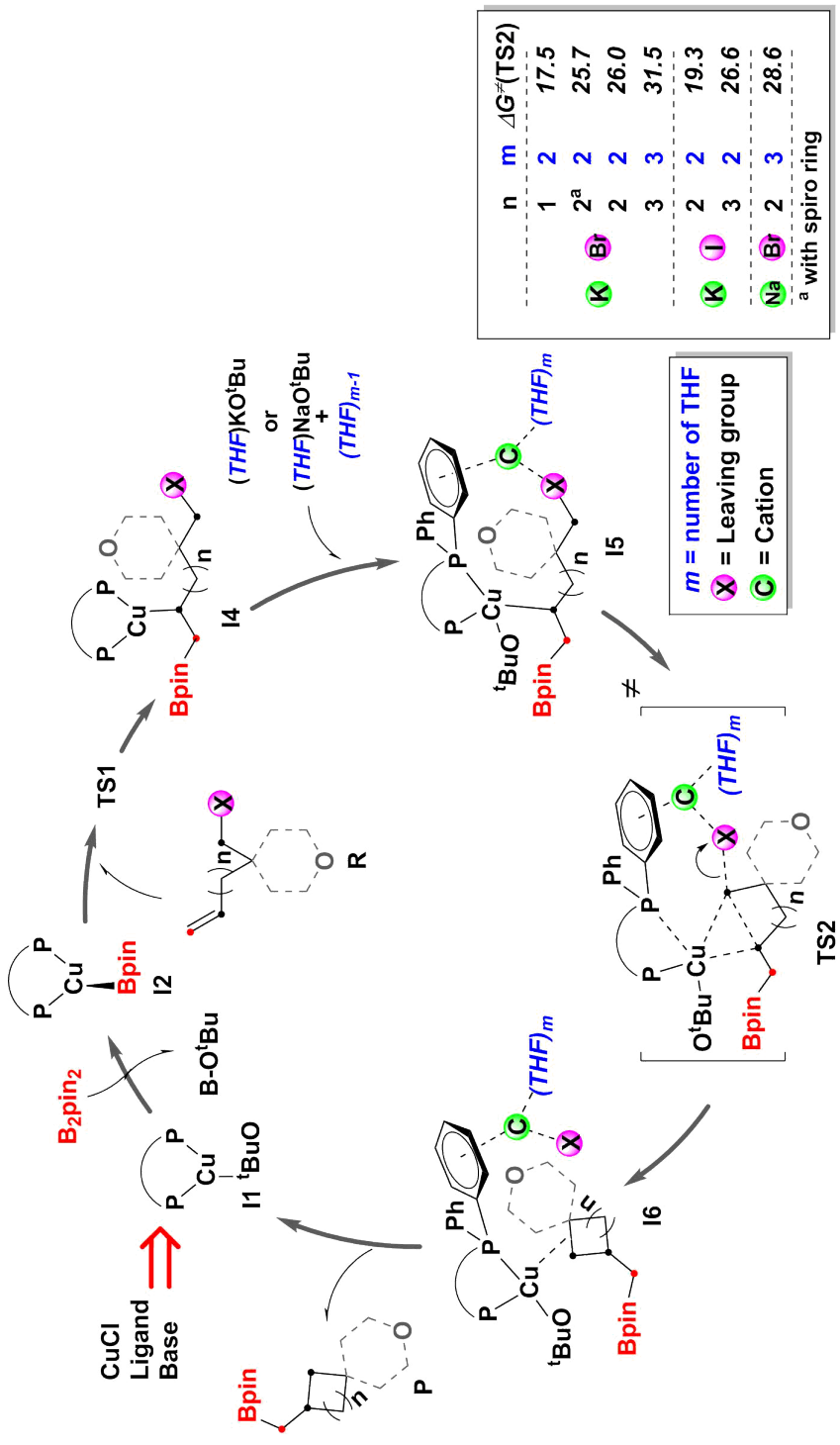

Fig. 3.14 The summary of the catalytic cycle.

Chapter 4

Enantioselective Cyanotrifluoromethylation of Alkenes

4.1 Background

Functionalization of simple alkenes has been a long-standing research topic in organic chemistry that has developed into a powerful tool for the synthesis of highly functionalized skeletons.[100, 101] Among the efforts in this area, transition-metal-catalyzed vicinal difunctionalization of alkenes has been particularly relevant. The introduction of two different functional groups across a double bond is a step-economic strategy to access multiple carbon–carbon and carbon–heteroatom bonds.[102–105] The pioneering work was reported by Bäckvall and co-workers on the palladium-catalyzed amination of alkenes to afford the 1,2-functionalized products.[106]

Two types of metal-catalyzed reactions - nucleophilic [101, 107–109] and radical difunctionalization - dominate this research field for both the intramolecular and intermolecular versions(see Figure 4.1). The mechanism for the radical processes is particularly intriguing. The general mecha-

nism of the intramolecular radical difunctionalization is shown in Figure 4.1 (b). The reaction takes place with alkenes containing tethered nucleophilic groups. After the extrinsic radical addition an alkyl radical or carbocation intermediate is generated. The reaction terminates with the intramolecular C-Nu (Nu = C, N, O) bond formation and release the product. A variety of intramolecular radical difunctionalizations have been shown to increase molecular complexity.[110, 111]

The intermolecular radical process starts with the addition of the radical to the C=C double bond. This generates a C-centered radical intermediate, as shown in Figure 4.1 (d). This intermediate has two options: further functionalization by combination with an extrinsic radical donor (Path A) or further oxidation to a carbocation (Path B). For example, the copper-catalyzed intermolecular azidotrifluoromethylation of alkenes using the Tog-CF_3 reagent as the CF_3 source was developed by Liu and co-workers in 2014.[112] This provided a new strategy for the construction of a variety of CF_3-containing organoazides from a wide range of olefins. Regiospecific additions of the CF_3 radical to the terminal carbon of the alkenes were observed,[113–117] and could be further extended to the trifluoromethylation of alkynes, allenes, and enynes.[105, 118, 119]

Some of the reactions described above for radical difunctionalization of alkenes described above are good examples of atom- or group-transfer radical addition (ATRA). ATRA and ATRA-type reactions are becoming increasingly popular, as they allow the conversion of simple alkenes into complex molecules in a rapid and convenient manner. Within this context, the issue of asymmetric ATRA-type reactions has been traditionally challenging. This is mainly due to the difficult of enantioselective control in the presence of radicals.[100, 120, 121] These challenges have been circumvented in selected cases. A pioneering work on asymmetric intramolecular oxytrifluoromethylation of alkenes was reported by Buchwald and coworkers in 2013.[103, 122]. Later on, the intramolecular enantioselective amino-di/trifluoromethylation,

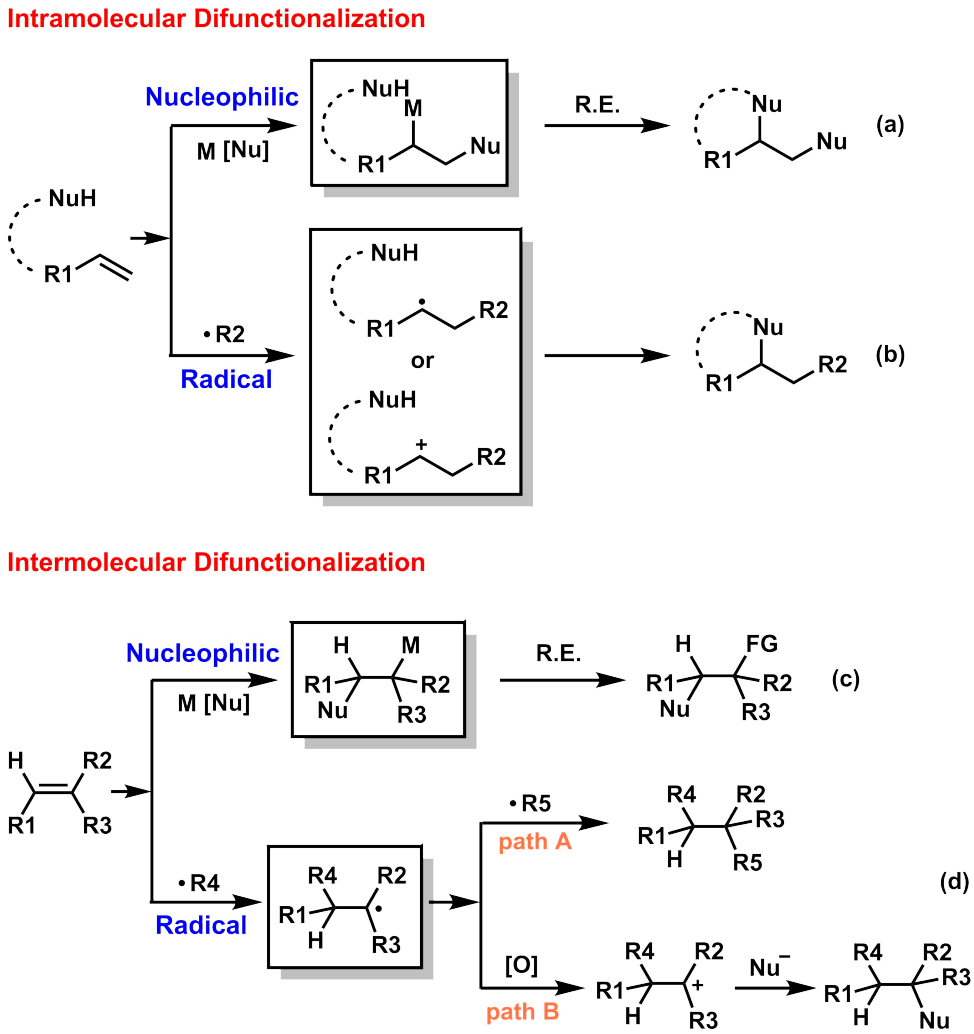

Fig. 4.1 Mechanisms for difunctionalization of alkenes.

aminoperfluoroalkylation, diamination and oxytrifluoromethylation of alkenes were discovered successively by Liu and coworkers employing a chiral phosphoric acid/Cu(I) dual catalyst system.[120, 123–125] Another successful combination has been obtained with Cu and Rh systems, which have led to enantioselective intermolecular ATRA-type difunctionalization reactions such as enantioselective aminoarylation, aminocyanation, azidocyanation, trifluoromethylarylation, and trifluoromethylcyanation of styrene.[126–134]

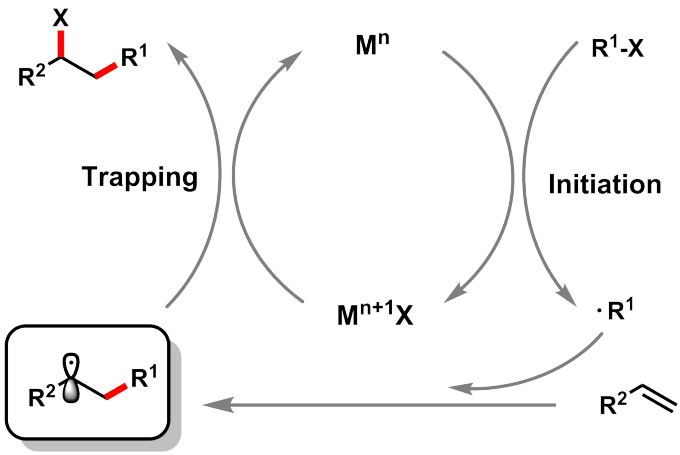

Fig. 4.2 Mechanism of ATRA difunctionalization.

The mechanistic understanding of this ATRA-type difunctionalization reactions is still superficial and incomplete. Two of the main issues are the role of the transition metal catalysts in the radical generation, and the origin of enantioselectivity in the whole process. Because of this, we decided to study computationally the mechanism for a representative process.

We chose one example involving the CF_3 group. The CF_3 group is common in bioactive compounds and has a wide application in a number of modern industries.[135–140] The enantioselective intermolecular cyanotrifluoromethylation of styrenes by using a chiral bis(oxazoline)/CuI catalyst was developed by Liu and coworkers in 2016.[128] As shown in Figure 6.1

(a), the reaction furnished CF_3-containing alkylnitriles with high yield (up to 96%) and excellent enantioselectivity (up to 99% ee).

The proposed mechanism in the experimental publication is shown in Figure 6.1 (b). It consists of some off-cycle steps and a catalytic cycle. In a first off-cycle step the reaction between the monocationic $[L*Cu(I)]^+$ complex, the Togni's reagent (which we label as Tog-CF_3) and TMSCN produces the Tog-TMS molecule, the monocationic $[L*Cu(II)(CN]^+$ complex and a CF_3 radical. The copper is oxidized in this step, which includes a single electron transfer (SET). The CF_3 radical subsequently attacks the styrene molecule to yield a benzylic radical. In the next step, the copper is reduced back to Cu(I) through an outer-sphere single electron transfer (OSET) process with the benzylic radical. This results **A**, which is postulated to be the active species in the catalytic cycle.

In the proposed catalytic cycle, **A** reacts with new molecules of Tog-CF_3 and TMSCN, resulting in intermediate **C**, containing a Cu(II) center and two cyanide ligands. **C** reacts with a benzylic radical to generate the Cu(III) species **D**. The final reductive elimination from Cu(III) leads to release of the products and regeneration of **A**, which can reinitiate the catalytic cycle. Mechanisms involving similar intermediates to **D**, with two CN groups have been proposed in other Cu-catalyzed processes of alkene difunctionalization(see Figure 6.1 (c)).[105, 129, 132, 141]

While some mechanistic research have been carried out, [105, 141] the whole picture remains still superficial and incomplete. This is why we decided to carry out a DFT study on the process experimentally reported by Liu and co-workers. Our main goal is to explain how the active radical is captured by the metal center in order to achieve the high enantioselectivity.

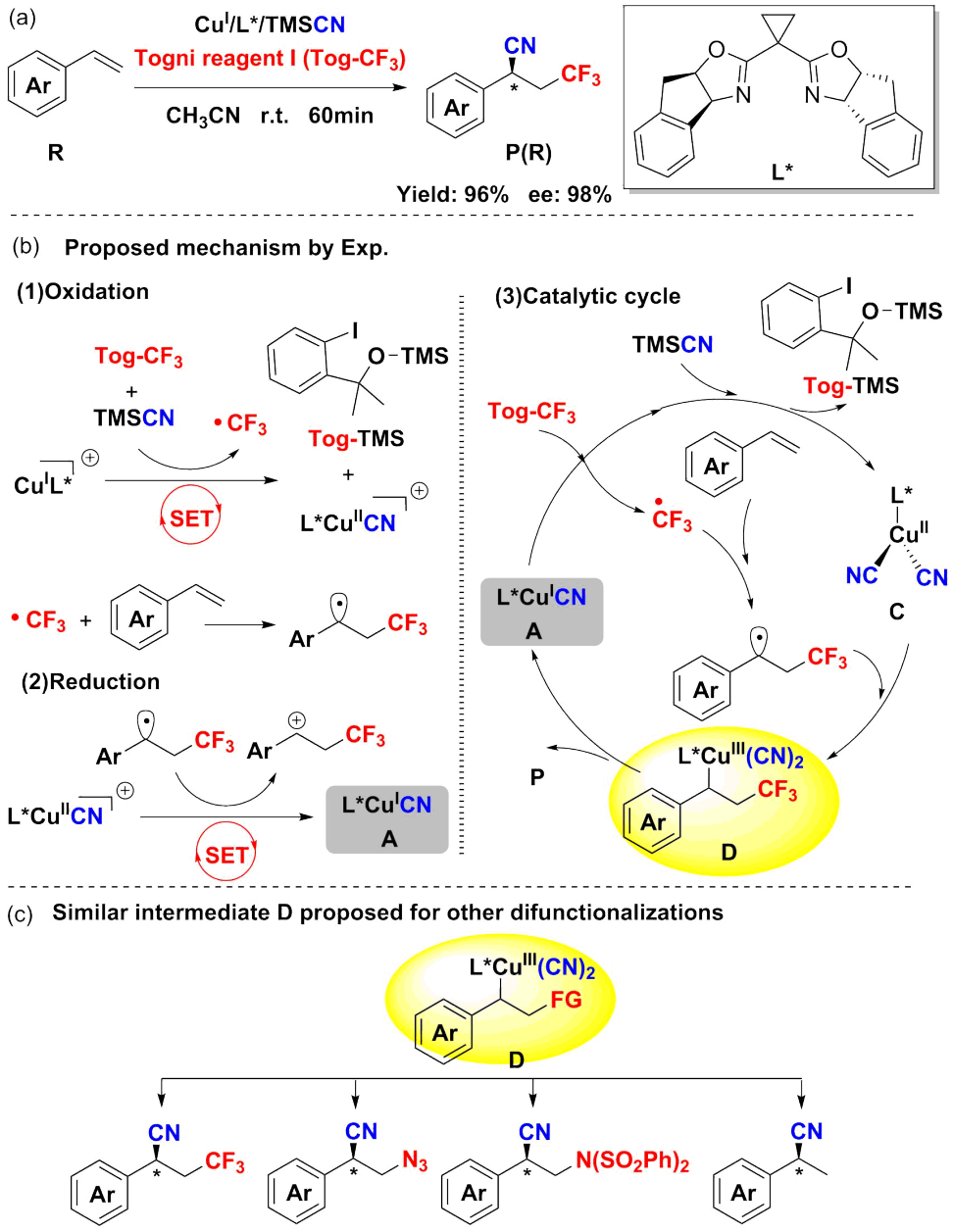

Fig. 4.3 Enantioselective intermolecular cyano-trifluoromethylation of styrenes by using chiral bis(oxazoline)/CuI catalyst.

4.2 Computational details

The structures of all species were optimized using the ωB97X-D[87] functional in the Gaussian 09 program.[88] The effective core potentials (ECPs) of Hay and Wadt with a double-ζ valence basis set (LANL2DZ) were used for Cu and I atoms,[89–92] complemented with polarization functions (f with exponent 3.525 for Cu) and (d with exponent 0.289 for I).[93] The all-electron basis set 6-31+G(d) was used in describing all other atoms.[94] Potential energies were refined by using a larger basis set: LANL2TZ(f) on Cu, LANL8(d) on I, and 6-311++g(d,p) on other atoms.[95–97] Solvent effects were taken into account in all calculations through the continuum model SMD for CH_3CN solvent. The harmonic vibrational frequencies and the number of imaginary frequencies determine the nature of all intermediates (no imaginary frequency) and transition state structures (only one imaginary frequency). The latter were confirmed to connect appropriate intermediates, reactants, or products by intrinsic reaction coordinate (IRC) calculations. Free energy corrections were considered at a concentration of 1 M and a temperature of 298.15 K. The charge decomposition analysis was carried out by the Multiwfn program.[142] The non-covalent interactions (NCI) were visualized by NCIplot 3.0.[143, 144] The 3D molecular structures of all the species were drawn by using the CYLview program. All the reported energies correspond to Gibbs free energies in solution.

4.3 Results

4.3.1 Mechanistic proposal from the experimental publication

In this section, the feasibility of the mechanism outlined in Figure 6.1 (b) will be analyzed with DFT calculations.

Figure 4.4 presentws the reaction between the Cu(I) precursor $Cu(CH_3CN)_4$ and the chiral ligand **L***. We find out that the preferred species **I2** retains one molecule of CH_3CN coordinating the Cu(I) center. We will use this species **I2** as the starting point for discussion that follows.

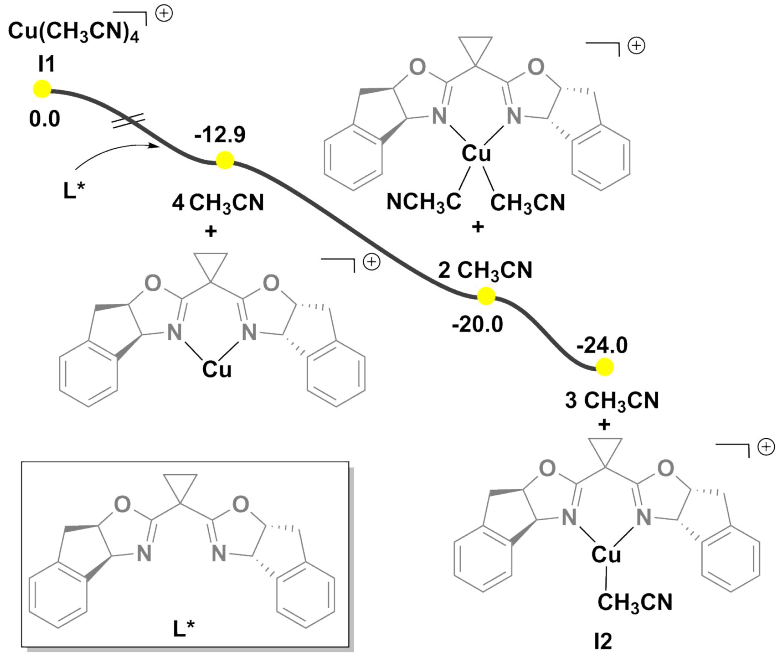

Fig. 4.4 Rapid ligand exchange process.

We started our investigation on the reaction between the copper intermediate **I2** and Tog-CF_3. The resulting free energy profile is shown in Figure 4.5. The replacement of CH_3CN by Tog-CF_3 in the nickel coordination sphere leads to the slightly unstable intermediate **I3**, where the Togni's reagent coordinates to the Cu(I) center through the O atom. Then, the single electron transfer occurs from the Cu(I) center to the O-I(III) bond of Togni's reagent, promoting the homolytic cleavage of the C-I α-bond, and the formation of the CF_3 radical. The oxidation state of copper increases to Cu(II) in complex **I4**, which remains neutral because it contains the formally negative Tog^- ligand. The free energy barrier for the associated open shell singlet transition

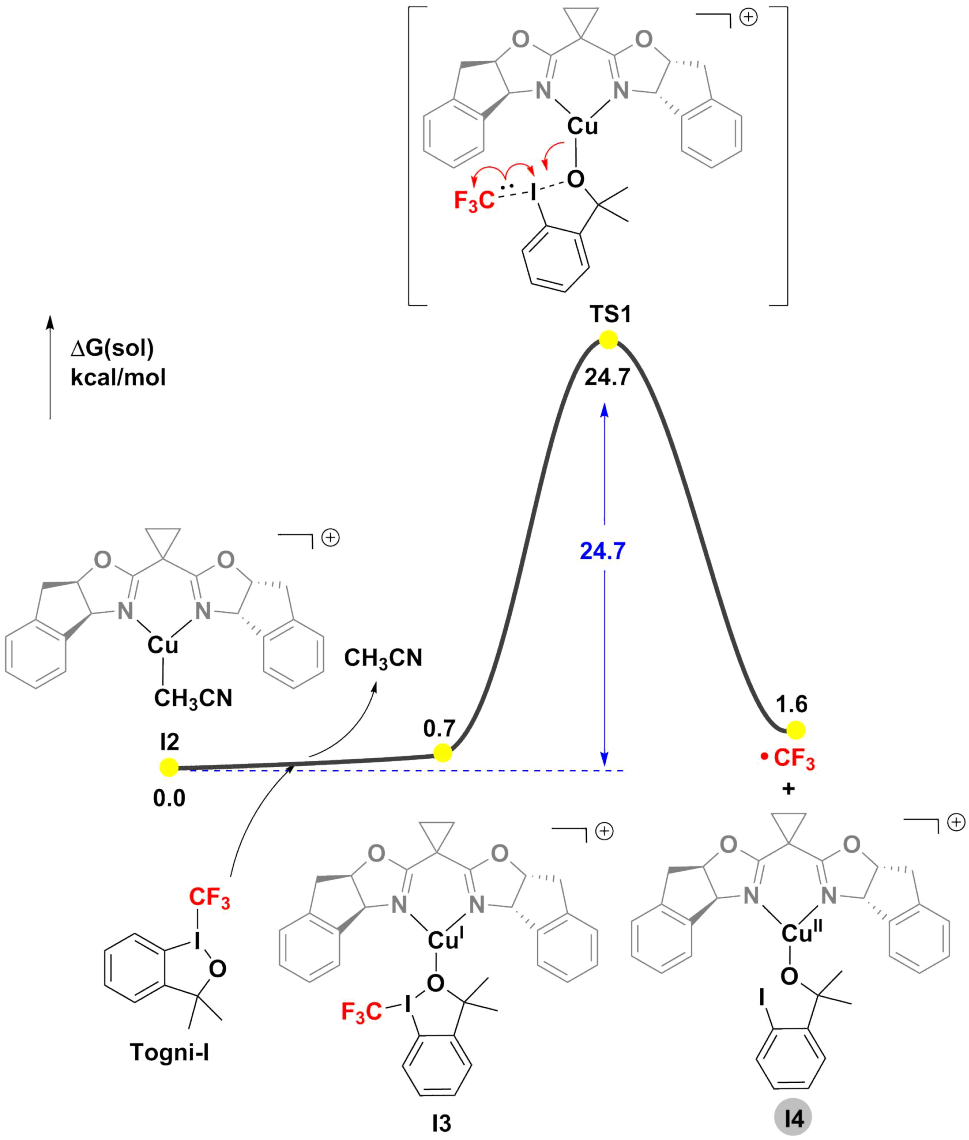

Fig. 4.5 Free energy profile of the CF_3 radical generation process.

Table 4.1 Benchmark of theoretical calculations with different basis sets.

	Cu	I	other atoms	$\Delta G^{\neq}$
BS1	LANL2TZ(f)	LANL8(d)	6-311+g**	24.8
BS2	LANL2TZ(f)	LANL8(d)	def2tzvp	26.5
BS3	LANL2TZ(f)	LANL8(d)	cc-pvtz	25.8
BS4	LANL2TZ(f)	LANL8(d)	def2tzvpp	26.4
BS5	SDD	SDD	6-311++g**	26.1
BS6	LANL2TZ(f)	LANL8(d)	6-311++g**	24.7

state **TS1** is 24.7 kcal/mol. The spin density diagram of **TS1** presented in Figure 4.6 shows that the β spin is mainly located on the CF_3 moiety while the α spin is delocalized on the Cu-O moiety.

We used this specific step to make a method calibration. Different basis set were tested for Cu, I, and the other atoms, the results are presented in Table 4.1. They show that the difference of the barriers with associated to changes in the basis set is quite small. This further demonstrates the reliability of our computational method.

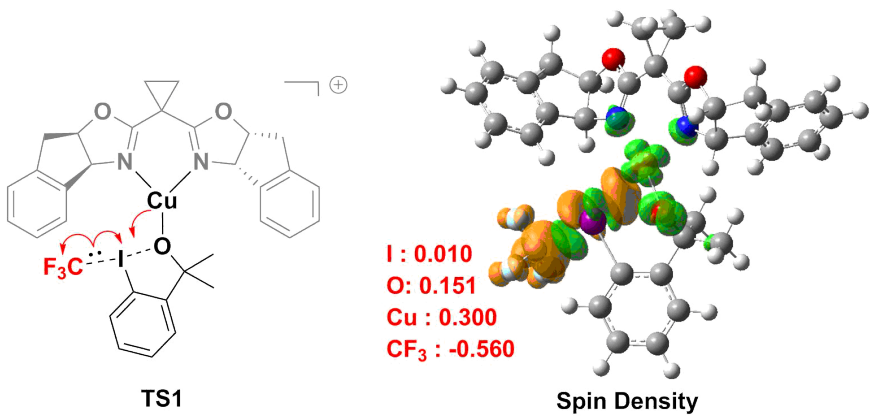

Fig. 4.6 The spin density of **TS1** (isovalue 0.0018).

An alternative process for the reaction of copper with Tog-CF_3 without the participation of the chiral ligand was also considered. The calculated results

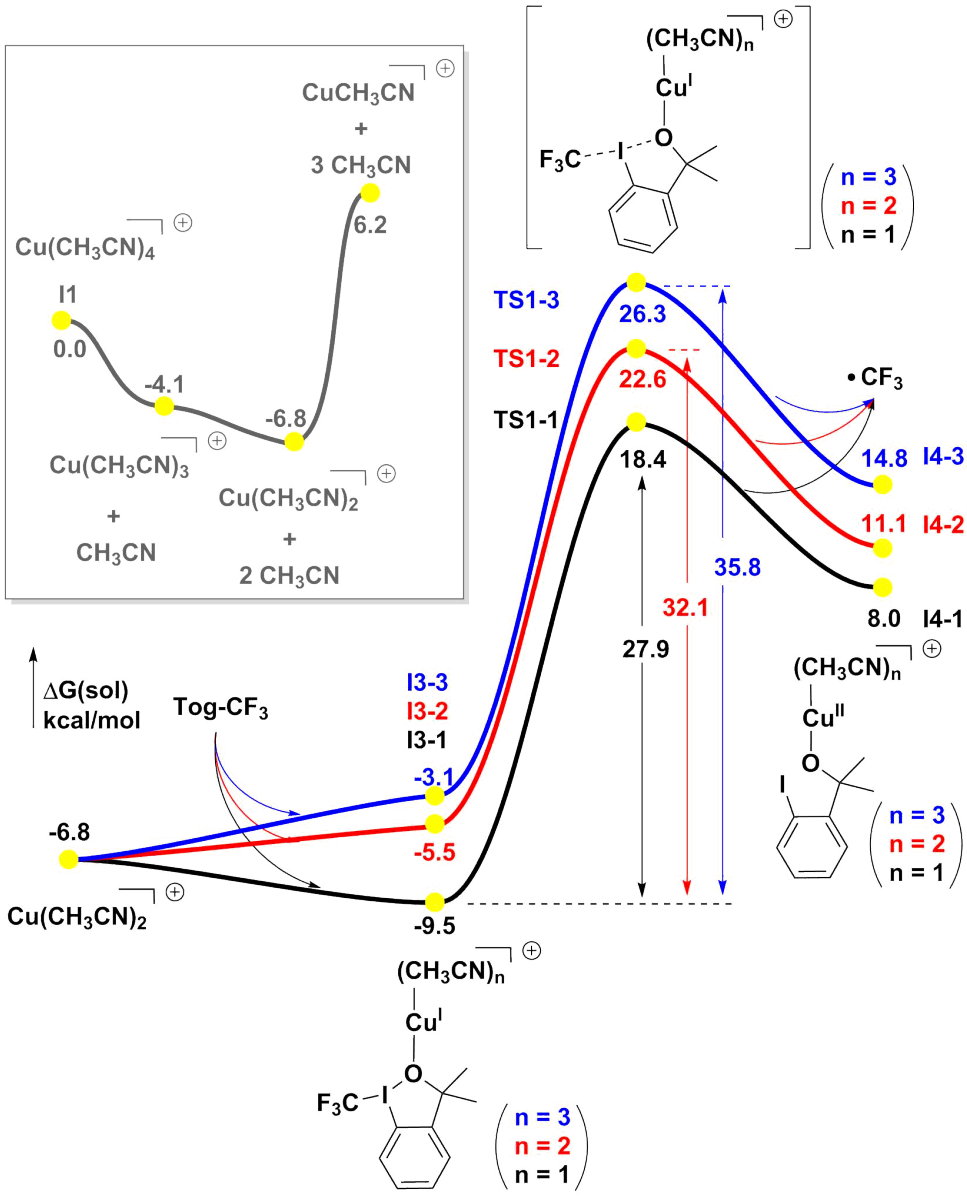

Fig. 4.7 The release of CF_3 radical by CuI catalyst without the participation of chiral ligand.

are shown in Figure 4.7. Three different transition states (**TS1-1**, **TS1-2**, and **TS1-3**) with different numbers of CH_3CN coordinated to Cu(I) center were considered. The barriers are 27.9, 32.1, and 35.8 kcal/mol for **TS1-1**, **TS1-2**, and **TS1-3**, respectively. They are higher than that of **TS1** in Figure 4.5. This agrees well with the experimental observation that the reaction proceeds more slowly in absence of the chiral ligand (yield = 19 % 30h).[128] Thus reaction routes without the chiral ligand will no longer be discussed in this work.

Another alternative process consisting of the reaction between Tog-CF_3 and TMSCN was also evaluated and the profile is shown in Figure 4.8. This activation mode is also thermodynamically disfavored despite the fact that it had been proposed by previous experimental investigations.[117, 128, 130]

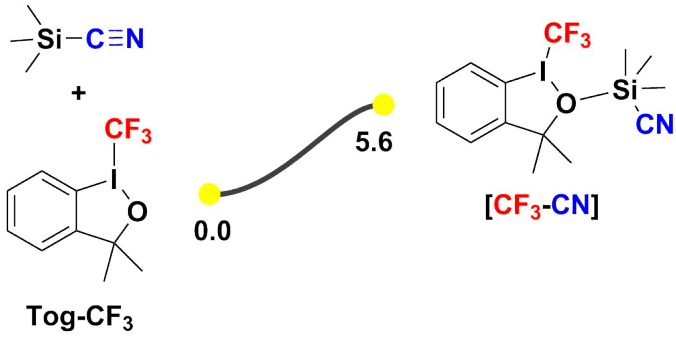

Fig. 4.8 The mutual activation of Tog-CF_3 and TMSCN.

The reaction continues following the profile outlined in Figure 4.9. The Cu(II) intermediate **I4** undergoes a rapid transmetalation process with TMSCN to give intermediate **I6**, which could be further stabilized by the coordination of one molecular of CH_3CN to give **I7**. All attempts to get this transmetalation transition state failed as all geometry optimizations led to intermediate **I6**. We consider that given the very close energies, the barrier must be quite low.

The CF_3 radical generated in a previous step can react with styrene to produce the benzylic radical **I8** *via* **TS2**. The intermolecular outer-sphere

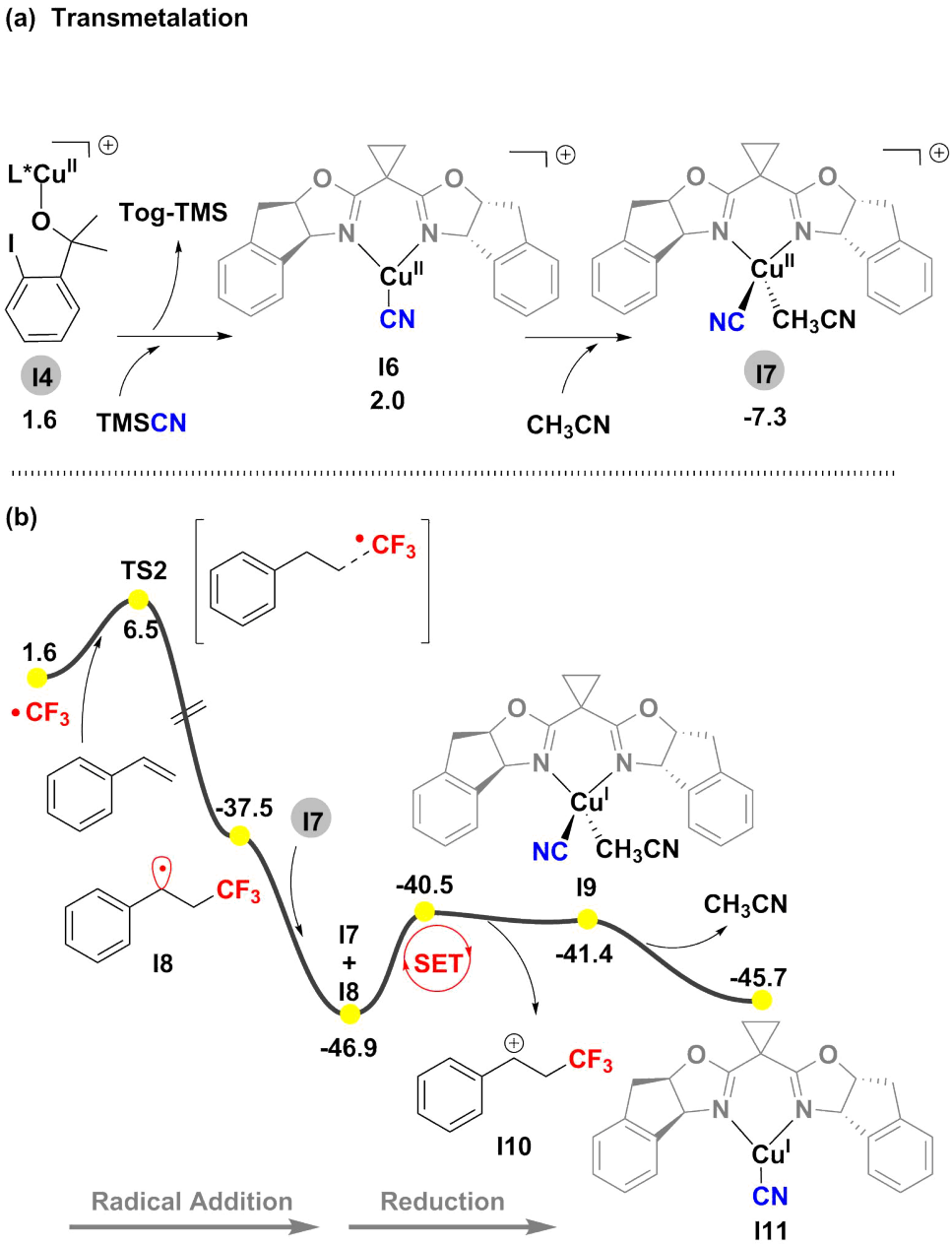

Fig. 4.9 Free energy profile of the preliminary oxidation and reduction process leading to the Cu(I) active species.

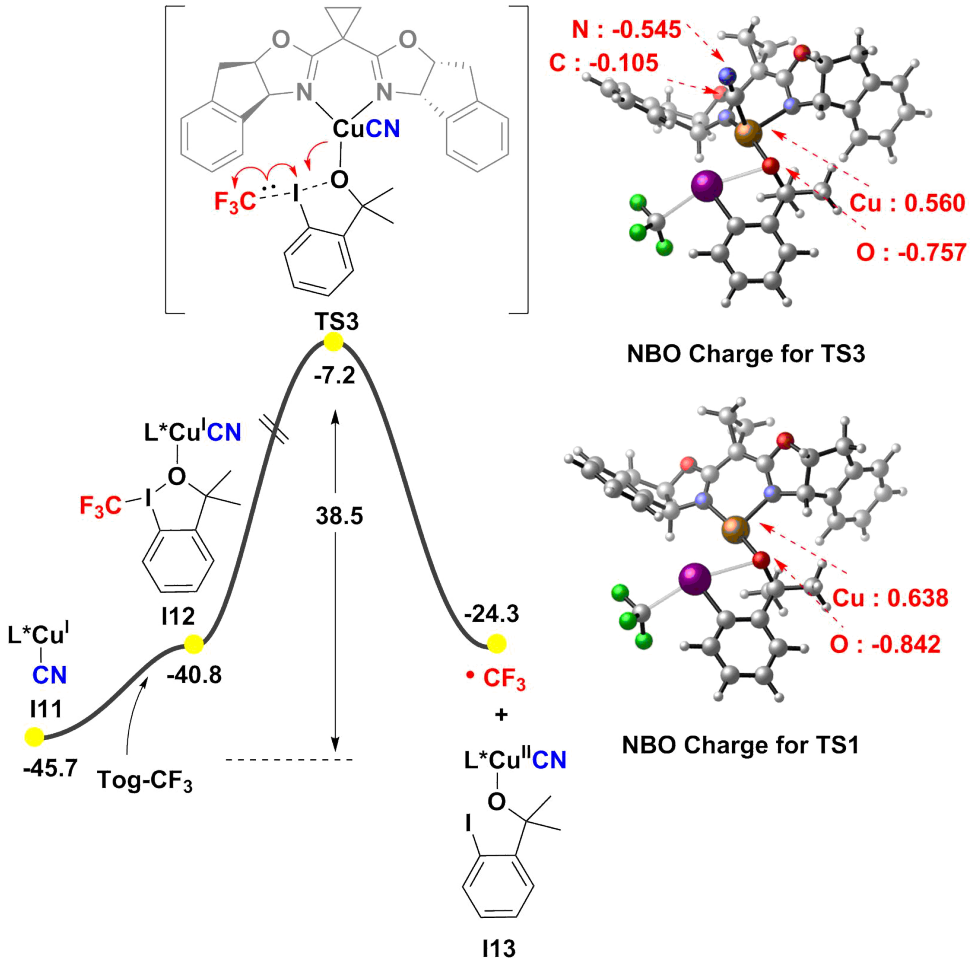

Fig. 4.10 Calculated potential energy surface of the experimental proposed radical generation process by **I11** and NBO charge of the key transition states **TS1** and **TS3**.

single electron transfer (SET) between **I8** and **I7** can then take place to produce the Cu(I) intermediate **I9** and the benzylic cation **I10**.[120, 137, 145–150] A low free energy barrier of 6.4 kcal/mol for this outer-sphere SET process was estimated through the Marcus-Hush theory and related formulations.[151–153] After, the disassociation of CH_3CN from **I9** yields a stable Cu(I) intermediate **I11**, which is the active species **A** in Figure 6.1 (b) proposed by the experimental group.[128] Intermediate **A**, labeled here as **I11** is thus accessible through relative low barriers, and from the calculations presented so far, it could indeed be the catalytic species.

The problem appears when we try to use this species in the catalytic cycle proposed in Figure 6.1(b). The first step should be a SET process between **I11** and the Tog-CF_3 reagent. The calculated free energy barrier, shown in Figure 4.10, is 38.5 kcal/mol, which is obviously too high for the experimental conditions.[128] The presence of a strong ligand such as cyanide on the Cu center seems to be sufficient to block the reaction. In transition state **TS3**, the charge transfer from the Cu center to the $\sigma*$ I-CF_3 orbital is more difficult than that in **TS1**. The results of the NBO charge analysis, in **TS1** and **TS3** are interesting. The NBO charges on Cu and O in **TS1** are 0.638 and -0.842, respectively, while the corresponding values are 0.560 and -0.757 for **TS3**. It is important to realize that the high barrier from **I11** to **TS3** is the only block for an easy reaction, as the subsequent steps would occur rapidly: transmetalation, radical addition, and the final reductive elimination, as shown in Figure 4.11.

We summarize our calculations on the experimentally proposed mechanism in Figure 4.12. The reaction proceeds smoothly until transition state **TS3**. The SET process from **I11** is calculated to be unfavorable, with a high barrier of 38.5 kcal/mol. A further complication is that our DFT calculations in Figure 4.11 (b) show that the final reductive elimination product of this would be in the S configuration (**P(S)** *via* **TS5(S)**), which also contradicts the

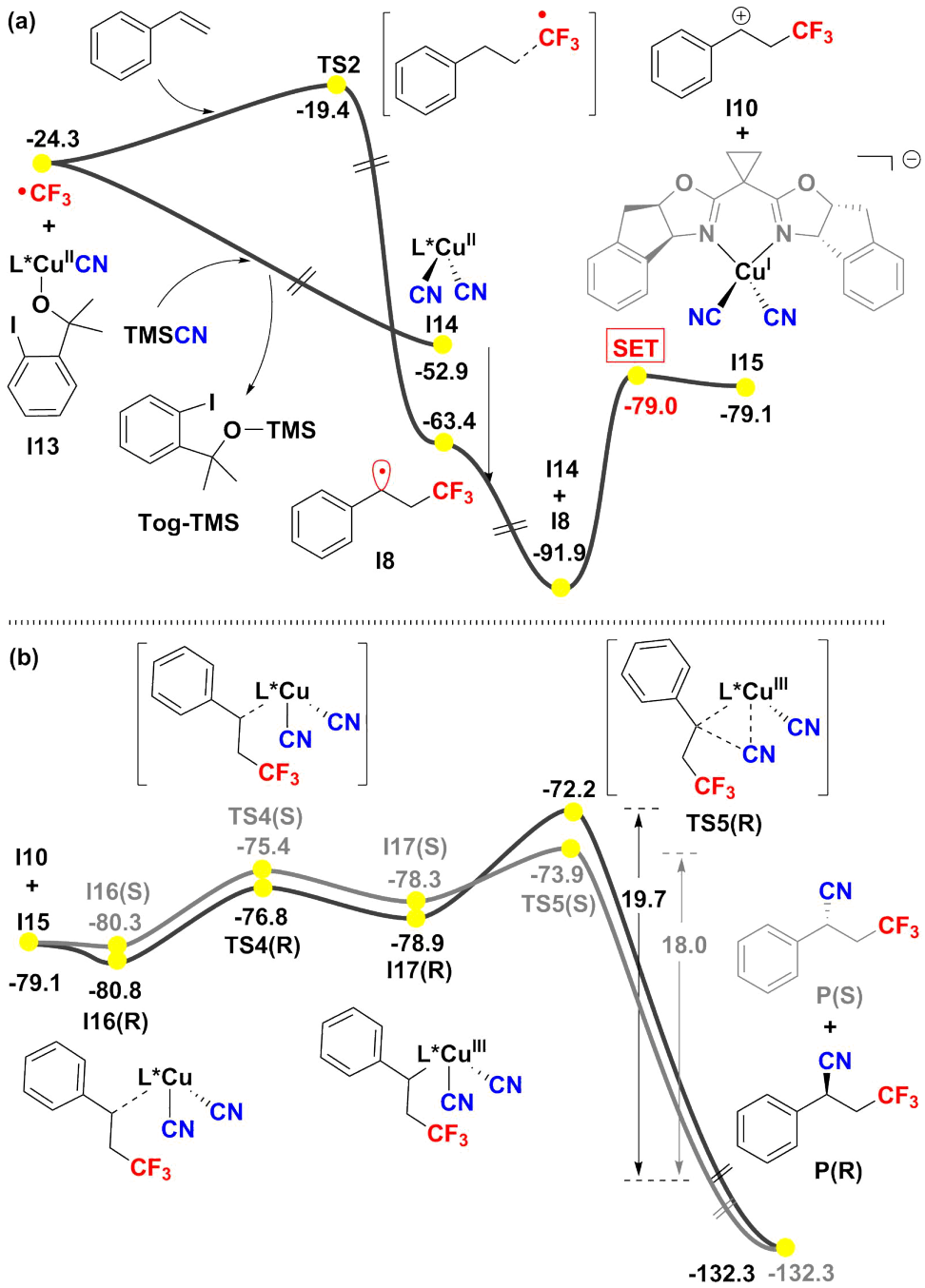

Fig. 4.11 Calculated potential energy surface of the experimental proposed mechanism.

experimental observation that the **R** configuration is the main product. As a result, the mechanism proposed in Figure 4.12 must be discarded.

4.3.2 Revised mechanism

We were able to find an efficient mechanism using many of the steps reported above, but introducing a significant change. This was the possibility of having the Cu(I) intermediate **I11** to react with the benzylic cation **I10**. This mechanism is shown in Figure 4.13. The 4-coordinated Cu(III) intermediates **I19(R)** and **I19(S)** could be formed quickly by trapping the benzylic cation asymmetrically *via* the transition states **TS6(R)** and **TS6(S)**. Similar to the mechanism that was proposed by the previous study about the reductive elimination at the Cu(III) centers,[154–156] the current reductive elimination via transition states **TS7(R)** and **TS7(S)** leads to the chiral CF_3-containing alkyl nitrile products **P(R)** and **P(S)** and regenerates the catalyst. The free energy barriers for the enantioselectivity-determining transition states are 6.7 and 8.3 kcal/mol for **TS7(R)** and **TS7(S)**, respectively. This is in accordance with the experimental observation that the **R** configuration is the main product (ee 98%).[128] We also considered the possibility of the rebound of benzylic radical **I8** to the Cu(II) center as proposed in the previous theoretical reports.[105, 141] All the attempts to locate these radical-radical coupling transition states failed.

In summary, the reaction should finish the catalytic cycle by a different mechanism that is shown in Figure 4.14 (in green colour). Reaction should start with the SET oxidation and OSET reduction process to give the Cu(I) intermediate **I11**, that is the same as proposed experimentally. However, from **I11**, different from the oxidation process of Cu(I) to Cu(II) proposed by experimental study, the direct rebond of benzylic cation to Cu(I) gives the Cu(III) species **I19**, where the reductive elimination happens to give the products. The rate determining step for this new catalytic cycle is the generation of CF_3 radical via **TS1**, which needs a barrier of 24.7 kcal/mol.

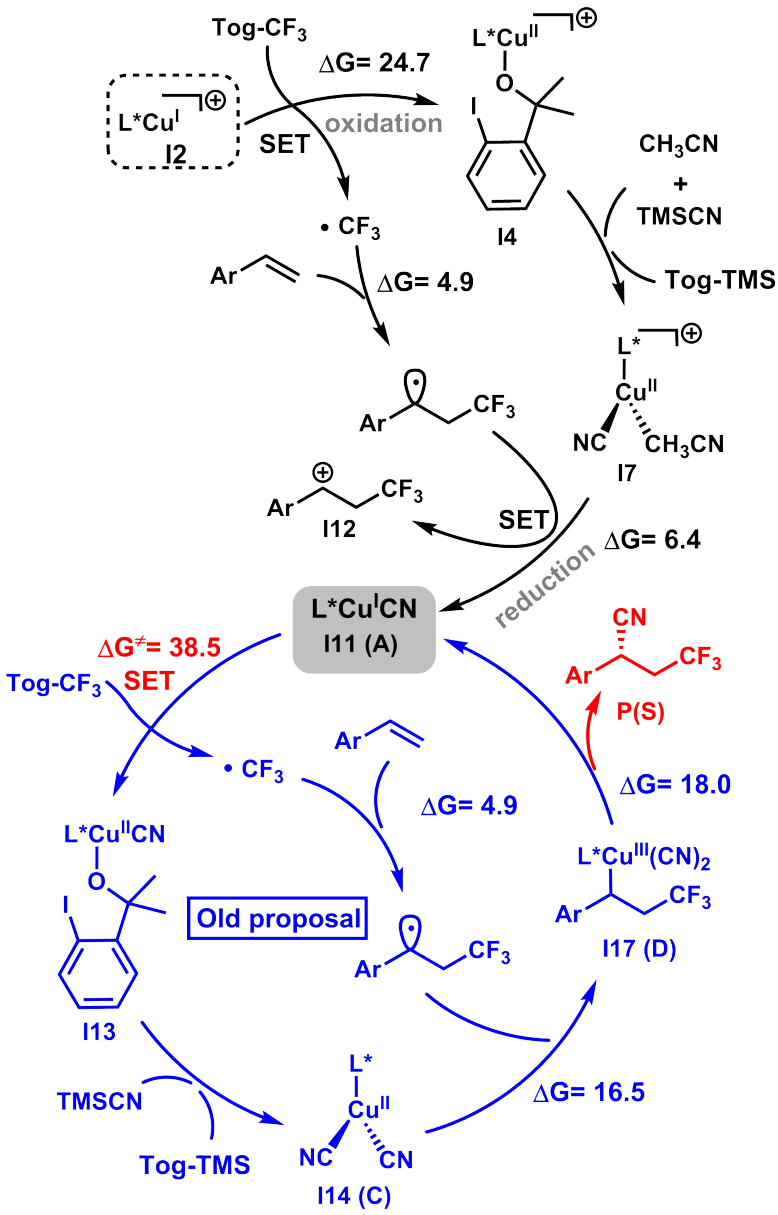

Fig. 4.12 Calculated potential energy surface of the experimental proposed mechanism.

The enantioselectivity determining step is the reductive elimination process. This newly proposed mechanism by our DFT calculation provides reasonable explanation about the reactivity and enantioselectivity of this copper-catalyzed intermolecular enantioselective cyanotrifluoromethylation of alkene.[128]

4.3.3 Non-covalent interaction (NCI) analysis

Having established the new mechanism of the catalytic cycle, a comprehensive analysis on the origin of the enantioselectivity process was performed. In particular, we pay our attention on the enantioselectivity determining transition states **TS7(R)** and **TS7(S)** in Figure 4.13. Rational explanation for the observed asymmetric induction could be provided by the clear presentation of the structures of transition states in Figure 4.15 and the non-covalent interaction (NCI) in Figure 4.16. As shown in the space-filling model in Figure 4.15, when the Re-face of benzylic cation coordinates to the Cu center, the CF_3 group is well accommodated in the binding pocket in **TS7(R)**. However, this is not the case when the benzylic cation coordinate to the Cu center by the Si-face. The CF_3 group will clash with the arm of the chiral ligand, which makes the benzylic cation cannot bury deeply into the chiral pocket in **TS7(S)**. This is quite in accordance with the bond length shown in Figure 4.16, both the bond length of Cu-C1 and C1-C2 in **TS7(R)** (Cu-C1 = 2.231 Å, C1-C2 = 2.095 Å) are shorter than that **TS7(R)** (Cu-C1 = 2.264 Å, C1-C2 = 2.133 Å). The NCI plots in Figure 4.16 give us a direct presentation of this steric repulsion. More repulsive area (red dashed circle of the front view and side view) between the ligand arm and the benzylic cation in the disfavored transition state **TS7(S)**, makes the formation of S-product unfavorable.

4.3.4 Energy decomposition analysis

To better understand the origin of the 1.6 kcal/mol difference between the barriers of the enantioselective determining transition states **TS7(R)** and

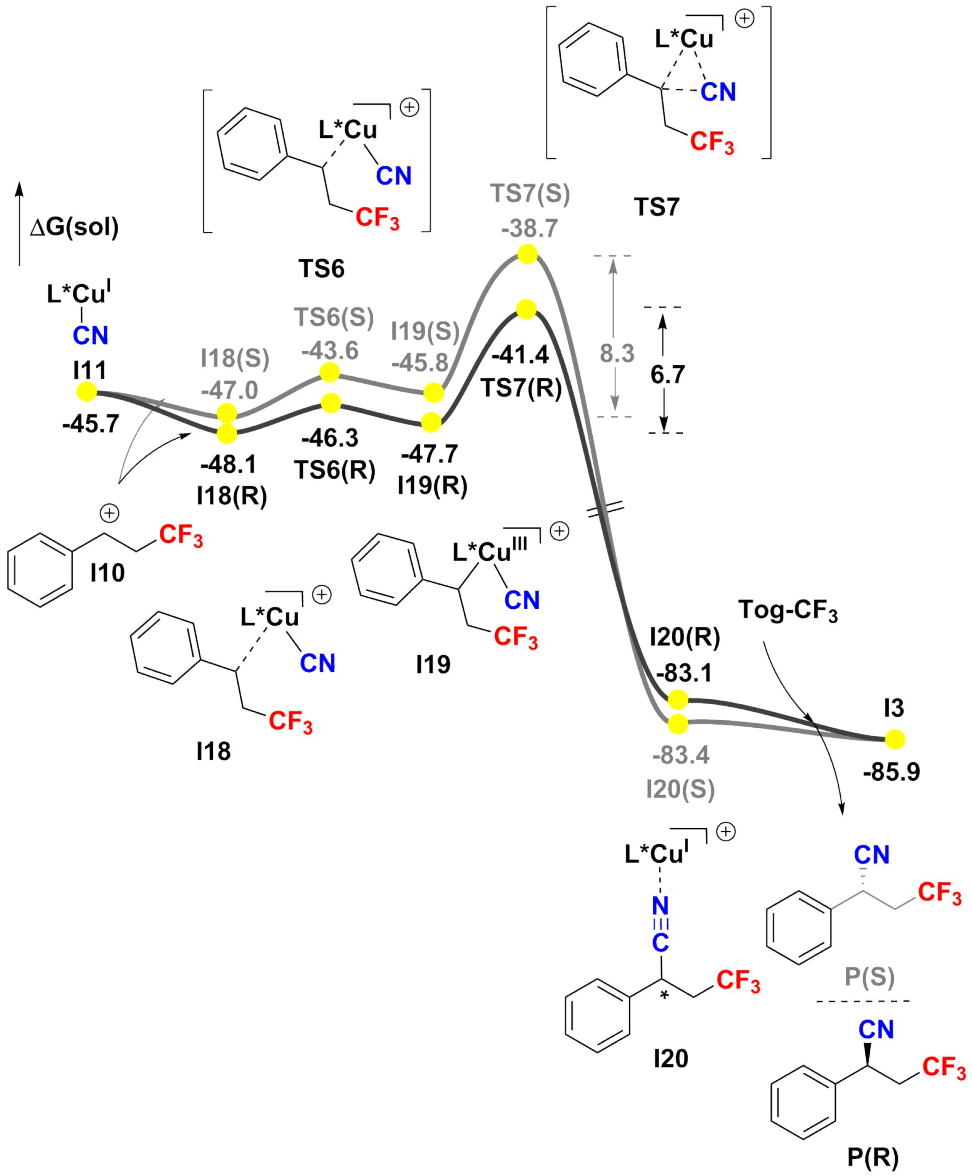

Fig. 4.13 Free energy profile of the alternative routes leads to the enantioselective formation of the products.

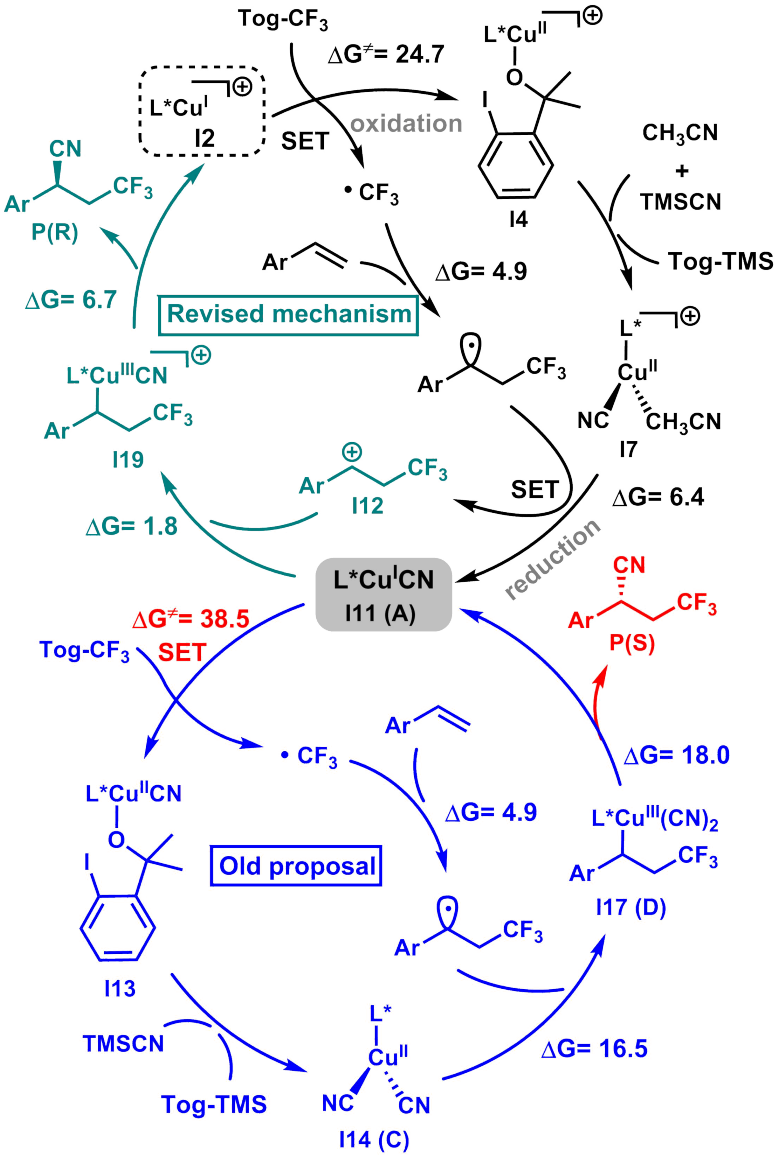

Fig. 4.14 The new mechanism confirmed by our theoretical calculations.

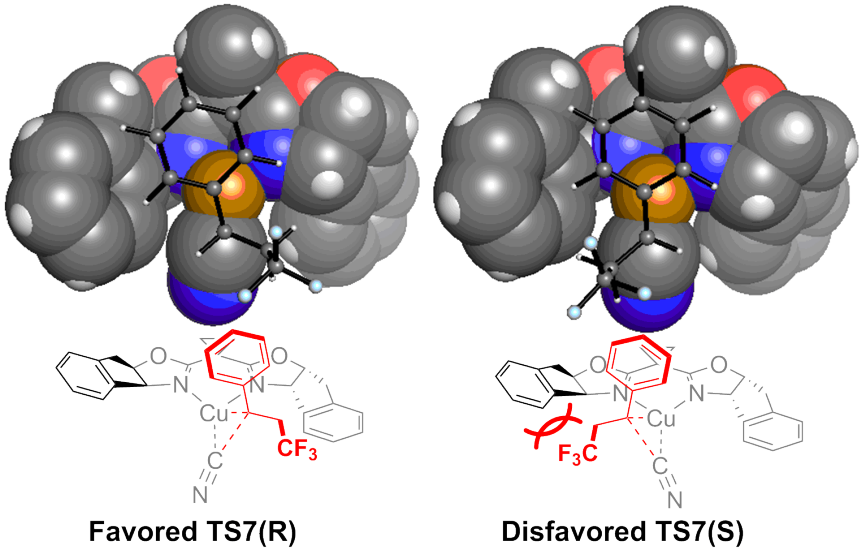

Fig. 4.15 Space-filling model for **TS7(S)** and **TS7(R)**.

TS7(S), we use Wheeler's energy decomposition model to analysis the energy difference.[157] First of all, we noticed that the gas-phase energy difference, $\Delta\Delta E^{\neq}$ is 0.8 kcal/mol, which means that the entropic and solvent effect increased the energy gap by 0.8 kcal/nol. The $\Delta\Delta E^{\neq}$ in gas-phase can be decomposed into three components as shown in Figure 4.17. The $\Delta\Delta E_{sub}$ is the energy difference between the benzylic cation in **TS7(R)** and **TS7(S)**; $\Delta\Delta E_{cat}$ is the difference of the energy of the catalyst in **TS7(R)** and **TS7(S)** geometries; and $\Delta\Delta E_{int}$ is the difference of the interaction energies between the substrates and catalysts in these two transition states. Remarkably, we noticed that the interaction energy ΔE_{int} (repulsion interaction, 1.7 kcal/mol) dominates the energy difference in gas-phase. While the $\Delta\Delta E_{sub}$ and $\Delta\Delta E_{cat}$ are negative and the substrate and catalyst in **TS7(S)** are 0.1 and 0.8 kcal/mol lower than in **TS7(R)**, the strong repulsion still makes the gas-phase energy of **TS7(S)** 0.8 kcal/mol higher than that in **TS7(R)**.

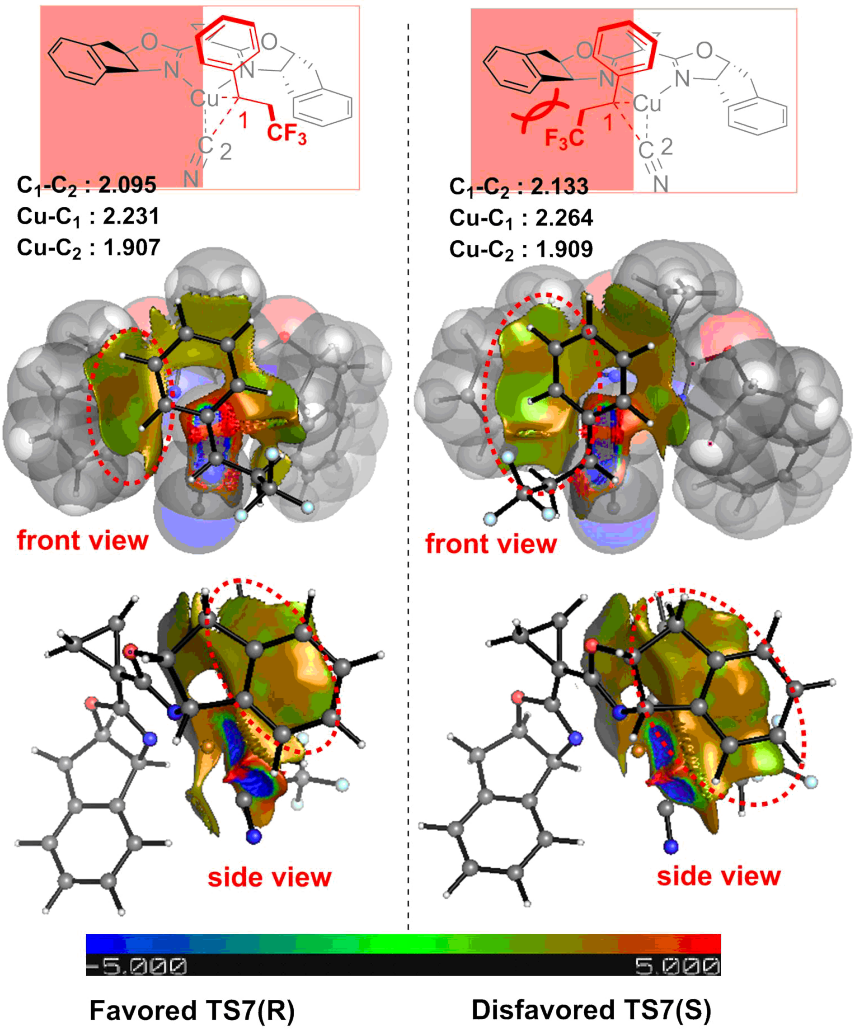

Fig. 4.16 Structure parameters and visualization of the NCI plot of the key enantioselevtive determining TSs, NCI surface shows only intermolecular interactions. (red : strong and repulsive; green : weak interaction; blue : strong and attractive).

These results suggest that the enantioselectivity arises from the more favorable binding of benzylic cation to Cu center in **TS7(R)**, the strong repulsion in **TS7(S)** plays a crucial role in elevating the energy barrier.

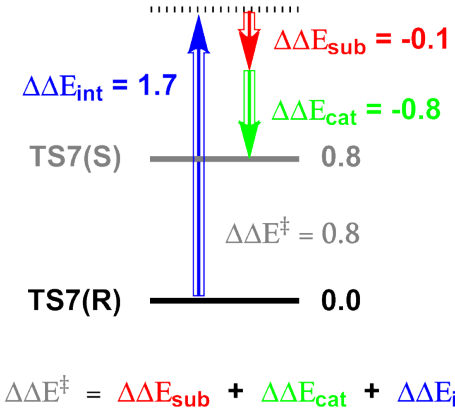

Fig. 4.17 Energy decomposition analysis of the energy difference of the enantioselective transition states.

4.3.5 Charge decomposition (CDA) analysis

The charge decomposition analysis (CDA) could further give us a qualitative explanation for the origin of the enantioselectivity,[158] which also has been successfully used on the discussion of the C-C bond cleavage mechanism before.[159, 160] Here, the reductive elimination transition states **TS7(R)** and **TS7(S)** were divided into two fragments, the C-C bond formation moiety (Labeled as C-C, red) and the Cu catalyst moiety (Labeled as Cu, gray) in Figure 4.18. For both of these two C-C σ-bond formation transition states, electron transfer from the HOMO (the highest occupied molecular orbital) of the C-C moiety to the LUMO (the lowest unoccupied molecular orbital) of the Cu moiety. The charge transfer for the favored transition state **TS7(R)** is 0.180 e, which is less than that of the disfavored **TS7(S)** (0.194 e). More charge transfer from C-C bond to Cu center in **TS7(S)** makes the new emerging C-C

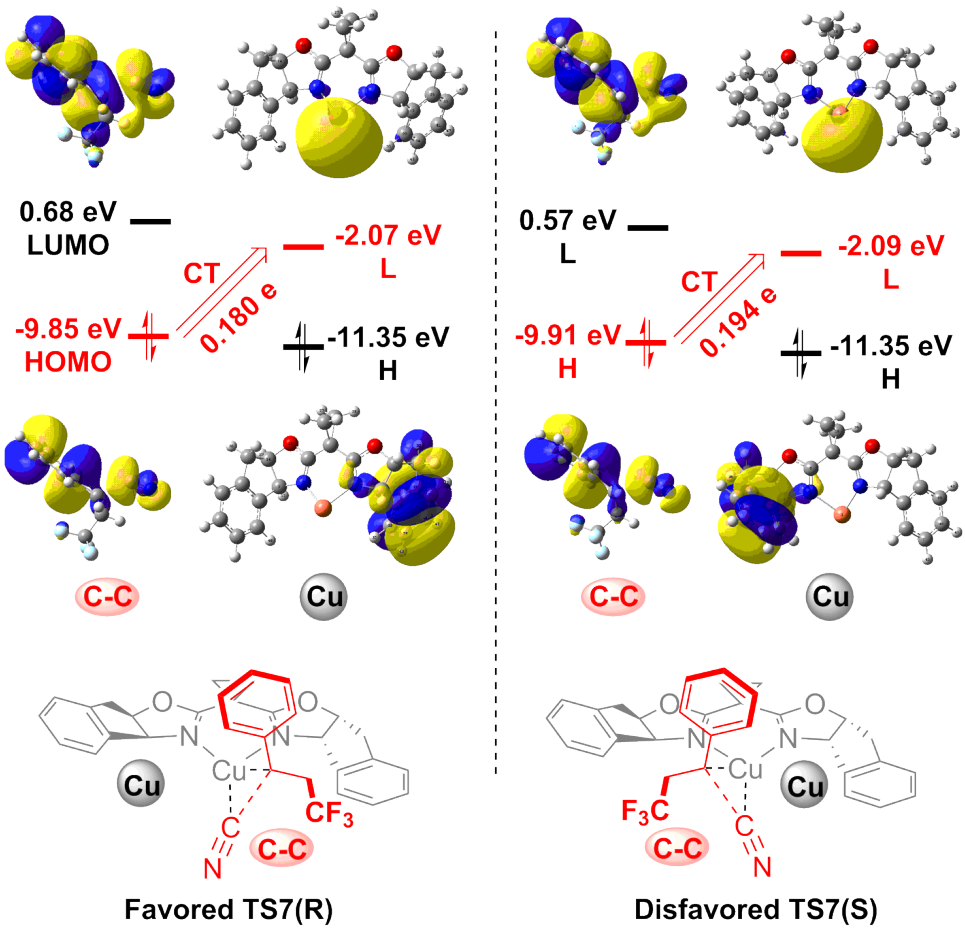

Fig. 4.18 Fragment molecular orbital analysis and charge decomposition analysis (CDA) of the enantioselective transition states corresponding to the C-C bond formation processes. (isovalue 0.02).

bond not as strong as the one in **TS7(R)**, indicating the difficult of C-C bond formation in **TS7(S)**. This also agrees well with the structure parameters that the C-C bond in **TS7(S)** (2.133 Å) is longer than that in **TS7(R)** (2.095 Å) in Figure 4.16.

The visualization of the NCI plot, the qualitative energy decomposition and charge decomposition analysis give us rational explanation of the experimental outcome that the formation of **P(R)** product with excellent enantiomeric excess.

4.4 Conclusions

In summary, DFT calculations have been performed to investigate the reaction mechanism of copper-catalyzed intermolecular enantioselective cyanotrifluoromethylation of alkene. Different from the experimental proposed mechanism, our theoretical investigation reveals an alternative mechanism scenario where the reaction initiated with the preliminary oxidation (SET) to release the CF_3 radical, followed by the rapid radical addition and intermolecular SET process to give **I11**. The catalytic cycle finished by the reductive elimination from Cu(III) center as shown in Figure 4.14. The rate determining step is the release of CF_3 radical and the enantioselectivity determining step is the reductive elimination process from the Cu(III) center. By the structure parameters analysis, the non-covalent interaction (NCI) visualization, and the energy decomposition analysis, the small steric repulsion between the ligand and the benzylic cation makes the formation of the **R**-products more favorable. Also the charge decomposition analysis (CDA) shows that the more charge transfer from the emerging C-C bond to the Cu center, the more difficult the formation of the C-C bond will be, thus disfavors the formation of the **S**-product. This work uncovers a new general manifold for the copper-catalyzed intermolecular enantioselective difunctionalization of alkenes via

radical process and will give more implication to improve the reactivity and enantioselectivity on this ATRA-type reaction.

Chapter 5

Aerobic α,β-Dehydrogenation of γ,δ-Unsaturated Amides

5.1 Background

Dehydrogenation is an important strategy for the increase of the oxidation state of organic compounds. It can convert the relatively inert and low value alkane chains to reactive and valuable alkene functional group, which can be in turn used as precursors to aldehydes, polymers, and aromatics compounds.[161–163] Dehydrogenation requires the activation of the C-H bond,[164–168] a process that has been subject of high development during the last years. The intrinsic inertness of the C-H bond requires catalysis, usually based on inorganic complexes containing metals such such as Pd,[169, 170] Ru,[171] Fe,[172] and others.

The direct α,β-dehydrogenation strategy has allowed the straightforward conversion of aldehydes, [173–176] ketones, [175–185] esters, [186, 187] nitriles, [187] and amines [188] to the corresponding α,β-unsaturated compounds.[189–191] An important milestone in this type of processes was the first tandem dehydrogenative Diels-Alder reaction to yield complex cyclohexenyl rings from simple terminal olefins reported by the group of

White.[192] This dehydrogenation methodology has been used with success in the synthesis of natural producrs. Stahl and co-workers prepared cyclic enones *via* the Pd-catalyzed aerobic dehydrogenation of ketones, and the cyclopentene-α-dione precursor to the natural product (-)-terpestacin was obtained in 90% yield.[193] Newhouse and co-workers reported a palladium-catalyzed ketone dehydrogenation process where various precursors for biologically active compounds were prepared efficiently.[194] The generally accepted mechanism for these transformations, shown in Figure 5.1 (a), involves a metal enolate as key intermediate.[195–197] A computational study by Pihko and co-workers supported the involvement of a Pd-enolate species in a cross coupling reaction involving dehydrogenation.[198]

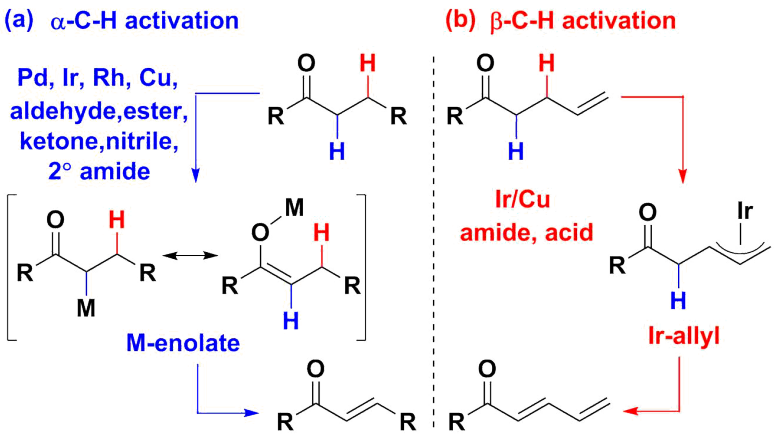

Fig. 5.1 Mechanism proposal of α,β-dehydrogenation.

Despite the large success achieved in the dehydrogenative synthesis of α,β-unsaturated ketones, aldehydes, and esters, the analogous α,β-dehydrogenation of amides remains challenging, probably due to the lower α-H acidity of these compounds. The traditional solution to increase amide reactivity has been the introduction of an α-leaving group such as halogen or sulfur.[195, 196, 199–202] The need for pre-functionalization and the usual requirement strong bases limit however the generality of this solution. New strategies to reach

α,β unsaturated amines from the corresponding saturated amides are thus highly desired. Several examples have been reported recently. In 2016, Newhouse *et al.* used an allyl-palladium catalyst to achieve unsaturated amides.[203] Later, the dehydrogenation of amides was also reported by the groups of Huang[204], Dong[199], and Maulide.[205] A transition metal-free process of α,β-dehydrogenation of saturated amides was also developed by Kang and co-workers under mild conditions.[206] These transformations are proposed to start with the α-C-H activation and the enolate intermediate is probably also involved in these reactions as shown in Figure 5.1 (a).

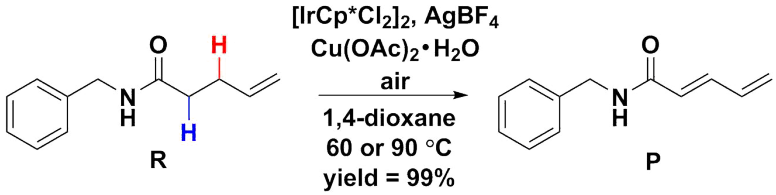

1	$[IrCp^*Cl_2]_2$	$Cu(OAc)_2 \cdot H_2O$ / air	$AgBF_4$	> 99%
2	$[IrCp^*Cl_2]_2$	$Cu(OAc)_2 \cdot H_2O$ / air	—	8%
3	$[IrCp^*Cl_2]_2$	air	$AgBF_4$	< 5%

Fig. 5.2 Aerobic α,β-dehydrogenation of γ,δ-unsaturated amides developed by Huang.

The scope of the amide dehydrogenation strategies indicated in the previous paragraph was relatively limited, as they did not apply to primary amides and acids. Things changed in 2018 when Huang and co-workers reported the direct iridium catalyzed aerobic α,β-dehydrogenation of γ,δ-unsaturated amides and acids under the presence of catalytic amounts of $Cu(OAc)_2 \cdot H_2O$ and O_2 as terminal oxidant.[207] This strategy tolerates primary amides and acids. It was proposed that the reaction does not proceed through an M-enolate intermediate, but through an M-allyl intermediate, as shown in Figure 5.1 (b). This M-allyl would be produced by a selective β-C-H activation, with the amides and acids work as directing groups.

The mechanism of the process is in any case far from being fully characterized. The control experiments presented in Figure 5.2 show that this reaction is only efficient when using the Ir catalyst with a combination of Cu(II) and Ag(I) salts. Although this mixture of Ag/Cu oxidant species with a transition metal catalyst has been demonstrated by our group to be a "privileged combination" in many oxidative couplings,[208–210] the mechanism and role of the Cu(II) and Ag(I) complexes has not been examined in dehydrogenations. We decided thus to carry out a DFT study on the mechanism of this reaction. We were interested in two specific issues: (1) the participation of either the Ir-allyl intermediate or the Ir-enolate in the catalytic cycle; (2) the roles of the Cu(II) and Ag(I) complexes.

5.2 Computational details

The structures of the reactants, products, intermediates and transition states were optimized in solution with the ωB97X-D [87] functional in the Gaussian 09 program.[88] The continuum model SMD was used to take account the solvent effects for solution in dioxane. Other functionals such as B3LYP-D3(BJ) and M06-D3 were used to calibrate the results(see Figure 5.3). A firs basis set was used for geometry optimizations and frequency calculations, It consisted of effective core potentials (ECPs) of Hay and Wadt with a double-ζ valence basis set (LANL2DZ) for Ir, Cu, and Ag atoms,[211] supplemented with polarization functions added for Ir (f = 0.938), Cu (f = 3.525) and Ag (f = 1.611),[93] and the all-electron basis set 6-31G(d) for all other atoms.[94] The potential energies were refined by carrying out single point calculations with a larger basis set: LANL2TZ(f) on Ir, Cu, and Ag, and 6-311++G(d,p) on other atoms.[95–97] The number of imaginary frequencies was used to determine the nature of all intermediates (no imaginary frequency) and transition state structures (only one imaginary frequency). The transition states were confirmed to connect the appropriate intermediates, reactants,

or products by intrinsic reaction coordinate (IRC) calculations. Free energy corrections were considered at a concentration of 1 M and a temperature of 298.15 K. All the 3D molecular structures of the species were drawn by using the CYLview program.

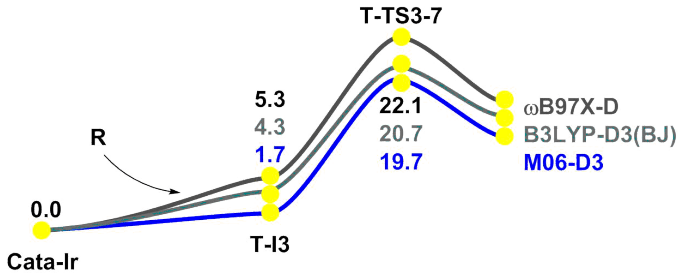

Fig. 5.3 Comparison of the free energy barriers of the rate determining transition states by using different functional

5.3 Results and discussion

5.3.1 Computational model

We chose γ,δ-unsaturated amide **R** shown in Figure 5.2 as the reactant. This substrate has been experimentally shown to undergo an α,β-dehydrogenation process to give the conjugated dienyl carbonyl product **P**. We investigated the mechanistic alternatives involving either the α-C-H and β-C-H activation routes leading to the M-enolate or M-allyl species, respectively, We also explored the role of the oxidant. Gibbs free energies in solution (in kcal/mol) are used throughout the discussion. The control experiments had shown the optimum Ir/Ag ratio to be 1/1, This suggests that the catalyst precursor $[IrCp^*Cl_2]_2$ is activated by one equivalent of $AgBF_4$ as shown in the equations in Figure 5.4. Because of this, the cationic Ir species $[IrCp^*Cl]^+$, labeled as **Cata-Ir**, was chosen as the starting point in our calculations.

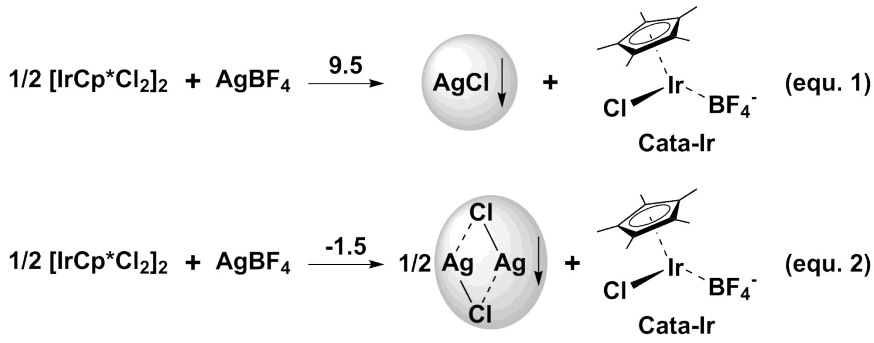

Fig. 5.4 Ligand exchange before the catalytic cycle.

5.3.2 The activation of the first C-H bond

We started exploring the first C-H bond activation. We considered both α- and β-C-H activation routes by Ir catalysts. We also considered mechanisms with and without the participation of $Cu(OAc)_2{\cdot}H_2O$. First of all, different adducts were obtained upon mixing of $[IrCp^*Cl_2]_2$, the $[Cu(OAc)_2{\cdot}H_2O]_2$, and the substrate. An adduct between **Cata-Ir** and substrate **R** is found to be the most stable. This adduct (**I3**), with an energy of -3.2 kcal/mol respect to the separated reactants (see Figure 5.5) will be used as resting state.

We first calculated the Ir-catalyzed β-C-H bond activation route proposed by the experimental investigation.[207] The results are shown in Figure 5.6. The process starts with a ligand exchange between the $[Cu(OAc)_2{\cdot}H_2O]_2$ and **Cata-Ir** complexes where an acetate ligand moves from the Cu(II) center to the Ir(III) center. This is mildly exergonic, and the acetate base on iridium is necessary to assist the C-H bond activation. A concerted metallation-deprotonation (CMD) transition state **TS1-4** leading to the Ir-allyl intermediate **I4** was located for the C-H activation; it is shown in Figure 5.6. However, the associated barrier is too high, 36.6 kcal/mol above the resting state **I3**, clearly unaffordable under the experimental conditions.[207]

This was not surprising. After all, the experimental data suggest participation of the co-catalyst $[Cu(OAc)_2{\cdot}H_2O]_2$, as a yield of less than 5% yield is

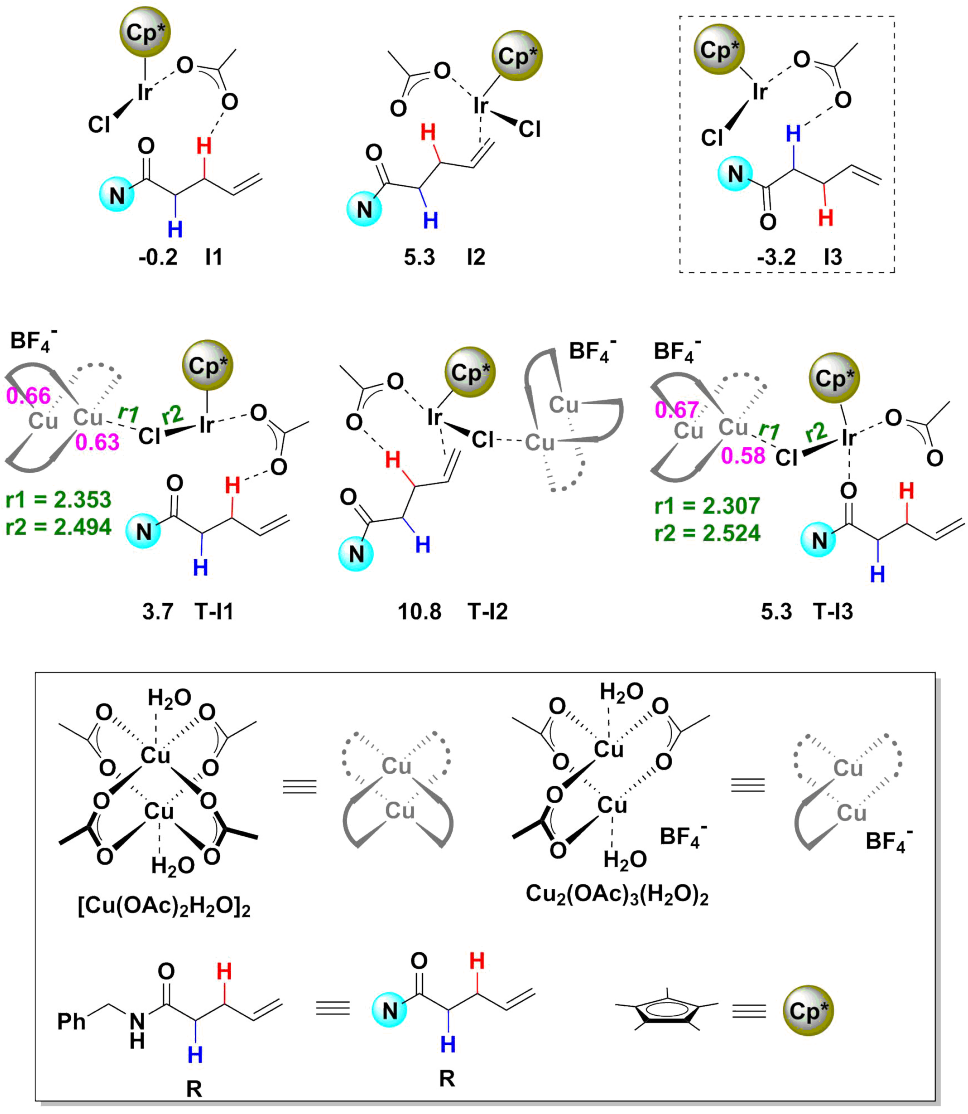

Fig. 5.5 Possible forms of the initial adduct.

observed when only air is used as oxidant(Figure 5.2).[207] So we decided to evaluate an alternative mechanism with involvement of the co-catalyst $Cu(OAc)_2{\cdot}H_2O$, results are also shown in Figure 5.6. $[Cu(OAc)_2{\cdot}H_2O]_2$, has been shown to be in a triplet dimeric state.[208–210, 212, 213] We hoped the acetate ligand coordinated to the Cu(II) center could exchange with other ligands such as the chloride from the Ir(III) catalyst precursor, and favor the process. A CMD transition state **T-TS1-4** with Cu(II) was located with the chlorine atom in the bridging position between the Cu(II) and Ir(III), being the Cu-Cl and Ir-Cl distances of 2.353 Å and 2.494 Å, respectively. The spin densities are concentrated on the Cu(II) center in **T-TS1-4**. The densities are practically the same as in $[Cu(OAc)_2{\cdot}H_2O]_2$, this indicates that no electron transfer happens during this process. In any case, contrary to our hope, the interaction between the Cu(II) and Ir(III) makes the β-C-H bond activation even more difficult, with a barrier of 44.9 kcal/mol. This mechanism must thus be discarded.

Other possibilities of β-C-H bond activation by using the C=C double bond as the directing group were also studied and all the transition states **TS2-6** and **T-TS2-6** have high barriers as shown in Figure 5.7. In summary, although the experimentally proposed Ir-allyl intermediate **T-I5** is more stable by 8.6 kcal/mol than the resting state, the high barriers found for the β-C-H bond activation preclude the formation of this Ir-allyl species.

This forced us to consider alternative α-C-H bond activation routes for this reaction. The free energy profile for the first set of them is shown in Figure 5.8. Transition state **TS3-7** leading to the Ir-enolate intermediate **I7** without the participation of $[Cu(OAc)_2{\cdot}H_2O]_2$ is calculated to have a free energy barrier of 38.3 kcal/mol, which makes the reaction more difficult when compared with the α-C-H activation transition state **TS1-4**. We next tried a cooperative transition state **T-TS3-7** with involvement of the $[Cu(OAc)_2{\cdot}H_2O]_2$ moiety. Similar to **T-TS1-4**, in the CMD transition state **T-TS3-7**, the chlorine atom is in the bridging position between the Cu(II) and Ir(III). To our delight, this

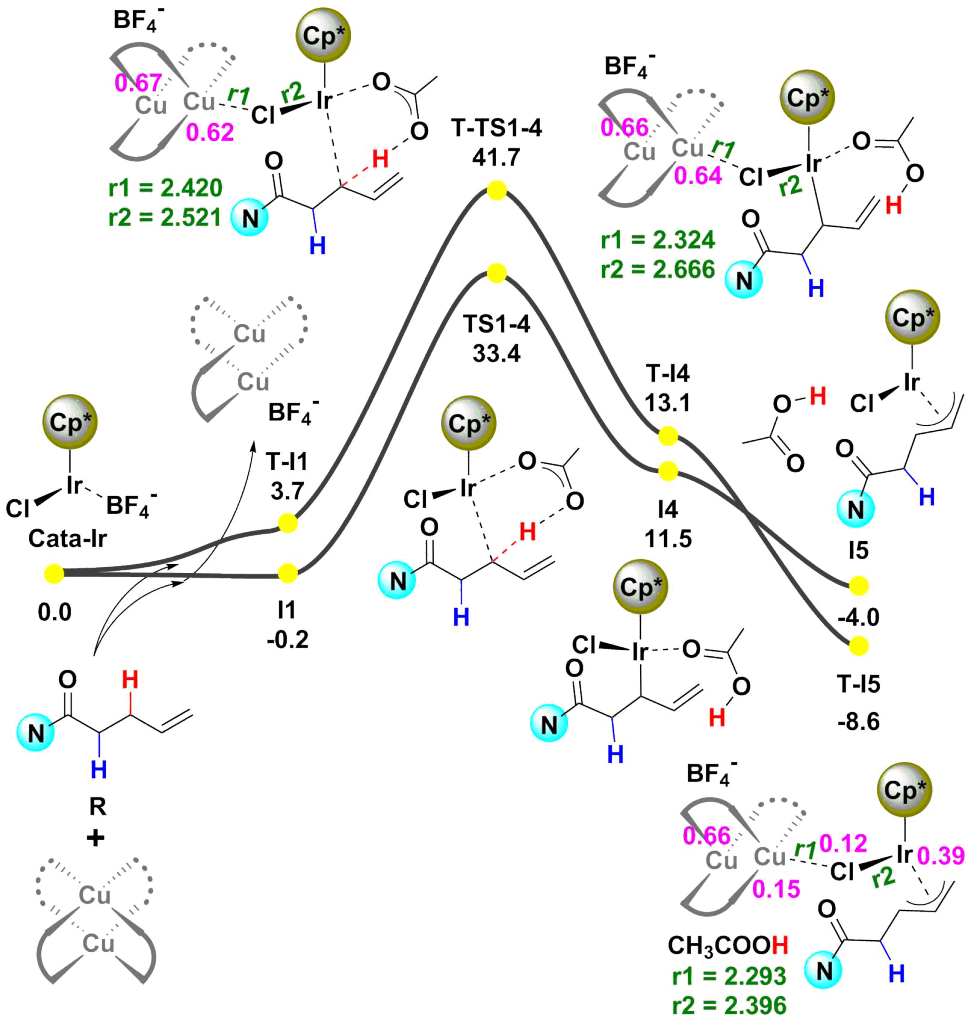

Fig. 5.6 Free-energy profiles (in kcal/mol) of the β-C-H bond activation routes. (Pink color: spin density; Green color: bond distance.)

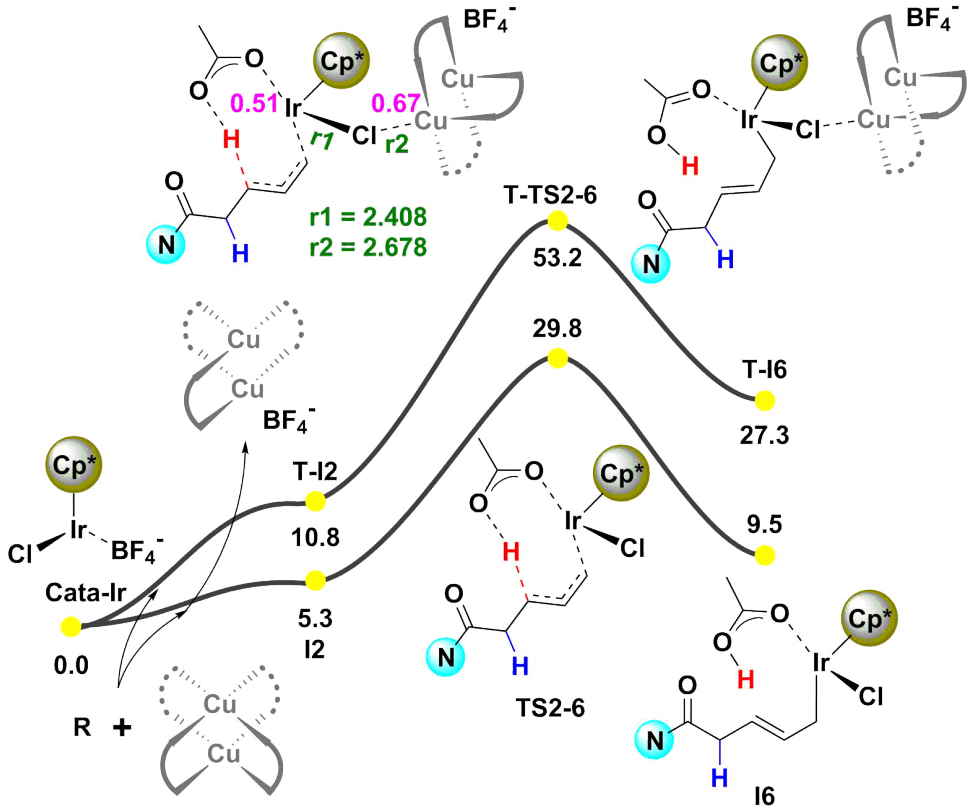

Fig. 5.7 Free-energy profiles (in kcal/mol) of the β-C-H bond activation routes by using C=C double bond as the directing group. (Pink color: spin density; Green color: bond distance.)

interaction makes the α-C-H activation much easier. An affordable barrier of 25.3 kcal/mol was found for this process. As shown in the 3D structure the copper center is connected with Ir(III) by Cl atom placed near the midpoint between the two centers (Cu-Cl : 2.395 Å; Ir-Cl : 2.474 Å). The spin densities in Cu(II)-Cu(II) center indicates that there is no electron transfer between copper(II) and Ir(III).

Other α-C-H activation transition states with the carbonyl **O** group of the substrate coordinated to the Ir center were also located; they are shown in Figure 5.9. Transition state **T-TS3-8** shows a free energy barrier similar to that **T-TS3-7**. The inclusion of an extra water molecule in **T-TS3-8-H_2O** shows no positive effect in terms of lowering the barrier of the α-C-H bond activation process.

All the mechanism reported above start with involvement of the Ag species through removal of Cl ligands from Ir. For the sake of completion, we evaluated also mechanisms where the Ag species was not available. The α- and β-C-H bond activation routes catalyzed by the $[IrCp^*Cl_2]_2$ and $[Cu(OAc)_2 \cdot H_2O]_2$ without the of Ag are not favorable, they have high barriers as shown in Figure 5.10. This further confirms the importance of the $AgBF_4$ salt in this reaction, and agrees well with the experimental observation of a low yield in its absence (Figure 5.2).[207]

Summarizing the calculations reported in this section, we conclude that the reaction starts with the α-C-H bond activation leading to an Ir-enolate intermediate. We discard thus the experimentally proposed Ir-allyl species.

5.3.3 The activation of the second C-H bond and the regeneration of the catalyst

We continued our study with the search for the second C-H bond activation. The computed free energy profile is presented in Figure 5.11. Once the alkyl chain is metalated at the α position forming the Ir-enolate intermediate **T-I7**, the reaction continues through a ligand exchange. One of the acetates from the

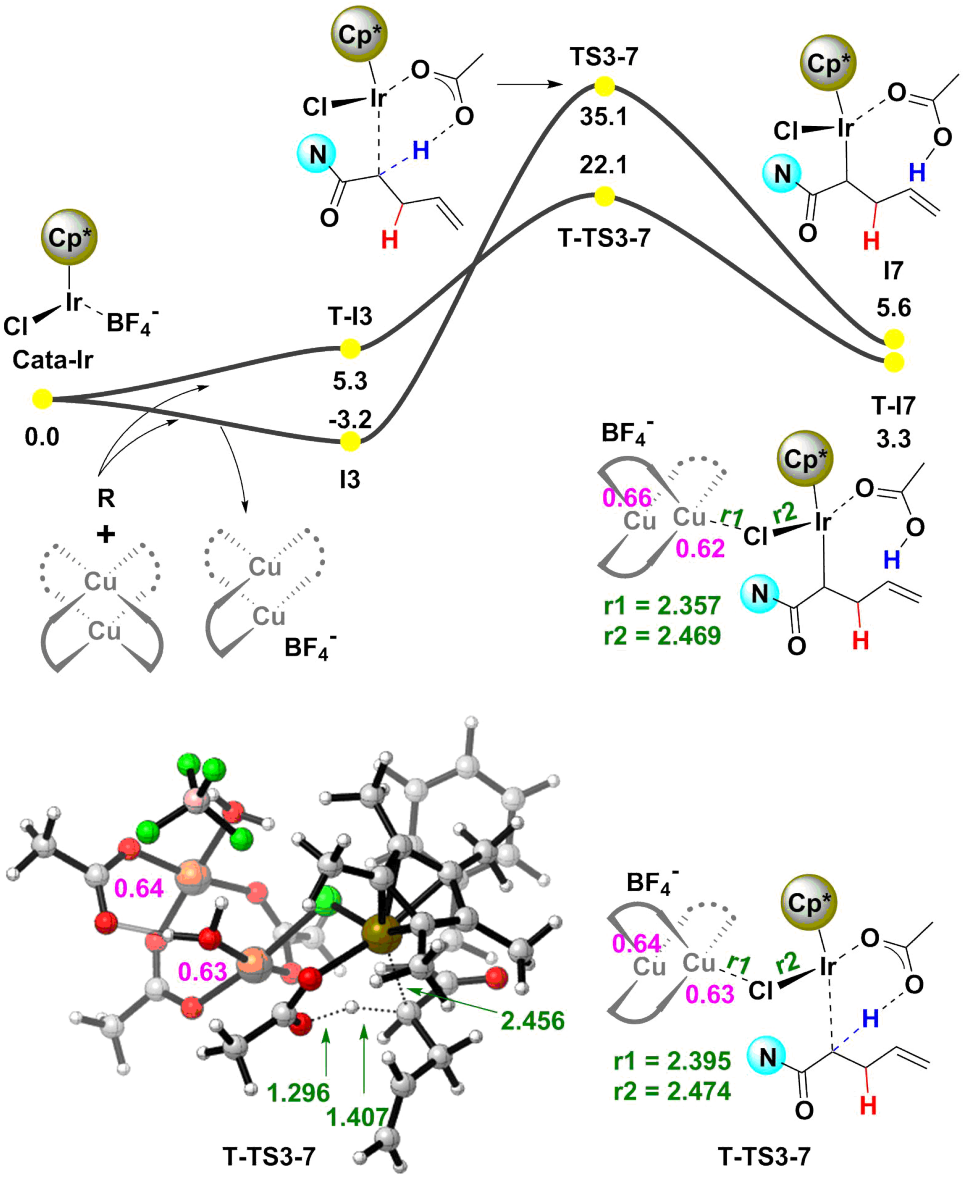

Fig. 5.8 Free-energy profiles (in kcal/mol) of the α-C-H bond activation routes. (Pink color: spin density; Green color: bond distance.)

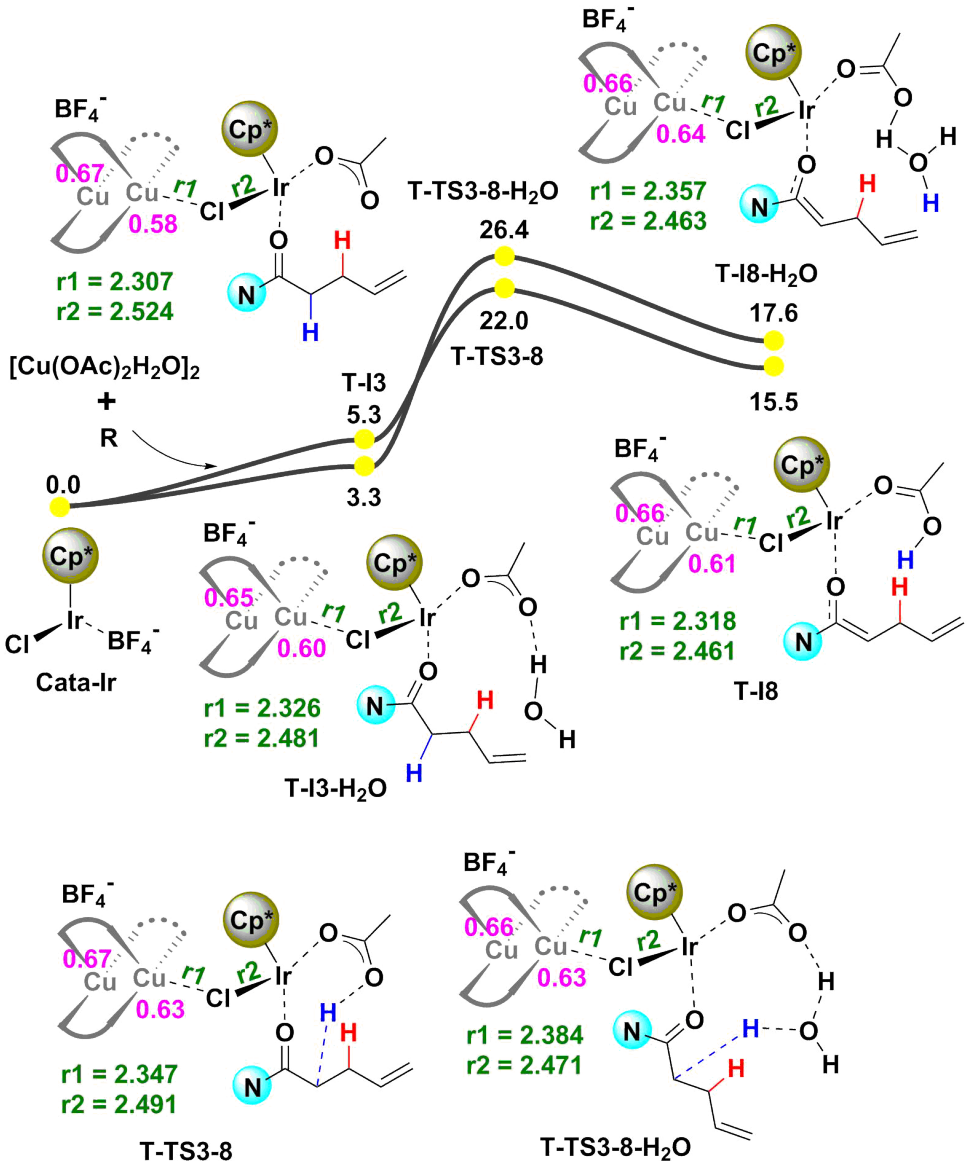

Fig. 5.9 Free-energy profiles (in kcal/mol) of the α-C-H bond activation routes involving coordination of the carbonylic **O** atom to Ir center. (Pink color: spin density; Green color: bond distance.)

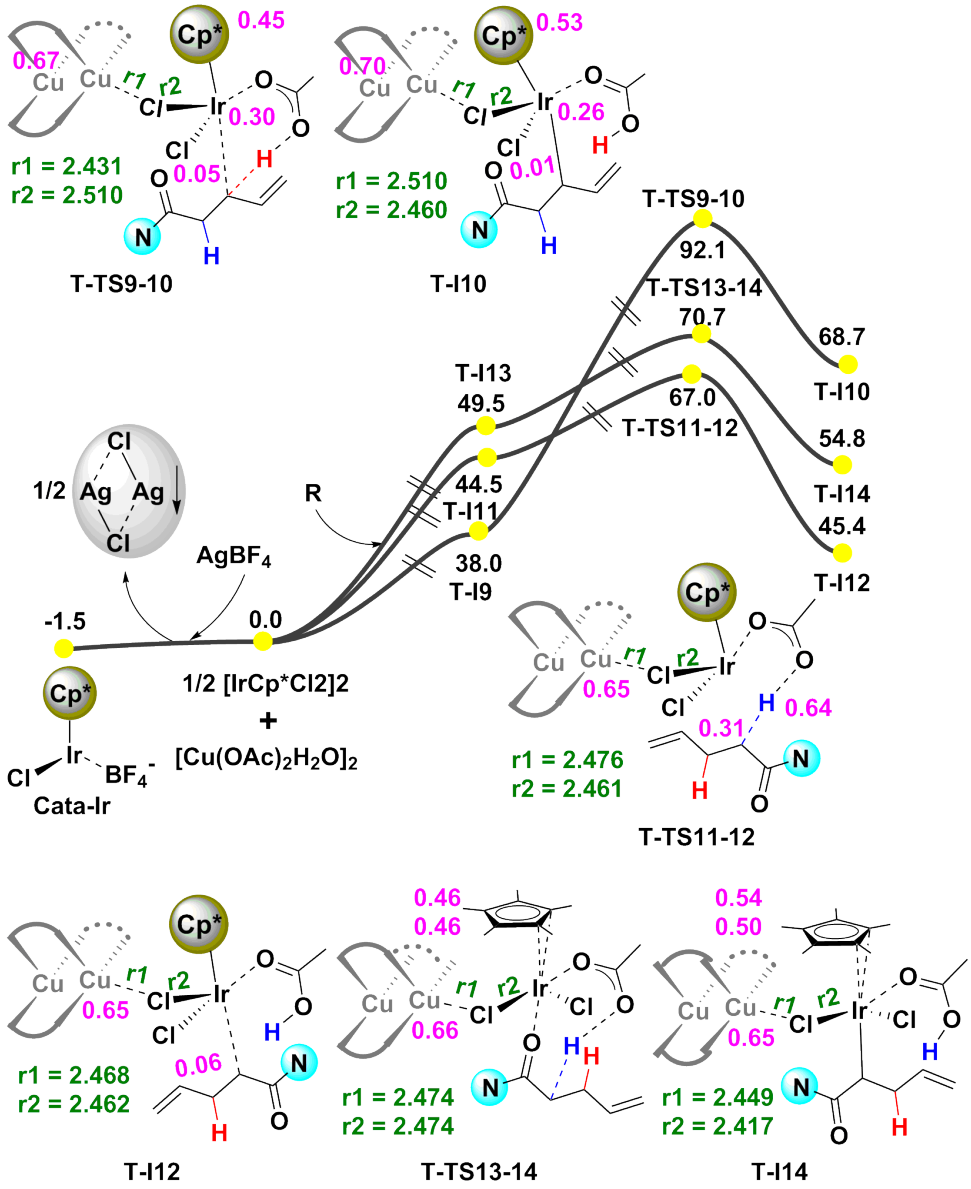

Fig. 5.10 Free-energy profiles (in kcal/mol) of the routes without Ag^+ abstracting the Cl^-.

copper dimer replaces the acetic acid resulting from the first CMD (Figure 5.8). The resulting intermediate **T-I15** undergoes activation of the β-C-H bond with a barrier of only 0.1 kcal/mol (**T-TS15-16**) respect to this intermediate **I15**. An Ir(III)-H-Cu(II)-Cu(II) intermediate **T-I16** is formed, with the α,β-dehydrogenated dienyl carbonyl product coordinated to the Ir(III) center. From this intermediate, the bridging acetate abstracts the hydride from the Ir-H bond through **T-TS16-17**, generating the reduced Cu(II)-Cu(II)-Ir(I) intermediate **T-I17**, where the spin density is still located on the Cu(II)-Cu(II) moiety. This spin location indicates that no electron transfer occurs between both metal fragments.

The lack of electron transfer between the iridium fragment and the di-copper unit means that the current mechanism differs sharply from the co-operative reductive elimination on Rh/Cu catalysis previously reported in our group.[208–210] In cooperative reductive elimination, Rh was partially reduced by one electron forming Rh(II), and the other electron went to the dicopper unit. Instead, in this dihydrogenation mechanism reported here, Ir accepts two electrons, forming the closed-shell Ir(I) intermediate. The two-electron transfer is consistent with the change in the Ir-Cl and Cu-Cl distances, which change from 2.457 Å to 2.502 Å and from 2.397 Å to 2.365 Å, respectively.

The continuation of the reaction is the regeneration of the catalyst from Ir(I) to Ir(III). This is accomplished from intermediate **T-I17**, which is in the triplet spin state, through a minimum energy crossing point (**MECP**). The free energy barrier of associated to this MECP is 2.6 kcal/mol. Again, the electron transfer can be followed by the displacement of the bridging Cl atom: the reduction of the copper dimer by two electron elongates the Cu-Cl bond (from 2.365 Å in **I17** to 3.679 Å in **S-I17**) while the oxidation of Ir center decreases the Ir-Cl bond distance from 2.502 Å to 2.391 Å. The electronic structure of the resulting intermediate **S-I17** consists on a cluster with Ir(III)-Cu(I)-Cu(I) oxidation steps. Finally, the $[Cu(OAc)_2 \cdot H_2O]_2$ co-catalyst is regenerated by

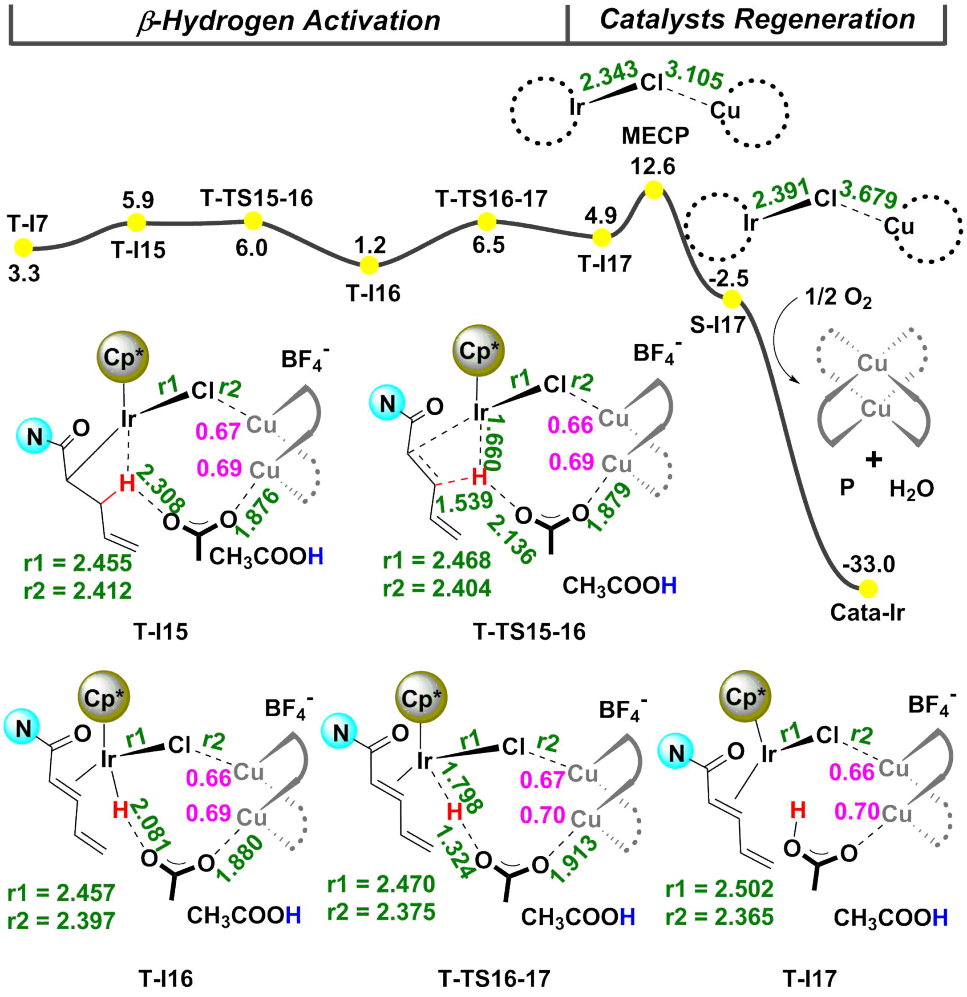

Fig. 5.11 Free-energy profiles (in kcal/mol) of the second C-H bond activation and catalyst regenaration.

Table 5.1 Comparison of the free energies of the triplet, open shell singlet and closed-shell singlet states.

	Triplet	Open-shell singlet	Closed-shell singlet
T-I3	5.3	5.0	48.1
T-TS3-7	22.1	22.8	81.8
T-I7	3.3	3.5	50.6
T-I15	5.9	6.4	\
T-TS15-16	6.0	6.7	\
T-I16	1.2	1.6	\
T-TS16-17	6.5	6.8	\
T-I17	4.9	4.9	\

consumption of O_2 with H_2O as the waste product. The overall process is exergonic by 33.0 kcal/mol. The consideration of open-shell singlet electronic states instead of closed-shell states brought only minor changes, as shown in Table 5.1

We were puzzled by the presence of the Ir(I) intermediate in the catalytic cycle, so we explored other alternative electron distributions for the key transition state in the second C-H bond activation. The results are summarized in Figure 5.12. Five different transition states were located in our calculations and these **TS**s cannot compete with the β-H elimination transition state **T-TS15-16** in Figure 5.11. All the spin density analysis of these five transition states shows that these **TS**s share a Cu(I-II)-Cu(I-II)-Ir(II) structure, which is similar to the previous reported Cu(I-II)-Cu(I-II)-Rh(II) species,[208–210], but different from the current Cu(II)-Cu(II)-Ir(I) structure **T-TS15-16**. The iridium center strongly disfavours the Ir(II) oxidation state. Further research will be necessary to see if this is an intrinsic feature or iridium or is related to the dehydrogenation process.

We can now present in Figure 5.13 the free energy profile for the full catalytic cycle. The reaction starts with the CMD type α-C-H activation with the participation of $[Cu(OAc)_2{\cdot}H_2O]_2$. An Ir-enolate intermediate is involved

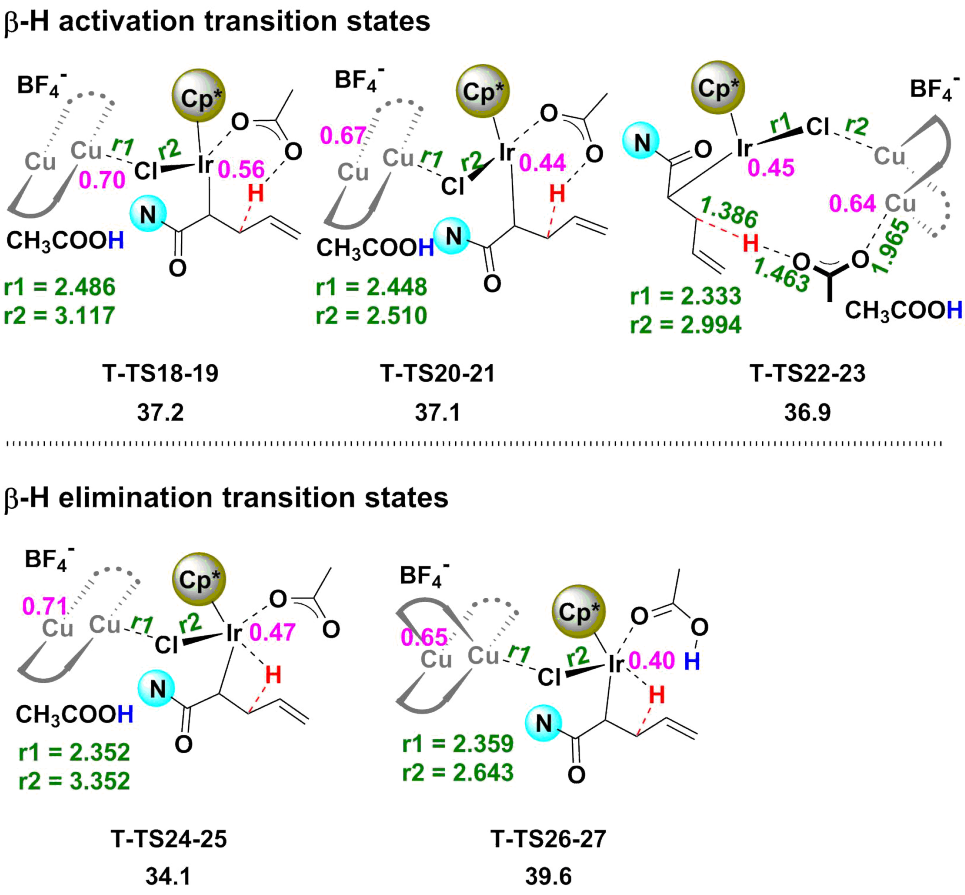

Fig. 5.12 Summary of the other possible transition states of the second C-H bond activation (Pink color: spin density; Green color: bond distance).

in the mechanism instead of the previously proposed Ir-allyl intermediate. After this, the β-H elimination occurs to give the α,β-dehydrogenated dienyl carbonyl product. The rate determining transition state is the α-C-H bond activation, where both the copper and iridium moieties play an important role in this process. The reaction does not operate through cooperative reductive elimination, as intermediates containing Ir(II) are not observed.

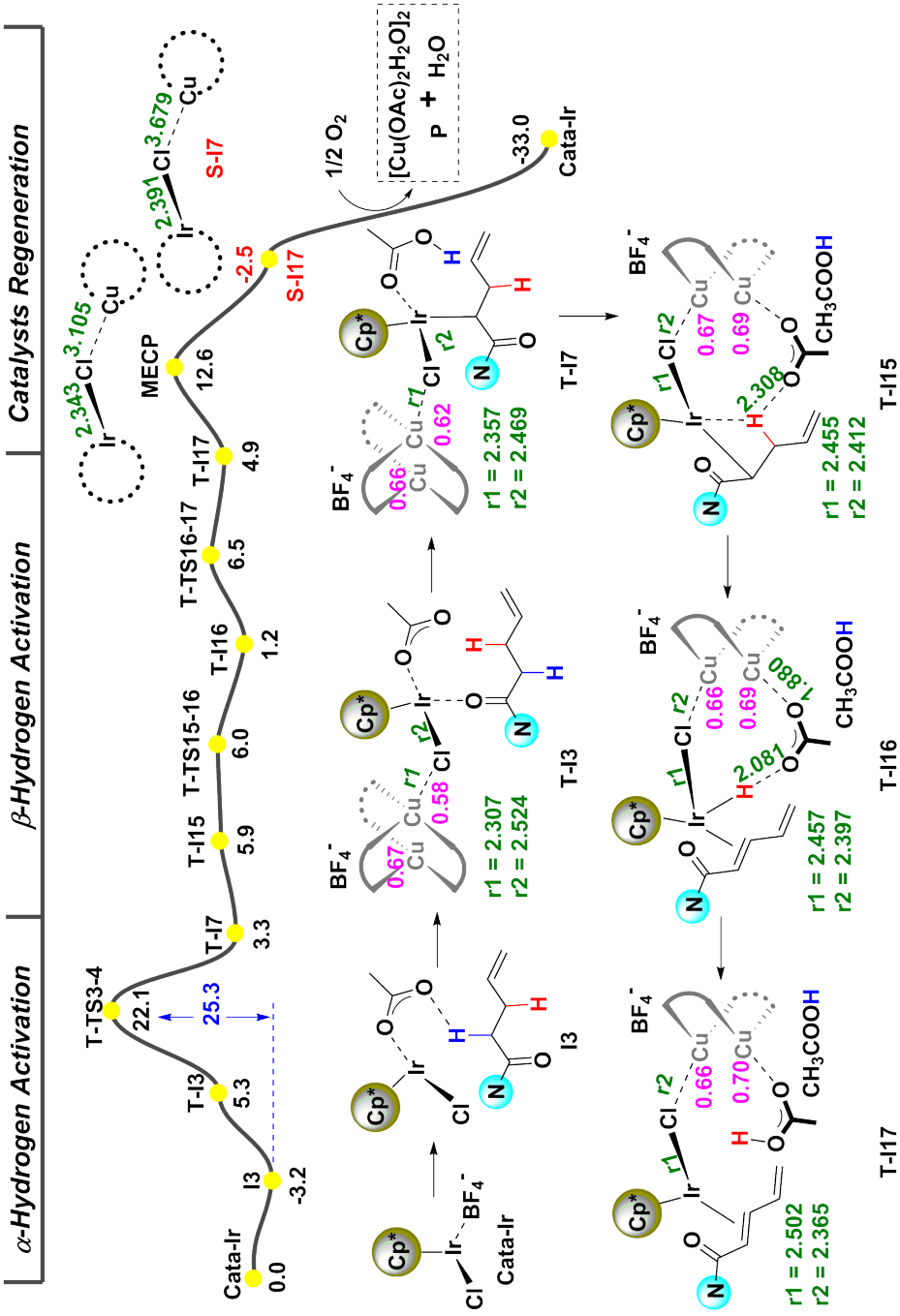

Fig. 5.13 Summary of the theoretically proposed mechanism.

5.3.4 The need for terminal alkenes

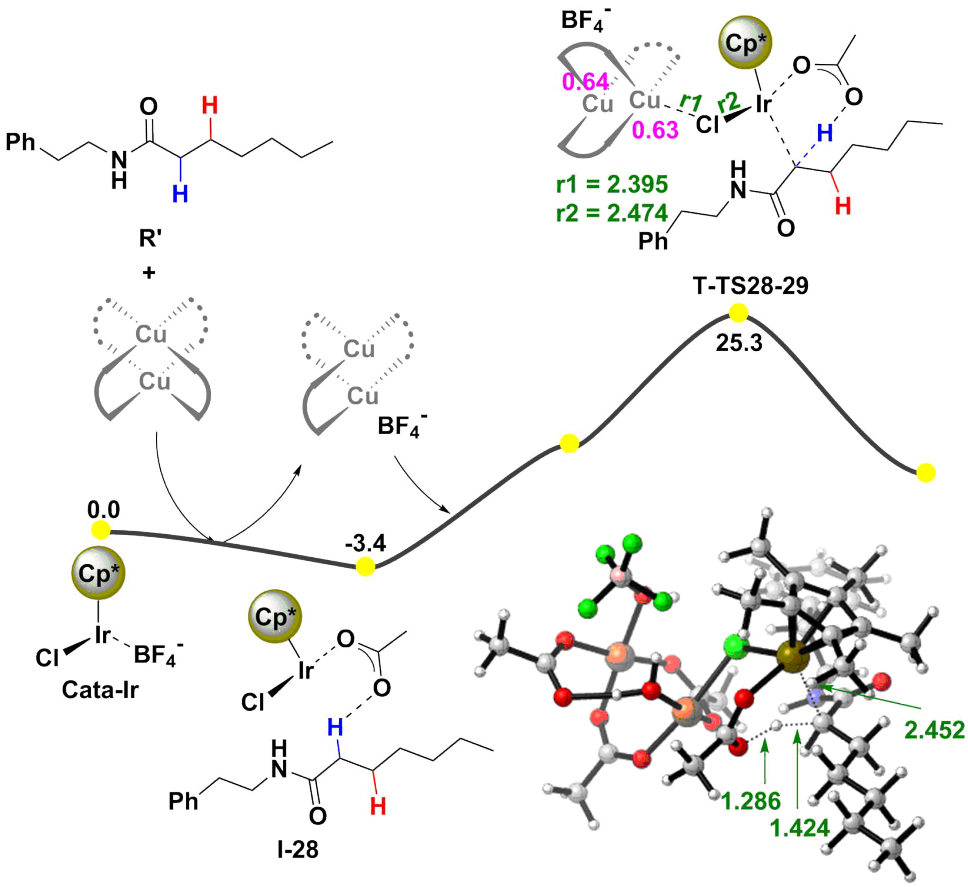

Fig. 5.14 Free-energy profiles (in kcal/mol) of the first C-H bond activation of substrates with an internal alkene.

Experimental studies indicate that a double bond must be in the terminal position for the reaction to be possible. Substrates containing long-chain amides do not react. We evaluated computationally the behavior of these systems. The α-C-H bond activation process of a saturated long-chain amide was studied at the same theoretical level, and the results are shown in Figure 5.14. A CMD transition state **T-TS28-29** with a free energy barrier of

28.7 kcal/mol could be located for the α-C-H bond activation. This is higher than for the substrate with terminal alkene, and the difference is sufficient to explain the lack of reaction.[207] The terminal C=C double bond makes the C-H bond more active for the formation of the conjugated products.

5.4 Concluding remarks

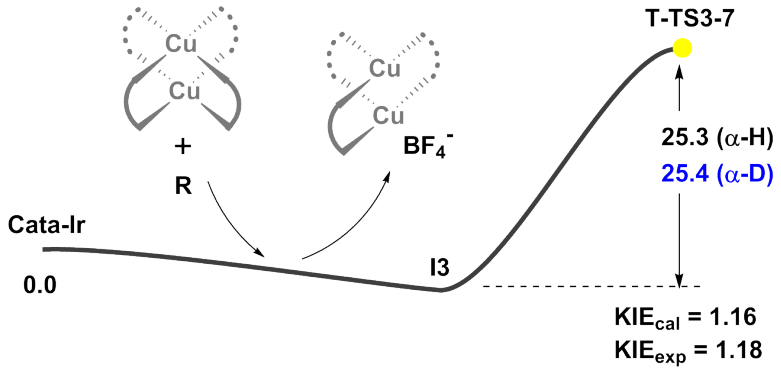

Fig. 5.15 The barrier of the a-deuterated amides used in the KIE calculation.

The mechanism of the Ir(III)/Cu(II) co-catalyzed dehydrogenation of amides has been elucidated by DFT computational means. The first C-H bond activated is in the α position. The reaction proceeds by cooperation between the main Ir(III) catalyst and the copper(II) acetate dimer leading to Ir-enolate intermediate. Then, the reaction continues through the β-H elimination to release the desired product. The computed mechanism confirms the need for the $AgBF_4$ and $[Cu(OAc)_2{\cdot}H_2O]_2$ species. The silver species activates the initial Ir(III) catalyst by Cl abstraction and the copper species cooperates in the C-H activation and is necessary for the regeneration of the iridium(III) catalyst.

The rate determining transition state is the α-C-H bond activation. We calculated a KIE value of 1.16 for the α-deuterated amides. This agrees well

with the experimental study measuring a KIE value of 1.18 for α-deuterated amides and a much smaller 1.04 value for β-deuterated amides.

Chapter 6

Synthesis of 1H-Indazoles through N-N bond formation

6.1 Background

Heterocycles, in particularly the nitrogen-containing heterocycles, are some of the most ubiquitous and important structural motifs with remarkable application in natural product research, pharmaceutials, and material sciences.[48, 214] Drived by these exceptional properties, the synthesis of nitrogen heterocycles has attracted tremendous attention, thus motivated the chemists to develop safe, convenient, and efficient synthetic strategies.[214, 215] With the rapid and significant development of transition metal-catalyzed C-H bond activation in organic synthesis, direct catalytic nitrogenation of ubiquitous and fundamental C-H bonds into valuable C-N bonds, have appeared as one of the most efficient and powerful procedures for the construction of N-containing heterocycles and other useful scaffolds.[48, 214, 216–221] Hence, extensive efforts have been devoted to developing new synthetic methods for this C-H bond cleavage and C-N bond formation transformation.[214, 222]

The nitrogen-nitrogen (N-N) containing heterocyclic compounds, such as the indazoles, are widely appeared in the drugs and drug candidates due to

the pronounced biological and pharmacological activities. These broad applications have prompted organic chemists to construct the structurally novel and biologically active N-N bond containing indazole frameworks from easily obtained starting materials under milder conditions.[223–230] Most of the approaches, both the transition metal-free and the newly developed transition metal catalyzed processes as summarized in Figure 6.1, take the advantage of the N-N bonds already inside the starting materials. For example, Pd-catalyzed C-H functionalization of tosylhydrazones was reported by Inamoto and Hiroya, which delivered the 3-substituted indazoles by the intramolecular amination.[231] Other methodology starting with hydrazones by using Fe-, Cu-catalysts were also explored by Bao,[232] Jiang,[233] Yamamoto[234], Larock[235], Kim[229, 236], You [237], Wang [238], Ellman [219, 239] and their coworkers. However, these strategies usually suffered from the harsh reaction conditions and expensive, limited or carcinogenic starting materials, such as organo-hydrazines (Figure 6.1 a), hydrazones(Figure 6.1 b), or diazos(Figure 6.1 c).[215, 240–245]

The alternative way to construct the indazole is by the N-N coupling (Figure 6.1 d) or ring transformation process(Figure 6.1 e). These processes have a lot of limitations including the synthetic efficiency and substrate scope, which limits their wide application.[243, 246–250] Therefor, other methods for the direct N-N bond formation processes are highly desired. In recent years, other alternative nitrogen sources, such as azides, nitrosobenzenes, have emerged in the transition-metal-catalyzed direct amination/amidation of aromatic C-H bonds as shown in Figure 6.1 f.[224, 251–255] Take some examples shown in Figure 6.2, Glorius and coworkers reported oxidative synthesis of 1H-indazole through C-H amidation and N-N bond formation with azides as amino sources by a Rh(III)/Cu(II)-cocatalyst system in 2013.[256] Subsequently, similar strategy using azides as amino sources under oxidant-free conditions has also been disclosed by the group of Zhu.[222] In 2016, several works by using nitrosobenzenes or anthranil reagent as convenient aminating reagent

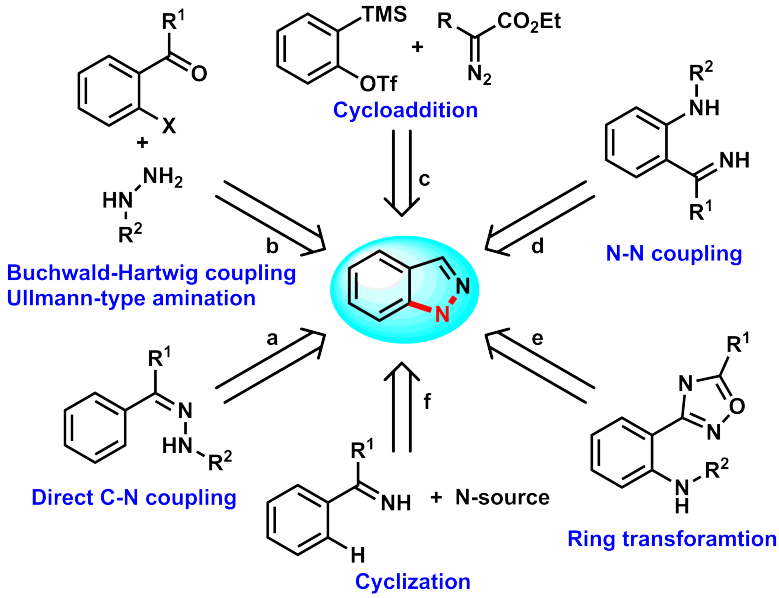

Fig. 6.1 The reported strategies for the synthesis of 1H-indazoles.

under synergistic Rh(III)/Cu(II) or Co(III)/Cu(II)-cocatalyst are reported by Li and workers.[221, 245, 257] Amines were also used as N-sources for the copper catalyzed sequential Ullmann-type process to construct N-N bond of indazoles by Jiang and workers.[244] Most recently, rhodium(III)-catalyzed intermolecular C-H amination of ketoxime and iodobenzene diacetate-enabled N-N bond formation by using sulfonamide as the nitrogen source has been developed.[258]

Despite the big success achieved to construct indazoles by the N-N bond formation strategies, challenges still remain.[214] On the one hand, the development of new catalytic strategies with increased efficiency under mild conditions are still highly desired; On the other hand, mechanistic understanding of the reported reactions are still superficial and on its early stage. We believe that the better understanding of the mechanism would provide more inspirations for the further development of this field. So in this project, we choose one of the pioneering work by Glorius and coworkers,[256] the

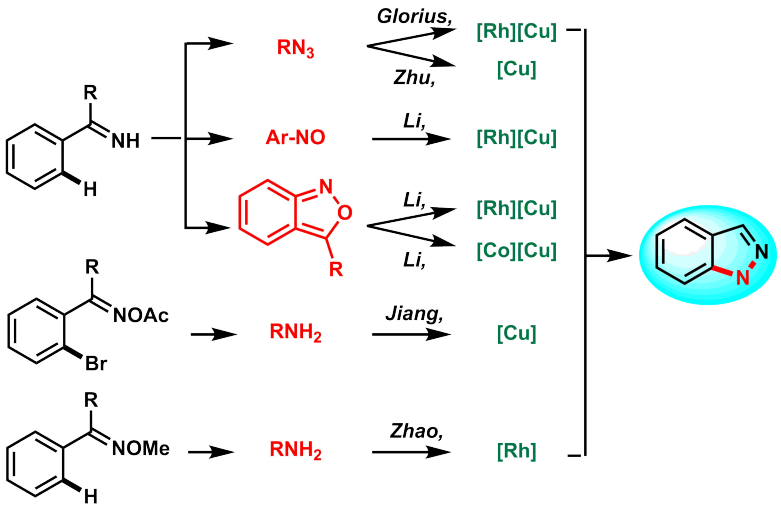

Fig. 6.2 Selected examples for the synthesis of indazoles through the N-N bond formation with different amino source.

oxidative synthesis of 1H-indazole through C-H amidation and N-N bond formation with azides as amino sources by a Rh(III)/Cu(II)-cocatalyst system, to conduct a comprehensive study on the mechanism of this kind reaction. As shown in Figure 6.3, this reaction uses the readily available substrates to construct the indazoles. O_2 is used as the terminal oxidant while leaving N_2 and H_2O as the byproducts. Only a trace amount of product was detected in the absence of either Rh(III) or Cu(II), indicating that both the two catalyst are quite important for this reaction. We are particularly interested in two aspects of this reaction from our DFT calculations: (1) the mechanism, especially the mechanism of N-N formation process; (2) the cooperative role of the Rh(III) and Cu(II) in the catalysis system.

6.2 Computational details

The ωB97X-D [87] functional was used to optimize all the structures of the reactants, products, intermediates and transition states at T = 298.15 K

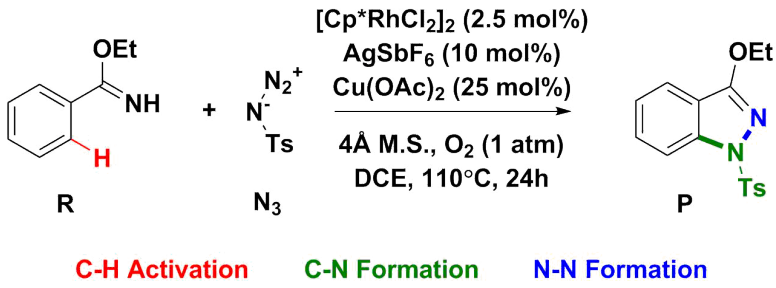

Fig. 6.3 Synthesis of indazole through N-N bond formation with zaide as amino source.

and 1 atm pressure by Gaussian 09 program.[88] All the optimizations were carried out in solvent by using the continuum model SMD with dichloroethane solution. The effective core potentials (ECPs) of Hay and Wadt with a double-ζ valance basis set (LANL2DZ) were used for Rh, Cu, and Sb atoms,[211] and polarization functions were also added for Rh (f = 0.350), Cu (f = 3.525) and Sb (f = 0.218),[93] whereas the all-electron basis set 6-31G(d) was used in describing all other atoms.[94] The Gibbs free energies in solvent were refined by carrying out single point calculations with larger basis set: LANL2DZ on Rh, Cu, and Sb, and 6-311++g(d,p) on other atoms.[95–97] All the intermediates (no imaginary frequency) and transition state structures (only one imaginary frequency) were confirmed by the harmonic vibrational frequencies and the number of imaginary frequency. The intrinsic reaction coordinate (IRC) calculations were used to confirm the transition states and the connected intermediates, reactants, or products. Free energy corrections were considered at a concentration of 1 M and a temperature of 298.15 K. All the 3D molecular structures of the species were drawn by using the CYLview program.

6.3 Results and discussion

In this work, arylimidate **R** is chosen as the reactant in Figure 6.3, which undergoes the C-H bond activation, C-N and N-N bond formation to give the desired 1H-indazole. Cationic Rh(III) species Cp*Rh(III)$(SbF_6)_2$ (name as **Cata-Rh**) is believed to be generated with the trap of chloride atoms by silver upon the mix of reactants, $AgSbF_6$ and catalysis precursor $[Cp^*RhCl_2]_2$. The **Cata-Rh** is used as the starting point, following the C-H bond activation, C-N and N-N bond formation processes to deliver the product **P**. The Gibbs free energies in solvent are used here for all the following discussions.

6.3.1 The C-H activation

We commence out theoretical investigation with the C-H bond activation process. As shown in Figure 6.4, the reaction is initiated by the rapid ligand exchange between the $[Cu(OAc)_2]_2$ and **Cata-Rh** together with the coordinate of reactant **R** to the Rh(III) center to generate the first intermediate **I1**. This process is calculated to be slightly endothermic with the energy of 2.0 kcal/mol higher than the starting point. In this process, one of the acetate ligand moves from the Cu(II) center to the Rh(III) center, which will participate in the *ortho* C-H bond activation process by the concerted metallation deprotonation (CMD) transition state **TS1-2** to afford the five-membered rhodacyclic complex **I2**. The further release of acetic acid gives the more stable rhodacyclic species **I3**, which is exothermic of 1.8 kcal/mol when compared with the starting point **Cata-Rh**.

Considering the role of Cu(II) in the C-H bond activation of our previous studies in the last chapter and the possibility of the acetate ligand works as the bridging ligand between the Cu(II) and the Rh(III), we decided to examine the possibility of involving the Cu(II) species in the C-H bond activation process. The calculated results are shown in Figure 6.4. Similar to the previous study, $[Cu(OAc)_2]_2$ is believed to be in its triplet dimeric state

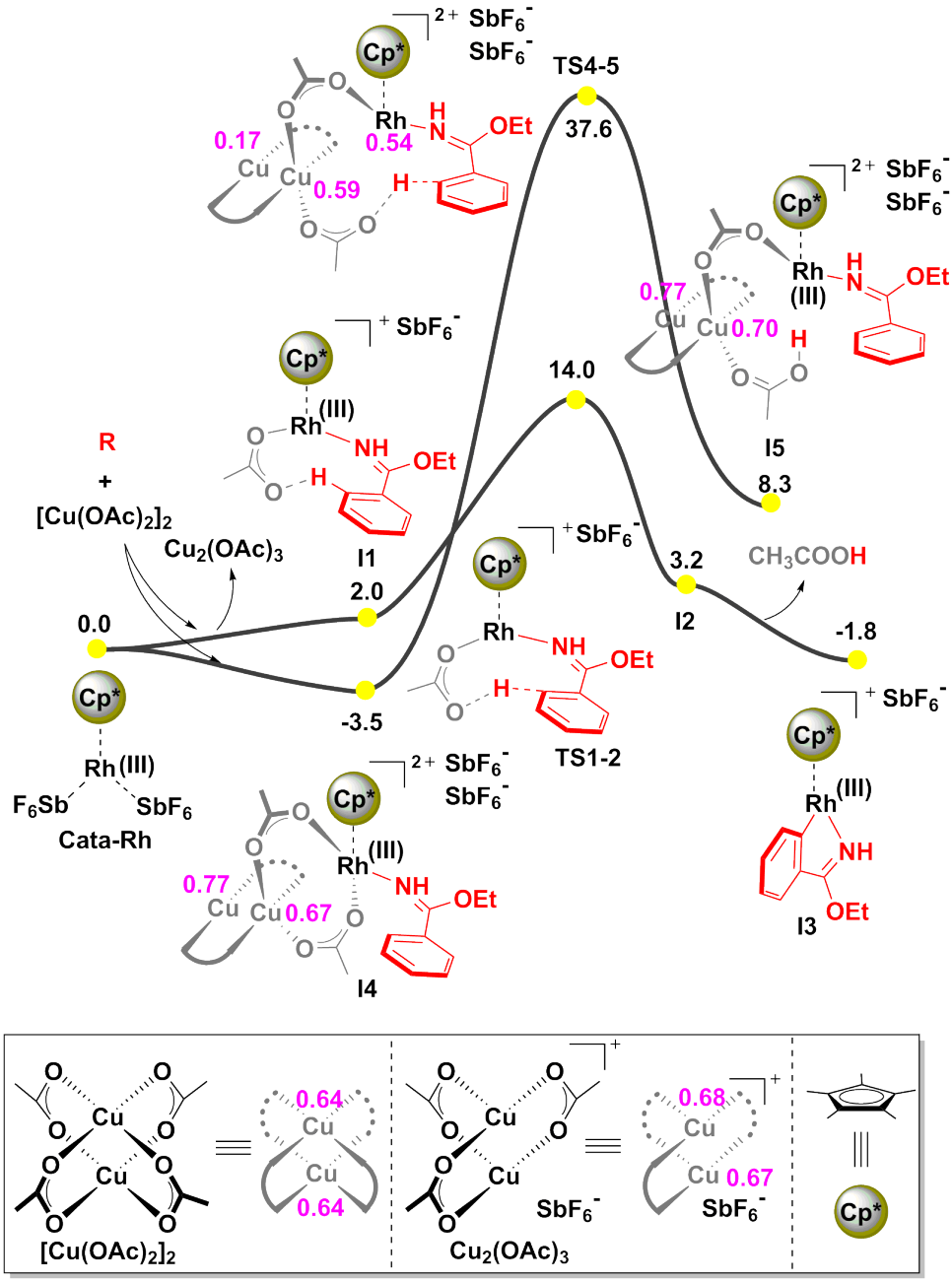

Fig. 6.4 DFT calculated potential energy surface of the C-H bond activation process with or without the help of Cu(II).

instead of the monometallic state.[208–210, 212, 213] The stable intermediate **I4** is therefore formed by using two of the acetates work as the bridging ligands between Cu(II) and Rh(III), which is 3.5 kcal/mol more stable than the reactants. One of the bridging acetate ligands will then participate in the deprotonation process of the CMD transition state **TS4-5**. However, a free energy barrier as high as 40.1 kcal/mol is needed for this C-H bond activation process, which is obviously different from our previous study and unfavorable for the current experimental conditions.[257] As a result, the C-H bond activation process for this reaction should work through a CMD process via **TS1-2** and the free energy barrier is estimated to be 17.5 kcal/mol.

6.3.2 The C-N bond formation

With the intermediate **I3** that produced through the C-H bond activation process in hand, we now start to search for the routes that corresponding to the C-N bond formation. An adduct **I6** in Figure 6.5 by the coordination of azide to the Rh(III) center is formed, which would release the N_2 passing through a transition state **TS6-7** with two electrons transferring from the Rh(III) center to the azide. A stable cycle Rh(V)-nitrenoid intermediate **I8** is generated with the free energy of -15.8 kcal/mol lower than the reactant. The calculated N-N bond length of the azide moiety in **I6** is 1.251 Å, which will elongate to 1.687 Å in the transition state **TS6-7**, and further be broken in the intermediate **I7** (N-N: 3.203 Å). This bond elongation process also suggested the exist of π-back-donation from the Rh center to an anti-bonding orbital of azide.[259–261] The Rh(V)-nitrogen bonds in **I7** and **I8** are calculated to be 1.830 Å and 1.838 Å, which are consistent with the double bond feature, confirming the oxidation process of the metal center from Rh(III) in **I6** to Rh(V) in **I7** and **I8**. The kinetic barrier for this process is 26.9 kcal/mol, higher than the previous C-H bond formation process. Other possible routes with the release of N_2 are also considered in our study and all the transition

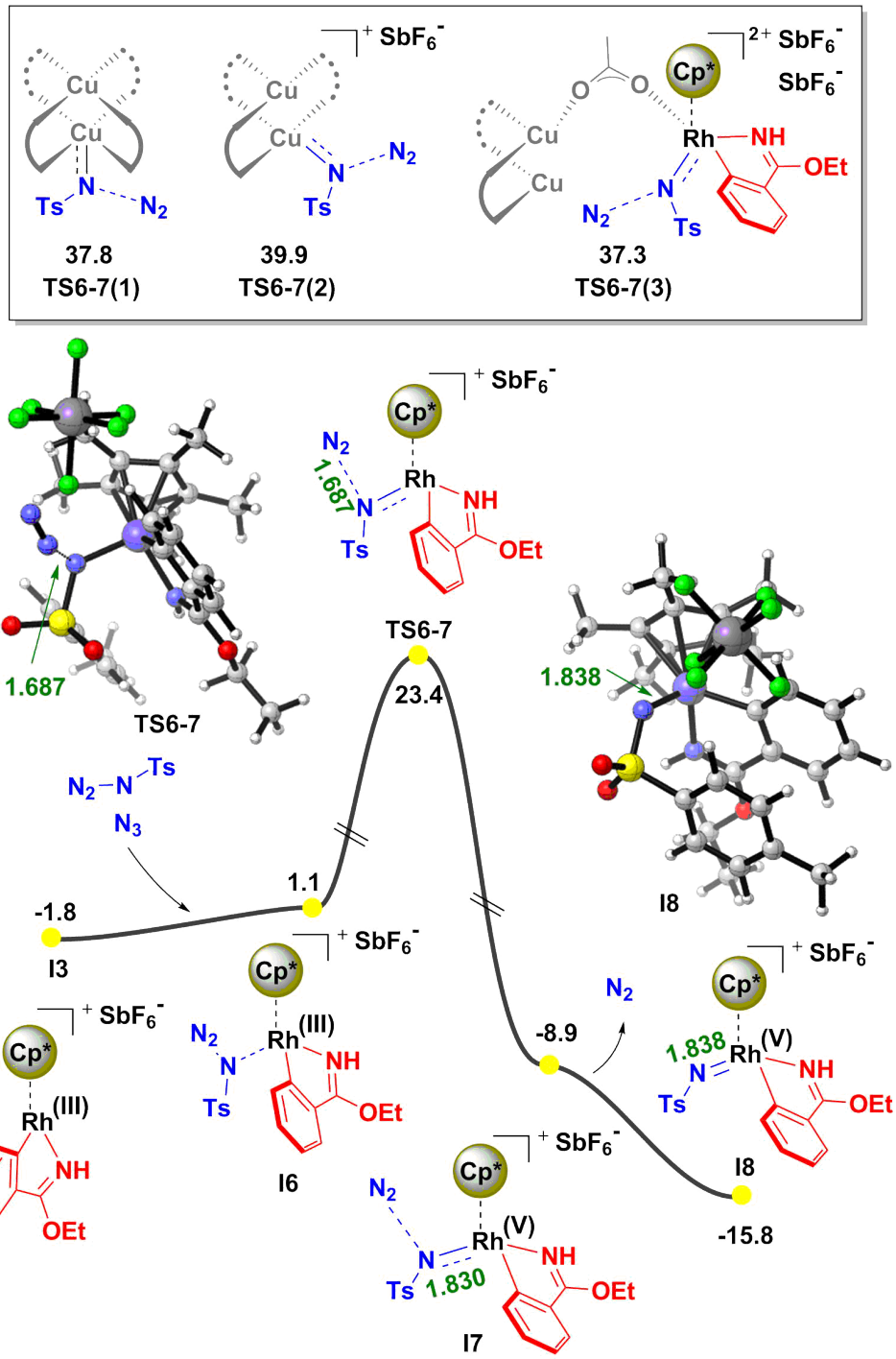

Fig. 6.5 DFT calculated potential energy surface for the formation of Rh(V)-nitrenoid.

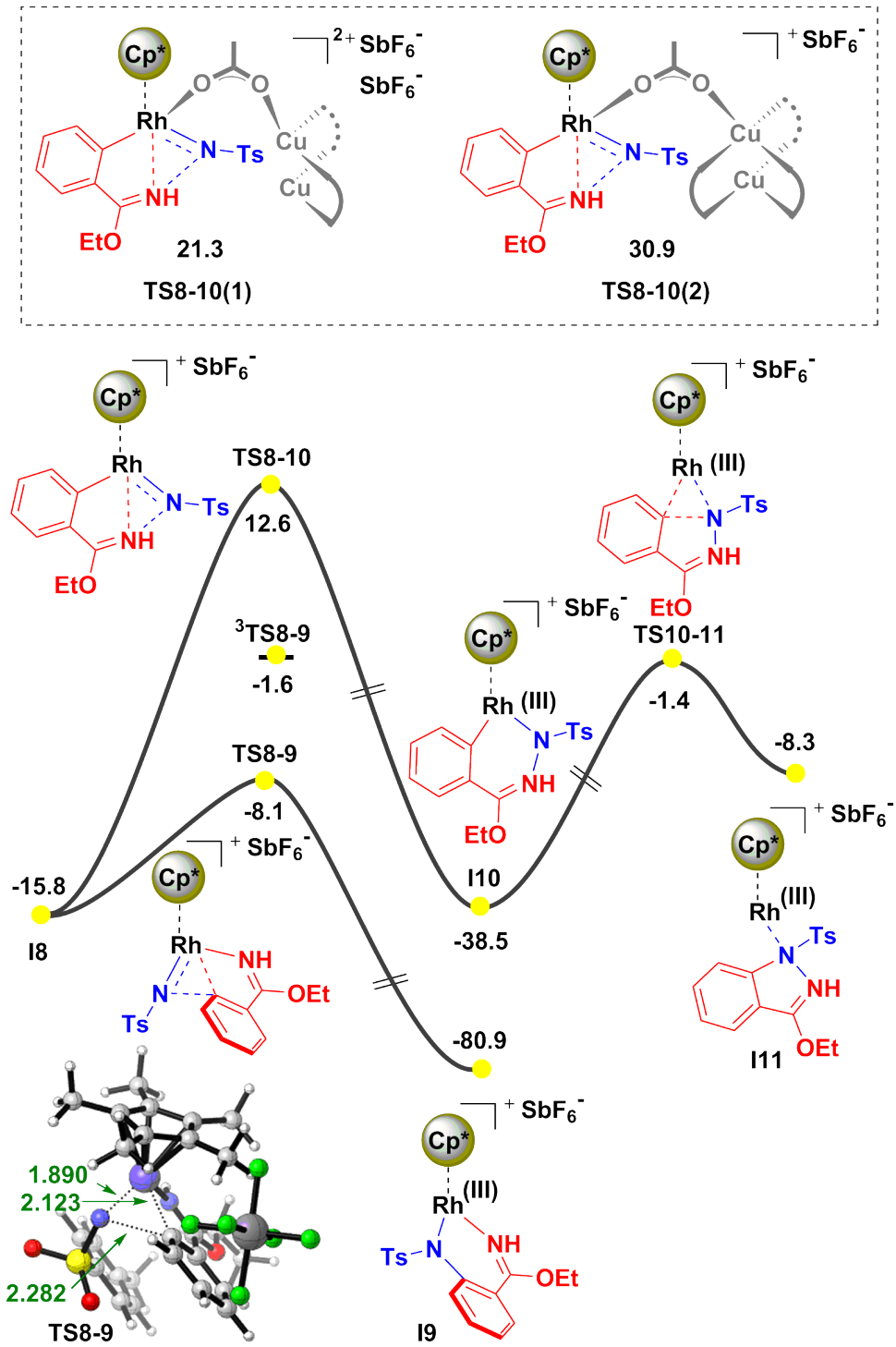

Fig. 6.6 DFT calculated potential energy surface of the C-N bond formation process.

states **TS6-7(1)**, **TS6-7(2)**, and **TS6-7(3)** possess high barriers about 40.0 kcal/mol, which obviously cannot compete with **TS6-7**.

I8 is confirmed to be in the closed-shell singlet state, by the migratory insertion process via a three-centered transition state **TS8-9** in Figure 6.6, the six-membered Rh(III)-amido species **I9** is generated. This is a super fast process with a shallow barrier of 7.7 kcal/mol, confirming that once the Rh-nitrene complex is formed the reaction would proceed smoothly for the migratory insertion and this process is exothermic about 80.0 kcal/mol. The triplet version of this nitrene insertion process is also considered (^{3}**TS8-9**) and the barrier is 6.5 kcal/mol higher than the closed-shell singlet transition state **TS8-9**. This agrees well with the closed-shell singlet state features of the metal-nitrene of the previous studies.[261–263, 167, 264, 265] In addition, the possibility of the concerted loss of N_2 and C-N bond formation similar to the previous proposed mechanism is also considered, unfortunately, all the optimization lead to the step-wise transition state **TS6-7**.[266]

We also calculated the route related to the insertion of nitrene to the Rh-N bond and the results are shown in Figure 6.6. The barriers for these three-centered N-N bond formation transition states **TS8-10**, **TS8-10(1)**, and **TS8-10(2)** are much higher than that of the C-N bond formation transition state **TS8-9**. Therefore, the routes following the N-N bond formation will not be further considered.

6.3.3 The N-N bond formation from Rh-center

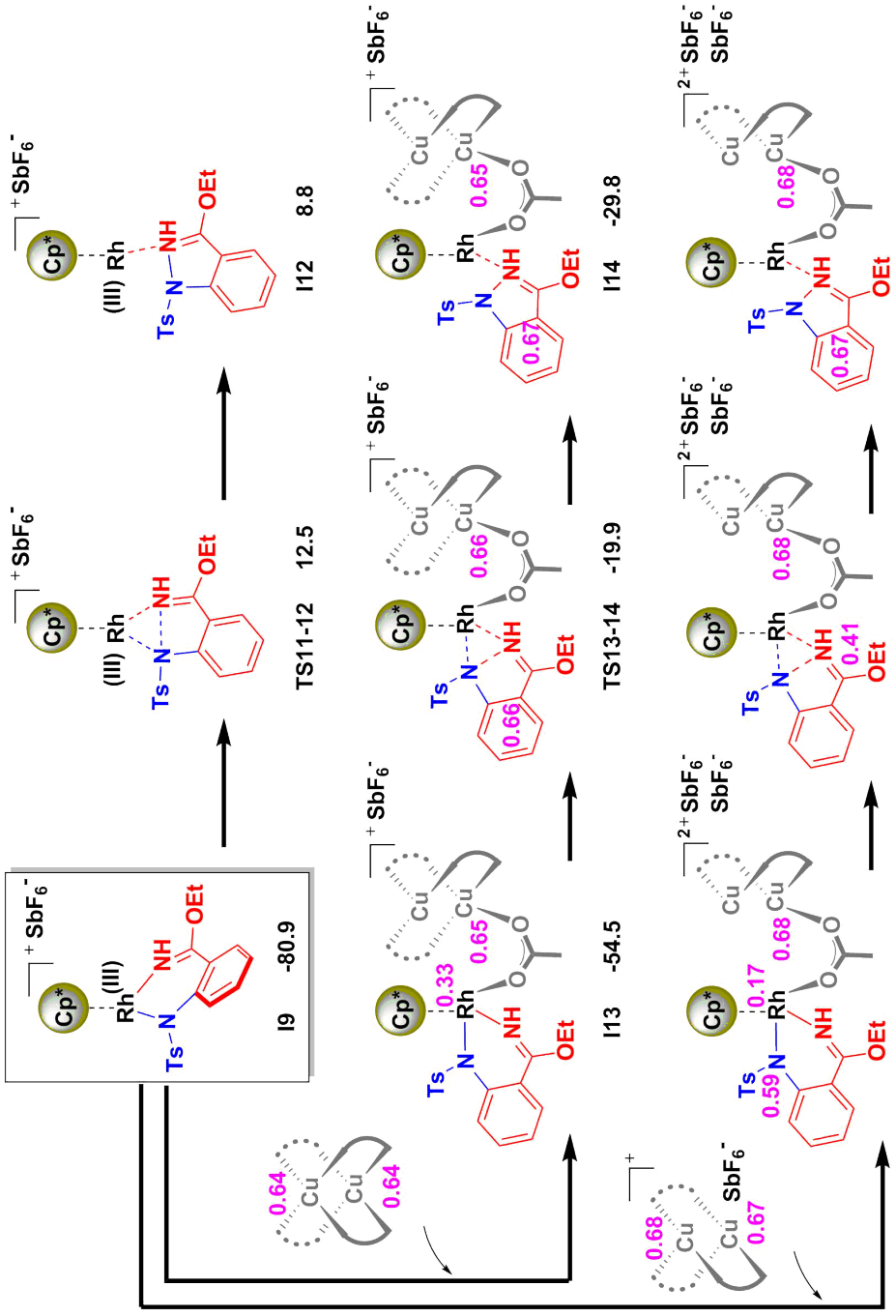

Fig. 6.7 DFT calculated mechanism for the reductive N-N bond formation from the Rh(III) center.

From the previous section, it have been confirmed that the C-H activation and C-N bond formation processes should occur successively at the beginning of this reaction to give the six-membered Rh(III)-amido species **I9**. Now we focus on the last N-N bond formation process. We firstly examined the N-N bond formation through the reductive elimination process from the Rh(III) center. Transition state **TS11-12** is located with the free energy barrier more than 90 kcal/mol shown in Figure 6.7. Further more, Cu(II) species are also introduced to the reductive elimination transition states as shown in **TS13-14** and **TS15-16**. The interactions between Rh(III) and Cu(II) bridged by the acetate ligand do help to decrease the reaction barriers with different extent. Unfortunately, all the barriers are still too much high under the current experimental conditions.[256]

Other possible routes by the deprotonation and reductive elimination process are shown in Figure 6.8. From **I9**, one of the acetate ligand could help the deprotonation process via a transition state **TS17-18** to yield the Rh(III) intermediate **I19**, which could go through a reductive elimination transition state **TS19-20** to deliver the desired indazole product. However, these deprotonation and reductive elimination processes possess very high barriers. Again, the interaction between Rh(III) and Cu(II) via the bridging acetate ligand helps to decrease the reductive elimination barrier (see **TS21-22**), but not enough.

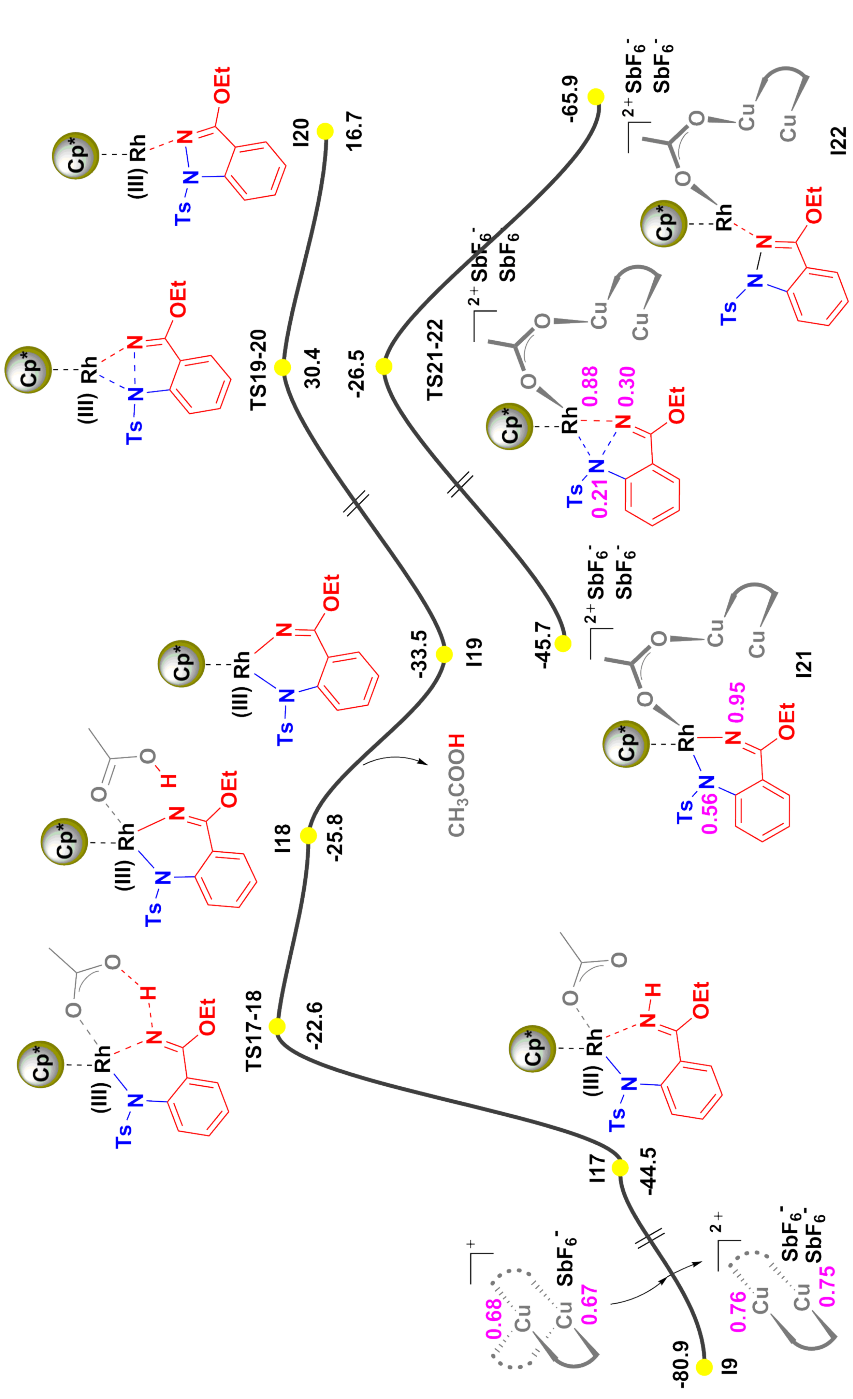

Fig. 6.8 DFT calculated mechanism for the deprotonation and reductive N-N bond formation from the Rh(III) center.

At last, the possible single electron transfer process between Rh(III) and Cu(II) is also taken into account in our calculations, which gives an Rh(IV) intermediate **I24**. The reductive elimination from Rh(IV) drive the reaction to a Rh(II) species **I25**. Unfortunately, this Rh(II) intermediate is quite unstable, which is in the energy level of 33.7 kcal/mol higher than **I9**, indicating that the Rh(IV)-Rh(II) pathway by the intermolecular single electron transfer is impossible for this reaction.

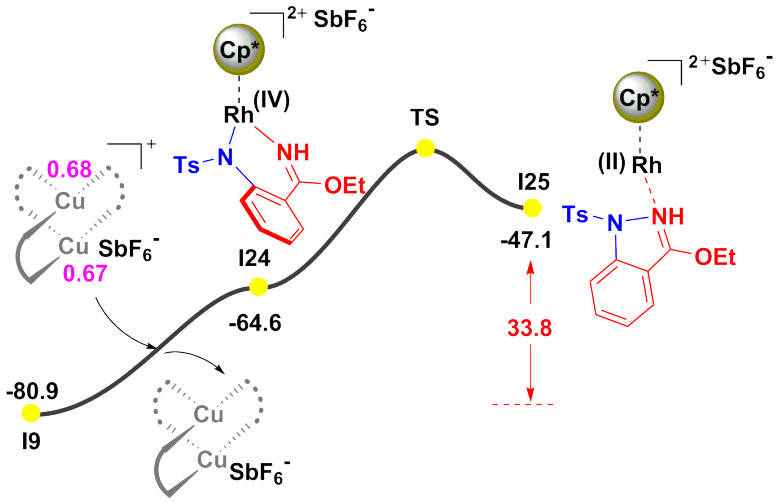

Fig. 6.9 DFT calculated mechanism for the reductive N-N bond formation from the Rh(IV) center.

6.3.4 The N-N bond formation from Cu-center

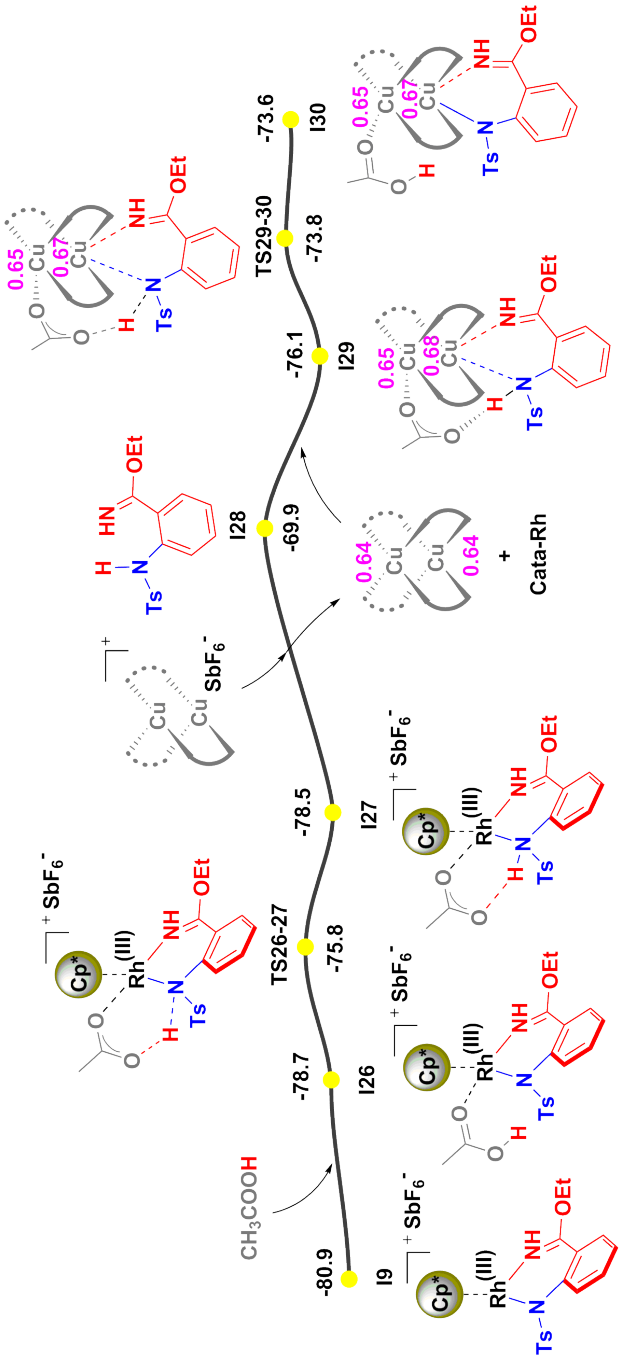

Fig. 6.10 The calculated mechanism of transfer N,N moiety from the Rh to Cu center.

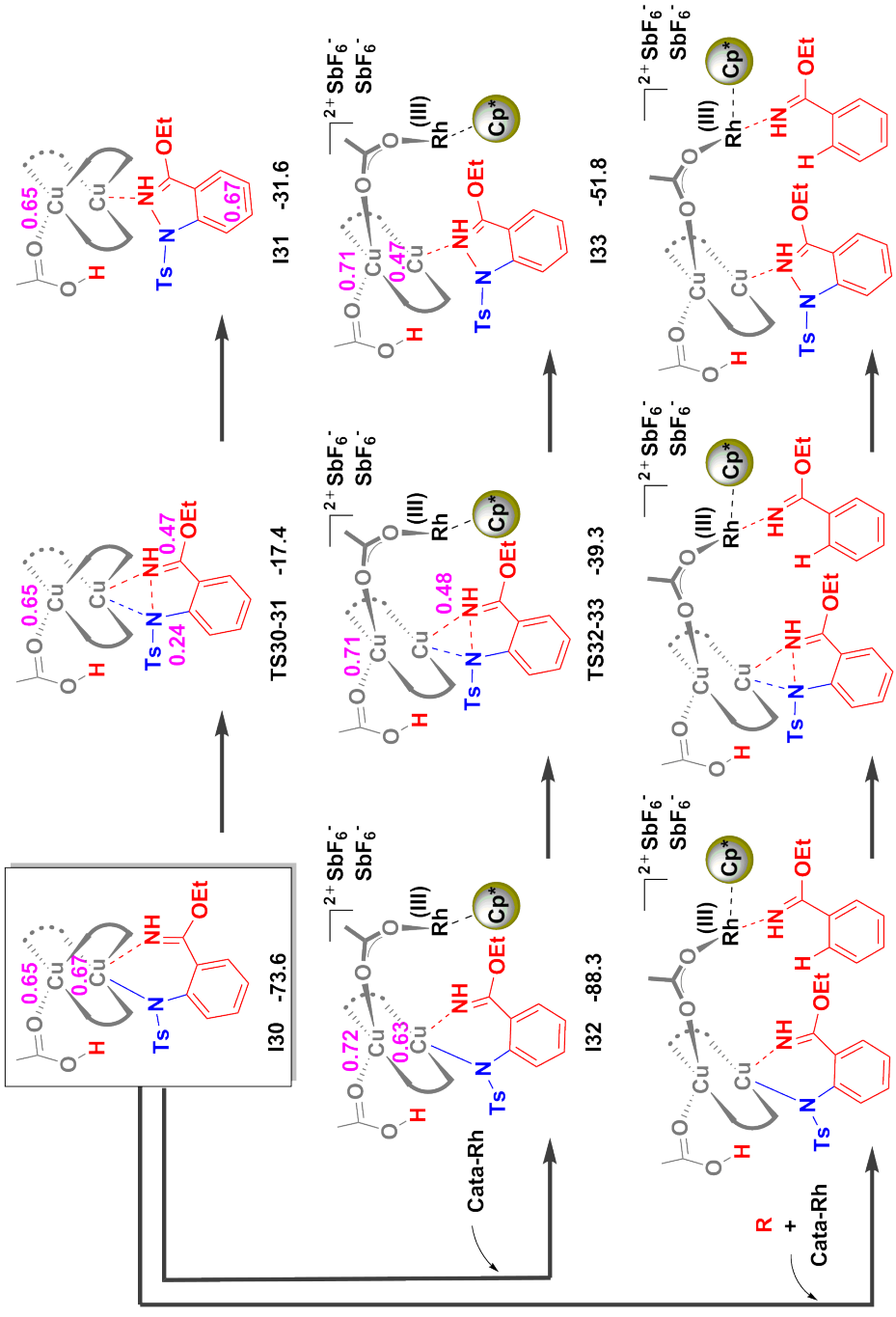

Fig. 6.11 DFT calculated mechanism for the reductive N-N bond formation from the Cu center.

Until now, from our DFT calculations, all the possibilities for N-N bond formation routes from the Rh(III) or Rh(IV) have been examined and confirmed to be unfavorable under the reported experimental conditions. This forces us to consider other N-N bond formation routes. As proposed by the experimental study, the N-N bond formation could happen through the reductive elimination from Cu center. Before the N-N bond formation, the transfer of N,N moiety from the Rh center to Cu is studied in Figure 6.10. **I9** may undergo the protonation process via transition state **TS26-27** to release the amidated **I28**, and regenerate the active Rh(III) catalyst **Cata-Rh**. **I28** will coordinate to the Cu center followed with the rapid deprotonation **TS29-30** to form the intermediate **I30**. The whole process goes smoothly and slightly endothermic about 7.0 kcal/mol from **I9** to **I30**.

From **I30**, different routes for the reductive elimination process are studied by DFT calculations. We will discuss these possibilities one by one in this section. Similar to the reductive elimination from Rh center, the direct reductive elimination from the Cu(II) center of **I30** is firstly calculated as in Figure 6.11. However, reaction needs to overcome a barrier more than 60.0 kcal/mol(compared with **I9**) through **TS30-31**, which is unfavorable for this reaction. In addition, the interactions between Rh and Cu center are also taken into account in our studies, and the barriers of the computationally located transition states **TS32-33** and **TS34-35** are both lower than that of **TS30-31**, indicating that the bridging interactions have a positive effect on the reaction. However, all these transition states still have high barriers and that should be ruled out from the current reaction.

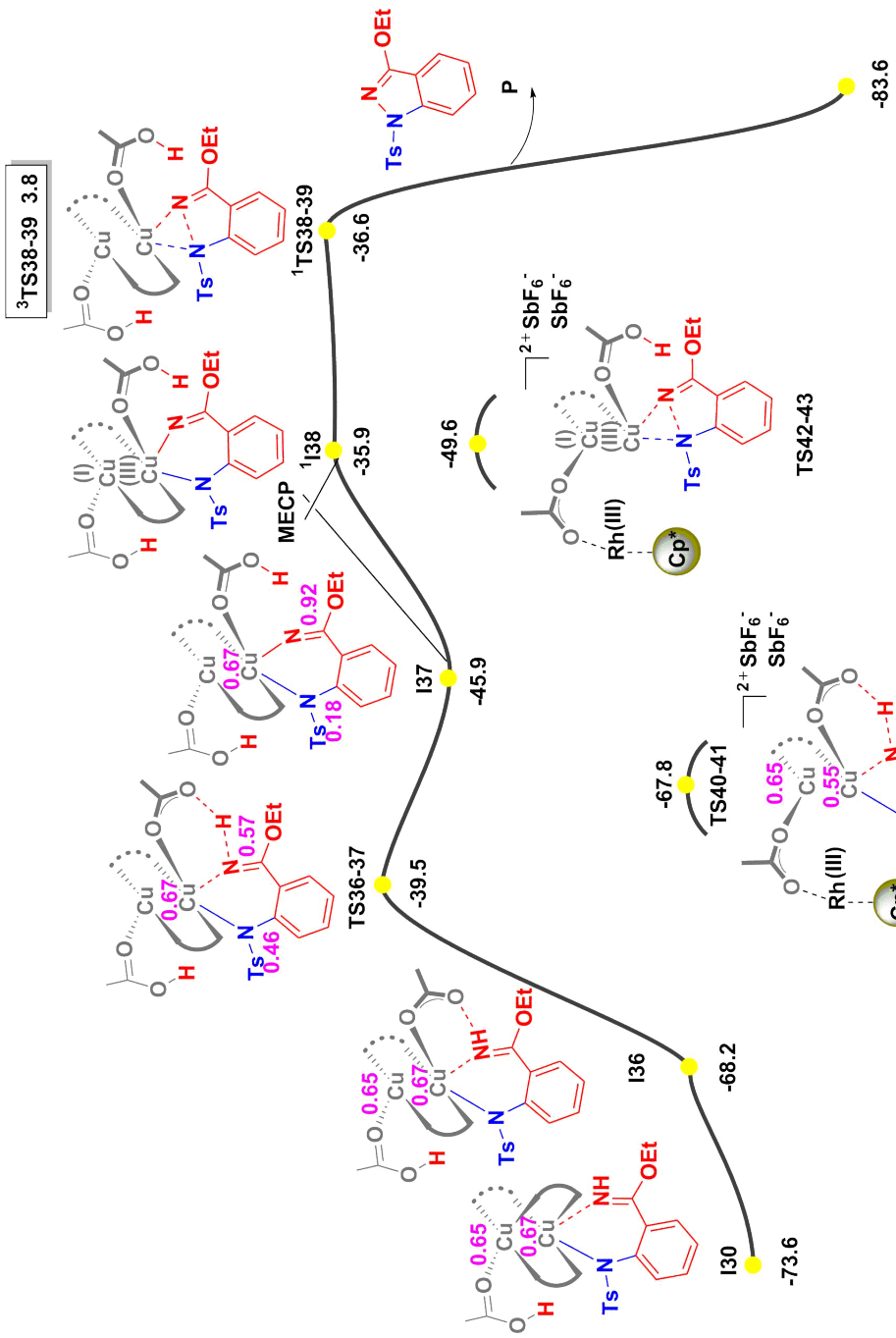

Fig. 6.12 DFT calculated mechanism for the deprotonation and reductive N-N bond formation from the Cu(III) center.

Another possible route is the oxidation of Cu(II) from **I36** by a deprotonation process via **TS36-37** and the following MECP (Minimum Energy Crossing Point) to give the closed-shell singlet Cu(III) intermediate ^{1}**I38** in Figure 6.12. Then, the reductive elimination from Cu(III) via transition state ^{1}**TS38-39** delivers the final indazole product. The direct reductive elimination via ^{3}**TS38-39** from the open-shell triplet state **I37** is calculated to have a much higher barriers compared with the singlet ^{1}**TS38-39**. However, both the high barriers of the singlet and triplet routes are unfavorable. We also considered the interactions between Cu and Rh by introducing the cationic Rh(III) (**Cata-Rh**) and all the barriers for these two transition states **TS40-41** and **TS42-43** decreased, but still not favorable for this experimental conditions.

As observed in the reductive elimination process from the Rh center in Figure 6.8, the coordination of another substrate could help to stabilize the intermediates and transition states with different extent. So inspired by this observation, another reactant **R** is involved in the mechanism as shown in Figure 6.13. Similar to the route calculated in Figure 6.12, from **I30**, the interactions between the bridged Rh and Cu centers and the coordination of **R** to the Rh(III) center lead the reaction to a quite stable intermediate **I44**, which is exothermic about 27.0 kcal/mol when compared with **I30**. The deprotonation process from **I44** goes smoothly via **TS44-45** to deliver the **I45**, where the spin densities are still around the Cu(II) centers, indicating that no electron transfer occurs until now. Then the MECP process corresponding to the spin change occurs from the open-shell triplet state **I45** to the closed-shell singlet state ^{1}**I45**. Release of acetic acid and the final N-N bond formation through ^{1}**TS46-47** give the desired indazole product. This process is downhill with the energy of -99.4 kcal/mol. At last, the Cu(I) will be oxidized by the $\mathbf{O_2}$ to regenerate the Rh(III) catalyst (**Cata-Rh**) and Cu(II), leaving H_2O as the byproduct.

As we already know that the coordination of another substrate **R** could help to stabilize the intermediate. So we re-calculated the route for the

transfer of the N,N organic part from the Rh to Cu in Figure 6.10, the updated energy profiles are shown in Figure 6.14. The interaction between Rh and Cu connected by the bridging acetate ligand stabilize the species **I29** from -76.1 kcal/mol to -87.1 kcal/mol of **I48**, and the coordination of **R** to the Rh(III) center further stabilize the intermediate to -93.6 kcal/mol (**I49**). **I49** undergoes the deprotonation process via **TS49-50** to the intermediate **I44** in Figure 6.13.

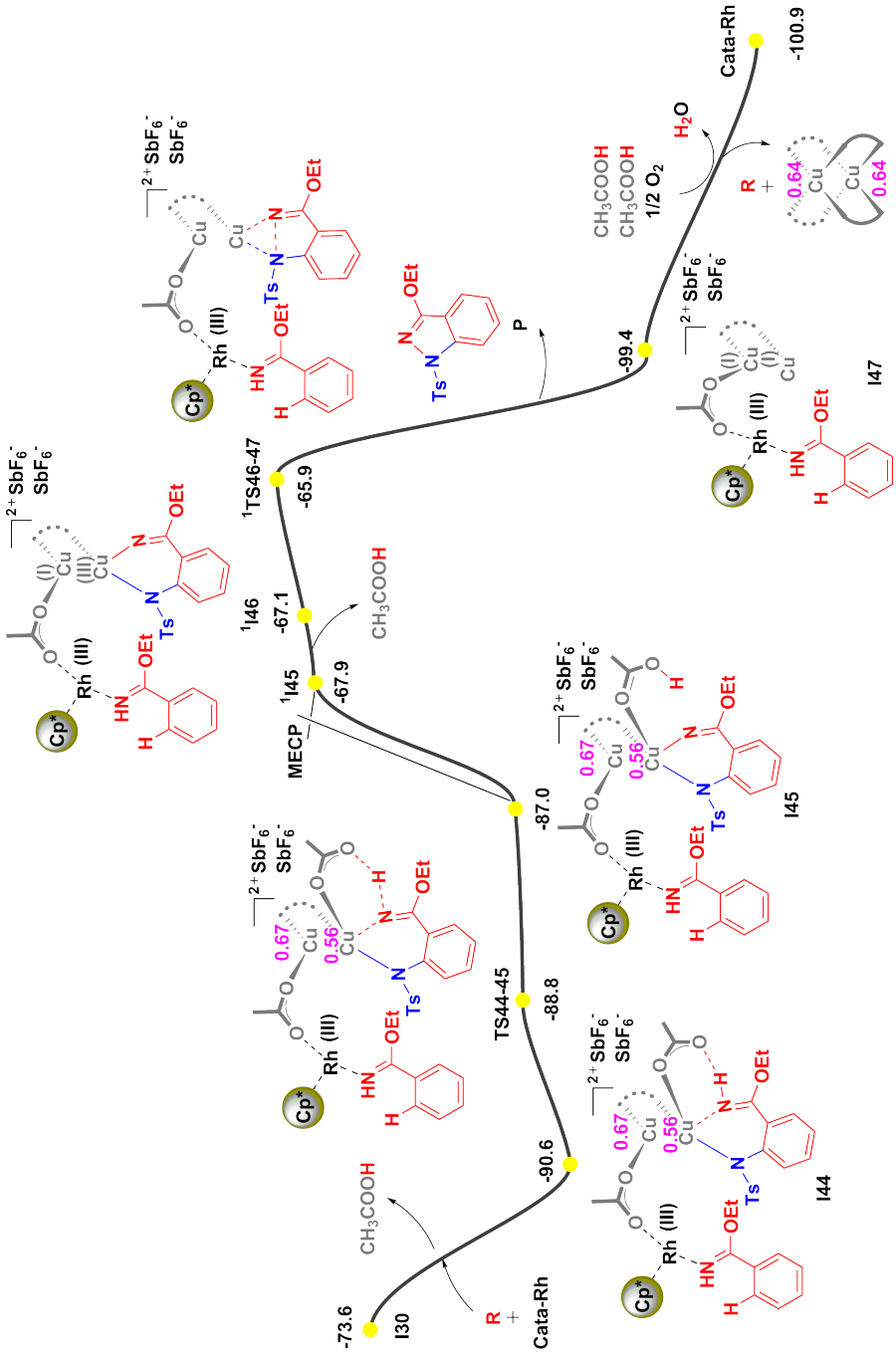

Fig. 6.13 DFT calculated mechanism for the deprotonation and reductive N-N bond formation from the Cu(III) center with the help of another substrate.

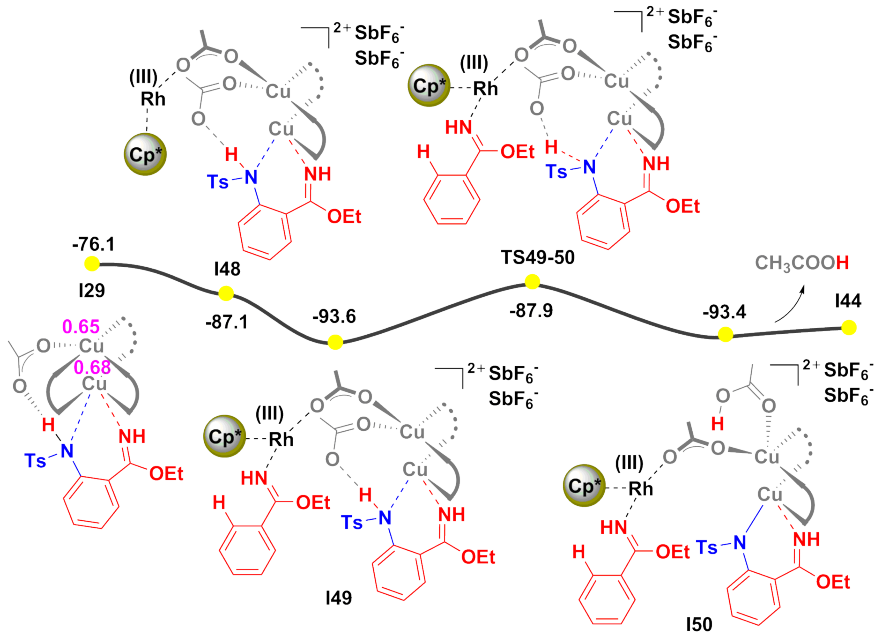

Fig. 6.14 The calculated mechanism of transfer N,N moiety from the Rh to Cu center with the help of Cu-Rh interactions.

The experimentally proposed single electron transfer process between the Cu and substrate is also calculated and the SET leads the reaction to unstable radical species **I51** and **I52** in Figure 6.15. Therefore, these routes will not be followed by our DFT studies.

From our DFT calculations in this section, the N-N bond formation process should proceed through the Cu center as shown in Figure 6.13. The interactions between Cu and Rh that connected by the acetate ligand and the coordination of substrate to the Rh(III) center is essential to make the reaction happen.

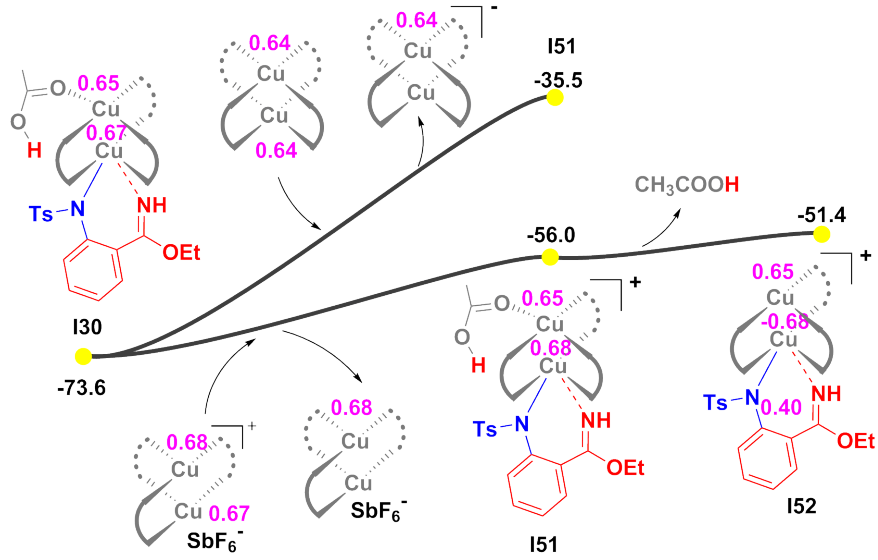

Fig. 6.15 The calculated mechanism of the single electron transfer process between Cu and substrate.

6.4 Conclusions

In summary, we have carried out DFT calculations to elucidate the mechanism of the leading reactions of synthesis of indazoles by the C-H amidation and N-N bond formation strategies. Our calculated results show that the reaction should start from the C-H bond activation from Rh(III) center via the CMD mechanism to give the rhodacyclic species. The release of N_2 and the following migratory insertion of the nitrene to the Rh-C bond gives the six-membered ring species. We proved that the N-N bond formation from the Rh(III) or Rh(IV) center is impossible for this case. Instead, the transfer of the N,N part from the Rh(III) center to the Cu(II) would deliver the Cu(III) intermediate, which will release the final N-N bond formation indazole product. The interactions between the Cu and Rh that connected by the acetate ligand and the coordination of substrate to the Rh(III) center is quite important for this N-N bond formation process. The whole process is

exothermic about 100.0 kcal/mol, and the rate determining transition state corresponding to the final N-N bond formation process. The overall barrier is 27.7 kcal/mol, agrees well with the experimental conditions that the reaction need a high temperature (110 C, 24h). Our calculations not only shed light on the mechanism of this reaction, we believe this could give some inspirations on the Rh-Cu co-catalyzed reactions, especially the related N-N bond formation process.

Chapter 7

Conclusions

Our DFT calculations have brought significant clarification to the rich mechanistic diversity of copper-catalyzed organic synthesis. The main results have been the following:

- The C-C bond formation by Cu-catalyzed borylative ring closing is ruled by two steps: halogen abstraction and C-C coupling. The more favorable formation of 4-membered rings is associated to the need for less distortion in the C-C coupling transition state, the preference for the I ligand group over Br is explained by the lower C-I bond strength, and the highest efficiency of K over Na as countercation is related to the better fit in the space available in the rate-limiting transition state.

- The rate determining step in the enantioselective intermolecular cyanotrifluoromethylation of styrenes with a chiral bis(oxazoline)/Cu(I) catalyst is the release of CF_3 radical and the enantioselectivity determining step is the reductive elimination from the Cu(III) center. The analysis of the structural parameters, the visualization of the non-covalent interactions (NCI), and the energy decomposition analysis show that the small steric repulsion between the ligand and the benzylic cation makes the formation of the R-products more favorable. This uncovers

a new general manifold for copper-catalyzed intermolecular enantioselective difunctionalization of alkenes via a radical process and can have important implications for the optimization of this ATRA-type reaction.

- An alternative mechanism, different from that proposed from experiment, has been characterized for the iridium-catalyzed aerobic α,β-dehydrogenation of γ,δ-unsaturated amides and acids under the presence of $Cu(OAc)_2 \cdot H_2O$ with O_2 as oxidant. An Ir-enolate intermediate is involved instead of the previously proposed Ir-allyl species. The $AgBF_4$ and $[Cu(OAc)_2 \cdot H_2O]_2$ units are shown to play an important role; the silver complex activates the initial Ir(III) catalyst by Cl abstraction and the copper complex cooperates in the C-H activation and facilitates the catalyst recovery by Ir(I) oxidation. The rate determining step is the α-C-H bond activation, with participation of both the copper and iridium centers.

- The key step in the synthesis of 1H-indazole through C-H amidation and N-N bond formation by a Rh(III)/Cu(II)-cocatalyst system is the N-N bond reductive elimination from the Cu(III) center. The interactions between the Cu and Rh connected by the acetate ligand and the coordination of the substrate to the Rh(III) center play an important role in the transition state for this step.

The joint consideration of these four specific studies shows the rich mechanistic complexity of copper as a catalyst, and the ability of computational chemistry to clarify the mechanisms and assist in the optimization of the existing processes and the design of more efficient ones,

References

[1] Gandeepan, P.; Müller, T.; Zell, D.; Cera, G.; Warratz, S.; Ackermann, L. *Chemical Reviews* **2018**, *119*, 2192–2452.

[2] Choy, P. Y.; Wong, S. M.; Kapdi, A.; Kwong, F. Y. *Organic Chemistry Frontiers* **2018**, *5*, 288–321.

[3] Baudoin, O. *Accounts of Chemical Research* **2017**, *50*, 1114–1123.

[4] Bras, J. L.; Muzart, J. *European Journal of Organic Chemistry* **2018**, *2018*, 1176–1203.

[5] Kakiuchi, F.; Kochi, T. *Israel Journal of Chemistry* **2017**, *57*, 953–963.

[6] Sun, C.-L.; Li, B.-J.; Shi, Z.-J. *Chemical Communications* **2010**, *46*, 677.

[7] Chen, X.; Engle, K.; Wang, D.-H.; Yu, J.-Q. *Angewandte Chemie International Edition* **2009**, *48*, 5094–5115.

[8] Neufeldt, S. R.; Sanford, M. S. *Accounts of Chemical Research* **2012**, *45*, 936–946.

[9] Ye, J.; Lautens, M. *Nature Chemistry* **2015**, *7*, 863–870.

[10] Nagamoto, M.; Nishimura, T. *ACS Catalysis* **2016**, *7*, 833–847.

[11] Yuan, C.; Liu, B. *Organic Chemistry Frontiers* **2018**, *5*, 106–131.

[12] Haldar, C.; Hoque, M. E.; Bisht, R.; Chattopadhyay, B. *Tetrahedron Letters* **2018**, *59*, 1269–1277.

[13] Sharninghausen, L. S.; Crabtree, R. H. *Israel Journal of Chemistry* **2017**, *57*, 937–944.

[14] Pan, S.; Shibata, T. *ACS Catalysis* **2013**, *3*, 704–712.

[15] Suzuki, T. *Chemical Reviews* **2011**, *111*, 1825–1845.

[16] Kim, J.; Chang, S. *Angewandte Chemie International Edition* **2014**, *53*, 2203–2207.

[17] Colby, D. A.; Bergman, R. G.; Ellman, J. A. *Chemical Reviews* **2010**, *110*, 624–655.

[18] Piou, T.; Rovis, T. *Accounts of Chemical Research* **2017**, *51*, 170–180.

[19] Yang, Y.; Li, K.; Cheng, Y.; Wan, D.; Li, M.; You, J. *Chemical Communications* **2016**, *52*, 2872–2884.

[20] Ye, B.; Cramer, N. *Accounts of Chemical Research* **2015**, *48*, 1308–1318.

[21] Song, G.; Wang, F.; Li, X. *Chemical Society Reviews* **2012**, *41*, 3651.

[22] Colby, D. A.; Tsai, A. S.; Bergman, R. G.; Ellman, J. A. *Accounts of Chemical Research* **2011**, *45*, 814–825.

[23] Satoh, T.; Miura, M. *Chemistry - A European Journal* **2010**, *16*, 11212–11222.

[24] Nareddy, P.; Jordan, F.; Szostak, M. *ACS Catalysis* **2017**, *7*, 5721–5745.

[25] Leitch, J. A.; Frost, C. G. *Chemical Society Reviews* **2017**, *46*, 7145–7153.

[26] Zha, G.-F.; Qin, H.-L.; Kantchev, E. A. B. *RSC Advances* **2016**, *6*, 30875–30885.

[27] Ruiz, S.; Villuendas, P.; Urriolabeitia, E. P. *Tetrahedron Letters* **2016**, *57*, 3413–3432.

[28] Thirunavukkarasu, V. S.; Kozhushkov, S. I.; Ackermann, L. *Chem. Commun.* **2014**, *50*, 29–39.

[29] De Sarkar, S.; Liu, W.; Kozhushkov, S. I.; Ackermann, L. *Advanced Synthesis & Catalysis* **2014**, *356*, 1461–1479.

[30] Kozhushkov, S. I.; Ackermann, L. *Chem. Sci.* **2013**, *4*, 886–896.

[31] Ackermann, L. *Accounts of Chemical Research* **2013**, *47*, 281–295.

[32] Arockiam, P. B.; Bruneau, C.; Dixneuf, P. H. *Chemical Reviews* **2012**, *112*, 5879–5918.

[33] Kallmeier, F.; Kempe, R. *Angewandte Chemie International Edition* **2017**, *57*, 46–60.

[34] Wolczanski, P. T. *Organometallics* **2018**, *37*, 505–516.

[35] Rajesh, N.; Barsu, N.; Sundararaju, B. *Tetrahedron Letters* **2018**, *59*, 862–868.

[36] Li, Y.; Hu, Y.; Wu, X.-F. *Chemical Society Reviews* **2018**, *47*, 172–194.

[37] Fukuzumi, S.; Lee, Y.-M.; Nam, W. *Coordination Chemistry Reviews* **2018**, *355*, 54–73.

[38] Chen, J.; Lu, Z. *Organic Chemistry Frontiers* **2018**, *5*, 260–272.

[39] Zweig, J. E.; Kim, D. E.; Newhouse, T. R. *Chemical Reviews* **2017**, *117*, 11680–11752.

[40] Webster, R. L. *Dalton Transactions* **2017**, *46*, 4483–4498.

[41] Pototschnig, G.; Maulide, N.; Schnürch, M. *Chemistry - A European Journal* **2017**, *23*, 9206–9232.

[42] Chirik, P. J. *Angewandte Chemie International Edition* **2017**, *56*, 5170–5181.

[43] Crossley, S. W. M.; Obradors, C.; Martinez, R. M.; Shenvi, R. A. *Chemical Reviews* **2016**, *116*, 8912–9000.

[44] Su, B.; Cao, Z.-C.; Shi, Z.-J. *Accounts of Chemical Research* **2015**, *48*, 886–896.

[45] Miao, J.; Ge, H. *European Journal of Organic Chemistry* **2015**, *2015*, 7859–7868.

[46] Allen, S. E.; Walvoord, R. R.; Padilla-Salinas, R.; Kozlowski, M. C. *Chemical Reviews* **2013**, *113*, 6234–6458.

[47] Patureau, F. W.; Gooßen, L. J. *Angewandte Chemie International Edition* **2014**, *53*, 5738–5739.

[48] Guo, X.-X.; Gu, D.-W.; Wu, Z.; Zhang, W. *Chemical Reviews* **2014**, *115*, 1622–1651.

[49] Chiba, S. *Bulletin of the Chemical Society of Japan* **2013**, *86*, 1400–1411.

[50] Zhang, C.; Tang, C.; Jiao, N. *Chemical Society Reviews* **2012**, *41*, 3464.

[51] Shi, Z.; Zhang, C.; Tang, C.; Jiao, N. *Chemical Society Reviews* **2012**, *41*, 3381.

[52] Wendlandt, A. E.; Suess, A. M.; Stahl, S. S. *Angewandte Chemie International Edition* **2011**, *50*, 11062–11087.

[53] Surry, D. S.; Buchwald, S. L. *Chemical Science* **2010**, *1*, 13.

[54] Monnier, F.; Taillefer, M. *Angewandte Chemie International Edition* **2009**, *48*, 6954–6971.

[55] Beletskaya, I. P.; Cheprakov, A. V. *Coordination Chemistry Reviews* **2004**, *248*, 2337–2364.

[56] Ley, S. V.; Thomas, A. W. *Angewandte Chemie International Edition* **2003**, *42*, 5400–5449.

[57] Hirano, K.; Miura, M. *Topics in Catalysis* **2014**, *57*, 878–889.

[58] Hirano, K.; Miura, M. *Chemical Communications* **2012**, *48*, 10704.

[59] Liu, T.; Shen, Q. *European Journal of Organic Chemistry* **2012**, *2012*, 6679–6687.

[60] Muñiz, K. *Angewandte Chemie International Edition* **2009**, *48*, 9412–9423.

[61] Xu, L.-M.; Li, B.-J.; Yang, Z.; Shi, Z.-J. *Chem. Soc. Rev.* **2010**, *39*, 712–733.

[62] Sehnal, P.; Taylor, R. J. K.; Fairlamb, I. J. S. *Chemical Reviews* **2010**, *110*, 824–889.

[63] Gamez, P.; Aubel, P. G.; Driessen, W. L.; Reedijk, J. *Chemical Society Reviews* **2001**, *30*, 376–385.

[64] Dong, J.; Wang, F.; You, J. *Organic Letters* **2014**, *16*, 2884–2887.

[65] McCann, S. D.; Stahl, S. S. *Accounts of Chemical Research* **2015**, *48*, 1756–1766.

[66] Ryland, B. L.; Stahl, S. S. *Angewandte Chemie International Edition* **2014**, *53*, 8824–8838.

[67] Zhang, N.; Samanta, S. R.; Rosen, B. M.; Percec, V. *Chemical Reviews* **2014**, *114*, 5848–5958.

[68] Wurtz, A. *Ann Chim Phys* **1855**, *44*, 275–312.

[69] Sandmeyer, T. *Berichte der deutschen chemischen Gesellschaft* **1884**, *17*, 2650–2653.

[70] Mulliken, R.; Person, W. B. *Annual Review of Physical Chemistry* **1962**, *13*, 107–126.

[71] Taube, H.; Myers, H.; Rich, R. L. *Journal of the American Chemical Society* **1953**, *75*, 4118–4119.

[72] Taube, H.; Myers, H. *Journal of the American Chemical Society* **1954**, *76*, 2103–2111.

[73] Taube, H. *Angewandte Chemie International Edition in English* **1984**, *23*, 329–339.

[74] Marcus, R. A. *Angewandte Chemie International Edition in English* **1993**, *32*, 1111–1121.

[75] Rosokha, S. V.; Kochi, J. K. *Accounts of Chemical Research* **2008**, *41*, 641–653.

[76] Muller, P. *Pure and Applied Chemistry* **1994**, *66*, 1077–1184.

[77] Barton, D. H.; McCombie, S. W. *Journal of the Chemical Society, Perkin Transactions 1* **1975**, 1574–1585.

[78] Carreira, E. M.; Fessard, T. C. *Chemical Reviews* **2014**, *114*, 8257–8322.

[79] Kotha, S.; Panguluri, N. R.; Ali, R. *European Journal of Organic Chemistry* **2017**, *2017*, 5316–5342.

[80] Royes, J.; Ni, S.; Farré, A.; Cascia, E. L.; Carbó, J. J.; Cuenca, A. B.; Maseras, F.; Fernández, E. *ACS Catalysis* **2018**, *8*, 2833–2838.

[81] Kubota, K.; Yamamoto, E.; Ito, H. *Journal of the American Chemical Society* **2013**, *135*, 2635–2640.

[82] Iwamoto, H.; Akiyama, S.; Hayama, K.; Ito, H. *Organic Letters* **2017**, *19*, 2614–2617.

[83] Iwamoto, H.; Ozawa, Y.; Kubota, K.; Ito, H. *The Journal of Organic Chemistry* **2017**, *82*, 10563–10573.

[84] Kleeberg, C.; Dang, L.; Lin, Z.; Marder, T. *Angewandte Chemie International Edition* **2009**, *48*, 5350–5354.

[85] Jover, J.; Maseras, F. *Organometallics* **2016**, *35*, 3221–3226.

[86] Song, H.; Ye, K.; Geng, P.; Han, X.; Liao, R.; Tung, C.-H.; Wang, W. *ACS Catalysis* **2017**, *7*, 7709–7717.

[87] Chai, J.-D.; Head-Gordon, M. *Physical Chemistry Chemical Physics* **2008**, *10*, 6615.

[88] Frisch, M.; Trucks, G.; Schlegel, H.; Scuseria, G.; Robb, M.; Cheeseman, J.; Scalmani, G.; Barone, V.; Mennucci, B.; Petersson, G.; et al. *J. Chem. Phys* **1993**, *98*, 785–789.

[89] Hay, P. J.; Wadt, W. R. *The Journal of Chemical Physics* **1985**, *82*, 270–283.

[90] Wadt, W. R.; Hay, P. J. *The Journal of Chemical Physics* **1985**, *82*, 284–298.

[91] Hay, P. J.; Wadt, W. R. *The Journal of Chemical Physics* **1985**, *82*, 270–283.

[92] Check, C. E.; Faust, T. O.; Bailey, J. M.; Wright, B. J.; Gilbert, T. M.; Sunderlin, L. S. *The Journal of Physical Chemistry A* **2001**, *105*, 8111–8116.

[93] Ehlers, A.; Böhme, M.; Dapprich, S.; Gobbi, A.; Höllwarth, A.; Jonas, V.; Köhler, K.; Stegmann, R.; Veldkamp, A.; Frenking, G. *Chemical Physics Letters* **1993**, *208*, 111–114.

[94] Binning, R. C.; Jr; of Chemistry, D.; of Puerto Rico, U.; Piedras, R.; Rico, P.

[95] Krishnan, R.; Binkley, J. S.; Seeger, R.; Pople, J. A. *The Journal of Chemical Physics* **1980**, *72*, 650–654.

[96] McLean, A. D.; Chandler, G. S. *The Journal of Chemical Physics* **1980**, *72*, 5639–5648.

[97] Frisch, M. J.; Pople, J. A.; Binkley, J. S. *The Journal of Chemical Physics* **1984**, *80*, 3265–3269.

[98] Li, J.-H.; Wang, D.-P.; Xie, Y.-X. *Tetrahedron Letters* **2005**, *46*, 4941–4944.

[99] Balcells, D.; Maseras, F.; Keay, B. A.; Ziegler, T. *Organometallics* **2004**, *23*, 2784–2796.

[100] Lan, X.-W.; Wang, N.-X.; Xing, Y. *European Journal of Organic Chemistry* **2017**, *2017*, 5821–5851.

[101] Yin, G.; Mu, X.; Liu, G. *Accounts of Chemical Research* **2016**, *49*, 2413–2423.

[102] Yasu, Y.; Koike, T.; Akita, M. *Organic Letters* **2013**, *15*, 2136–2139.

[103] Zhu, R.; Buchwald, S. L. *Angewandte Chemie International Edition* **2013**, *52*, 12655–12658.

[104] Pan, S.; Li, H.; Huang, Y.; Xu, X.-H.; Qing, F.-L. *Organic Letters* **2017**, *19*, 3247–3250.

[105] Wang, F.; Wang, D.; Zhou, Y.; Liang, L.; Lu, R.; Chen, P.; Lin, Z.; Liu, G. *Angewandte Chemie International Edition* **2018**, *57*, 7140–7145.

[106] Baeckvall, J. E. *Accounts of Chemical Research* **1983**, *16*, 335–342.

[107] McDonald, R. I.; Liu, G.; Stahl, S. S. *Chemical Reviews* **2011**, *111*, 2981–3019.

[108] Beccalli, E. M.; Broggini, G.; Gazzola, S.; Mazza, A. *Org. Biomol. Chem.* **2014**, *12*, 6767–6789.

[109] Mu, X.; Wu, T.; yang Wang, H.; long Guo, Y.; Liu, G. *Journal of the American Chemical Society* **2011**, *134*, 878–881.

[110] Dong, X.; Sang, R.; Wang, Q.; Tang, X.-Y.; Shi, M. *Chemistry - A European Journal* **2013**, *19*, 16910–16915.

[111] Hu, M.; Fan, J.-H.; Liu, Y.; Ouyang, X.-H.; Song, R.-J.; Li, J.-H. *Angewandte Chemie International Edition* **2015**, *54*, 9577–9580.

[112] Wang, F.; Qi, X.; Liang, Z.; Chen, P.; Liu, G. *Angewandte Chemie International Edition* **2014**, *53*, 1881–1886.

[113] Liang, Z.; Wang, F.; Chen, P.; Liu, G. *Journal of Fluorine Chemistry* **2014**, *167*, 55–60.

[114] Ilchenko, N. O.; Janson, P. G.; Szabó, K. J. *The Journal of Organic Chemistry* **2013**, *78*, 11087–11091.

[115] He, Y.-T.; Li, L.-H.; Yang, Y.-F.; Zhou, Z.-Z.; Hua, H.-L.; Liu, X.-Y.; Liang, Y.-M. *Organic Letters* **2013**, *16*, 270–273.

[116] Liang, Z.; Wang, F.; Chen, P.; Liu, G. *Organic Letters* **2015**, *17*, 2438–2441.

[117] Wang, F.; Wang, D.; Mu, X.; Chen, P.; Liu, G. *Journal of the American Chemical Society* **2014**, *136*, 10202–10205.

[118] Wang, F.; Zhu, N.; Chen, P.; Ye, J.; Liu, G. *Angewandte Chemie International Edition* **2015**, *54*, 9356–9360.

[119] Zhu, N.; Wang, F.; Chen, P.; Ye, J.; Liu, G. *Organic Letters* **2015**, *17*, 3580–3583.

[120] Lin, J.-S.; Dong, X.-Y.; Li, T.-T.; Jiang, N.-C.; Tan, B.; Liu, X.-Y. *Journal of the American Chemical Society* **2016**, *138*, 9357–9360.

[121] Li, Z.-L.; Li, X.-H.; Wang, N.; Yang, N.-Y.; Liu, X.-Y. *Angewandte Chemie International Edition* **2016**, *55*, 15100–15104.

[122] Zhu, R.; Buchwald, S. L. *Journal of the American Chemical Society* **2015**, *137*, 8069–8077.

[123] Lin, J.-S.; Wang, F.-L.; Dong, X.-Y.; He, W.-W.; Yuan, Y.; Chen, S.; Liu, X.-Y. *Nature Communications* **2017**, *8*.

[124] Wang, F.-L.; Dong, X.-Y.; Lin, J.-S.; Zeng, Y.; Jiao, G.-Y.; Gu, Q.-S.; Guo, X.-Q.; Ma, C.-L.; Liu, X.-Y. *Chem* **2017**, *3*, 979–990.

[125] Cheng, Y.-F.; Dong, X.-Y.; Gu, Q.-S.; Yu, Z.-L.; Liu, X.-Y. *Angewandte Chemie International Edition* **2017**, *56*, 8883–8886.

[126] Zhang, H.; Pu, W.; Xiong, T.; Li, Y.; Zhou, X.; Sun, K.; Liu, Q.; Zhang, Q. *Angewandte Chemie International Edition* **2013**, *52*, 2529–2533.

[127] Xu, L.; Mou, X.-Q.; Chen, Z.-M.; Wang, S.-H. *Chem. Commun.* **2014**, *50*, 10676–10679.

[128] Wang, F.; Wang, D.; Wan, X.; Wu, L.; Chen, P.; Liu, G. *Journal of the American Chemical Society* **2016**, *138*, 15547–15550.

[129] Wang, D.; Wang, F.; Chen, P.; Lin, Z.; Liu, G. *Angewandte Chemie International Edition* **2017**, *56*, 2054–2058.

[130] Wu, L.; Wang, F.; Wan, X.; Wang, D.; Chen, P.; Liu, G. *Journal of the American Chemical Society* **2017**, *139*, 2904–2907.

[131] Wang, D.; Wu, L.; Wang, F.; Wan, X.; Chen, P.; Lin, Z.; Liu, G. *Journal of the American Chemical Society* **2017**, *139*, 6811–6814.

[132] Wang, D.; Zhu, N.; Chen, P.; Lin, Z.; Liu, G. *Journal of the American Chemical Society* **2017**, *139*, 15632–15635.

[133] Sha, W.; Zhu, Y.; Mei, H.; Han, J.; Soloshonok, V. A.; Pan, Y. *ChemistrySelect* **2017**, *2*, 1129–1132.

[134] Chen, B.; Fang, C.; Liu, P.; Ready, J. M. *Angewandte Chemie International Edition* **2017**, *56*, 8780–8784.

[135] Parsons, A. T.; Buchwald, S. L. *Angewandte Chemie International Edition* **2011**, *50*, 9120–9123.

[136] Xu, J.; Fu, Y.; Luo, D.-F.; Jiang, Y.-Y.; Xiao, B.; Liu, Z.-J.; Gong, T.-J.; Liu, L. *Journal of the American Chemical Society* **2011**, *133*, 15300–15303.

[137] Wang, X.; Ye, Y.; Zhang, S.; Feng, J.; Xu, Y.; Zhang, Y.; Wang, J. *Journal of the American Chemical Society* **2011**, *133*, 16410–16413.

[138] Yang, X.; Wu, T.; Phipps, R. J.; Toste, F. D. *Chemical Reviews* **2014**, *115*, 826–870.

[139] Charpentier, J.; Früh, N.; Togni, A. *Chemical Reviews* **2014**, *115*, 650–682.

[140] Tomashenko, O. A.; Grushin, V. V. *Chemical Reviews* **2011**, *111*, 4475–4521.

[141] Seitz, L. C.; Dickens, C. F.; Nishio, K.; Hikita, Y.; Montoya, J.; Doyle, A.; Kirk, C.; Vojvodic, A.; Hwang, H. Y.; Norskov, J. K.; Jaramillo, T. F. *Science* **2016**, *353*, 1011–1014.

[142] Lu, T.; Chen, F. *Journal of Computational Chemistry* **2011**, *33*, 580–592.

[143] Johnson, E. R.; Keinan, S.; Mori-Sanchez, P.; Contreras-Garcia, J.; Cohen, A. J.; Yang, W. *Journal of the American Chemical Society* **2010**, *132*, 6498–6506.

[144] Contreras-Garcia, J.; Johnson, E. R.; Keinan, S.; Chaudret, R.; Piquemal, J.-P.; Beratan, D. N.; Yang, W. *Journal of Chemical Theory and Computation* **2011**, *7*, 625–632.

[145] Zhou, W.; Zhang, L.; Jiao, N. *Angewandte Chemie International Edition* **2009**, *48*, 7094–7097.

[146] Zhu, R.; Buchwald, S. L. *Journal of the American Chemical Society* **2012**, *134*, 12462–12465.

[147] He, Y.-T.; Li, L.-H.; Yang, Y.-F.; Zhou, Z.-Z.; Hua, H.-L.; Liu, X.-Y.; Liang, Y.-M. *Organic Letters* **2013**, *16*, 270–273.

[148] Chen, S.; Li, D.-Y.; Jiang, L.-L.; Liu, K.; Liu, P.-N. *Organic Letters* **2017**, *19*, 2014–2017.

[149] Wu, X.; Chu, L.; Qing, F.-L. *Angewandte Chemie International Edition* **2013**, *52*, 2198–2202.

[150] Lonca, G. H.; Ong, D. Y.; Tran, T. M. H.; Tejo, C.; Chiba, S.; Gagosz, F. *Angewandte Chemie International Edition* **2017**, *56*, 11440–11444.

[151] Jones, G. O.; Liu, P.; Houk, K. N.; Buchwald, S. L. *Journal of the American Chemical Society* **2010**, *132*, 6205–6213.

[152] Zhang, Q.; Zhang, Z.-Q.; Fu, Y.; Yu, H.-Z. *ACS Catalysis* **2016**, *6*, 798–808.

[153] Fernández-Alvarez, V. M.; Nappi, M.; Melchiorre, P.; Maseras, F. *Organic Letters* **2015**, *17*, 2676–2679.

[154] Yao, B.; Wang, D.-X.; Huang, Z.-T.; Wang, M.-X. *Chemical Communications* **2009**, 2899.

[155] Casitas, A.; Canta, M.; Solà, M.; Costas, M.; Ribas, X. *Journal of the American Chemical Society* **2011**, *133*, 19386–19392.

[156] Mayoral, J.; Rodríguez-Rodríguez, S.; Salvatella, L. *Chemistry - A European Journal* **2008**, *14*, 9274–9285.

[157] Seguin, T. J.; Lu, T.; Wheeler, S. E. *Organic Letters* **2015**, *17*, 3066–3069.

[158] Lu, T.; Chen, F. *Journal of Computational Chemistry* **2011**, *33*, 580–592.

[159] Guan, W.; Sakaki, S.; Kurahashi, T.; Matsubara, S. *ACS Catalysis* **2014**, *5*, 1–10.

[160] Ni, S.-F.; Yang, T.-L.; Dang, L. *Organometallics* **2017**, *36*, 2746–2754.

[161] Dobereiner, G. E.; Crabtree, R. H. *Chemical Reviews* **2010**, *110*, 681–703.

[162] Muzart, J. *European Journal of Organic Chemistry* **2010**, *2010*, 3779–3790.

[163] Choi, J.; MacArthur, A. H. R.; Brookhart, M.; Goldman, A. S. *Chemical Reviews* **2011**, *111*, 1761–1779.

[164] Balcells, D.; Clot, E.; Eisenstein, O. *Chemical Reviews* **2010**, *110*, 749–823.

[165] Davies, D. L.; Macgregor, S. A.; McMullin, C. L. *Chemical Reviews* **2017**, *117*, 8649–8709.

[166] Kim, D.-S.; Park, W.-J.; Jun, C.-H. *Chemical Reviews* **2017**, *117*, 8977–9015.

[167] Park, Y.; Kim, Y.; Chang, S. *Chemical Reviews* **2017**, *117*, 9247–9301.

[168] Huang, Z.; Lim, H. N.; Mo, F.; Young, M. C.; Dong, G. *Chemical Society Reviews* **2015**, *44*, 7764–7786.

[169] Cheng, G.-J.; Yang, Y.-F.; Liu, P.; Chen, P.; Sun, T.-Y.; Li, G.; Zhang, X.; Houk, K. N.; Yu, J.-Q.; Wu, Y.-D. *Journal of the American Chemical Society* **2014**, *136*, 894–897.

[170] He, J.; Wasa, M.; Chan, K. S. L.; Shao, Q.; Yu, J.-Q. *Chemical Reviews* **2016**, *117*, 8754–8786.

[171] Mack, J. B. C.; Gipson, J. D.; Bois, J. D.; Sigman, M. S. *Journal of the American Chemical Society* **2017**, *139*, 9503–9506.

[172] Shang, R.; Ilies, L.; Nakamura, E. *Chemical Reviews* **2017**, *117*, 9086–9139.

[173] Liu, J.; Zhu, J.; Jiang, H.; Wang, W.; Li, J. *Chemistry - An Asian Journal* **2009**, *4*, 1712–1716.

[174] Wang, M.-M.; Ning, X.-S.; Qu, J.-P.; Kang, Y.-B. *ACS Catalysis* **2017**, *7*, 4000–4003.

[175] Zhu, J.; Liu, J.; Ma, R.; Xie, H.; Li, J.; Jiang, H.; Wang, W. *Advanced Synthesis & Catalysis* **2009**, *351*, 1229–1232.

[176] Gao, W.; He, Z.; Qian, Y.; Zhao, J.; Huang, Y. *Chem. Sci.* **2012**, *3*, 883–886.

[177] Izawa, Y.; Pun, D.; Stahl, S. S. *Science* **2011**, *333*, 209–213.

[178] Bigi, M. A.; White, M. C. *Journal of the American Chemical Society* **2013**, *135*, 7831–7834.

[179] Diao, T.; Pun, D.; Stahl, S. S. *Journal of the American Chemical Society* **2013**, *135*, 8205–8212.

[180] Izawa, Y.; Zheng, C.; Stahl, S. S. *Angewandte Chemie International Edition* **2013**, *52*, 3672–3675.

[181] Jie, X.; Shang, Y.; Zhang, X.; Su, W. *Journal of the American Chemical Society* **2016**, *138*, 5623–5633.

[182] Shang, Y.; Jie, X.; Jonnada, K.; Zafar, S. N.; Su, W. *Nature Communications* **2017**, *8*.

[183] Huang, Z.; Dong, G. *Journal of the American Chemical Society* **2013**, *135*, 17747–17750.

[184] Ueno, S.; Shimizu, R.; Kuwano, R. *Angewandte Chemie International Edition* **2009**, *48*, 4543–4545.

[185] Shang, Y.; Jie, X.; Zhou, J.; Hu, P.; Huang, S.; Su, W. *Angewandte Chemie International Edition* **2012**, *52*, 1299–1303.

[186] Kusumoto, S.; Akiyama, M.; Nozaki, K. *Journal of the American Chemical Society* **2013**, *135*, 18726–18729.

[187] Chen, Y.; Romaire, J. P.; Newhouse, T. R. *Journal of the American Chemical Society* **2015**, *137*, 5875–5878.

[188] Chuentragool, P.; Parasram, M.; Shi, Y.; Gevorgyan, V. *Journal of the American Chemical Society* **2018**, *140*, 2465–2468.

[189] Nicolaou, K. C.; Zhong, Y.-L.; Baran, P. S. *Journal of the American Chemical Society* **2000**, *122*, 7596–7597.

[190] Uyanik, M.; Akakura, M.; Ishihara, K. *Journal of the American Chemical Society* **2009**, *131*, 251–262.

[191] Gandeepan, P.; Rajamalli, P.; Cheng, C.-H. *ACS Catalysis* **2014**, *4*, 4485–4489.

[192] Stang, E. M.; White, M. C. *Journal of the American Chemical Society* **2011**, *133*, 14892–14895.

[193] Diao, T.; Stahl, S. S. *Journal of the American Chemical Society* **2011**, *133*, 14566–14569.

[194] Chen, Y.; Huang, D.; Zhao, Y.; Newhouse, T. R. *Angewandte Chemie International Edition* **2017**, *56*, 8258–8262.

[195] Trost, B. M.; Salzmann, T. N.; Hiroi, K. *Journal of the American Chemical Society* **1976**, *98*, 4887–4902.

[196] Sharpless, K. B.; Lauer, R. F.; Teranishi, A. Y. *Journal of the American Chemical Society* **1973**, *95*, 6137–6139.

[197] Ito, Y.; Hirao, T.; Saegusa, T. *The Journal of Organic Chemistry* **1978**, *43*, 1011–1013.

[198] Leskinen, M. V.; Madarász, Á.; Yip, K.-T.; Vuorinen, A.; Pápai, I.; Neuvonen, A. J.; Pihko, P. M. *Journal of the American Chemical Society* **2014**, *136*, 6453–6462.

[199] Chen, M.; Dong, G. *Journal of the American Chemical Society* **2017**, *139*, 7757–7760.

[200] King, A. O.; Anderson, R. K.; Shuman, R. F.; Karady, S.; Abramson, N. L.; Douglas, A. W. *The Journal of Organic Chemistry* **1993**, *58*, 3384–3386.

[201] ichi Matsuo, J.; Aizawa, Y. *Tetrahedron Letters* **2005**, *46*, 407–410.

[202] Bhattacharya, A.; DiMichele, L. M.; Dolling, U. H.; Douglas, A. W.; Grabowski, E. J. J. *Journal of the American Chemical Society* **1988**, *110*, 3318–3319.

[203] Chen, Y.; Turlik, A.; Newhouse, T. R. *Journal of the American Chemical Society* **2016**, *138*, 1166–1169.

[204] He, Z.; Huang, Y. *ACS Catalysis* **2016**, *6*, 7814–7823.

[205] Teskey, C. J.; Adler, P.; Gonçalves, C. R.; Maulide, N. *Angewandte Chemie International Edition* **2018**, *58*, 447–451.

[206] Wang, M.-M.; Sui, G.-H.; Cui, X.-C.; Wang, H.; Qu, J.-P.; Kang, Y.-B. *The Journal of Organic Chemistry* **2019**, *84*, 8267–8274.

[207] Wang, Z.; He, Z.; Zhang, L.; Huang, Y. *Journal of the American Chemical Society* **2018**, *140*, 735–740.

[208] Funes-Ardoiz, I.; Maseras, F. *ACS Catalysis* **2018**, *8*, 1161–1172.

[209] Funes-Ardoiz, I.; Maseras, F. *Angewandte Chemie International Edition* **2016**, *55*, 2764–2767.

[210] Funes-Ardoiz, I.; Maseras, F. *Chemistry - A European Journal* **2018**, *24*, 12383–12388.

[211] Hay, P. J.; Wadt, W. R. *The Journal of Chemical Physics* **1985**, *82*, 299–310.

[212] Villuendas, P.; Ruiz, S.; Vidossich, P.; Lledós, A.; Urriolabeitia, E. P. *Chemistry - A European Journal* **2018**, *24*, 13124–13135.

[213] Jones, A. W.; Rank, C. K.; Becker, Y.; Malchau, C.; Funes-Ardoiz, I.; Maseras, F.; Patureau, F. W. *Chemistry - A European Journal* **2018**, *24*, 15178–15184.

[214] Zheng, Q.-Z.; Jiao, N. In *Nitrogenation Strategy for the Synthesis of N-containing Compounds*; Springer Singapore, 2016; pp 167–218.

[215] Zhu, J. S.; Kraemer, N.; Shatskikh, M. E.; Li, C. J.; Son, J.-H.; Haddadin, M. J.; Tantillo, D. J.; Kurth, M. J. *Organic Letters* **2018**, *20*, 4736–4739.

[216] Tiwari, V. K.; Mishra, B. B.; Mishra, K. B.; Mishra, N.; Singh, A. S.; Chen, X. *Chemical Reviews* **2016**, *116*, 3086–3240.

[217] Moses, J. E.; Moorhouse, A. D. *Chem. Soc. Rev.* **2007**, *36*, 1249–1262.

[218] Sadjadi, S.; Heravi, M. M.; Nazari, N. *RSC Advances* **2016**, *6*, 53203–53272.

[219] Lian, Y.; Bergman, R. G.; Lavis, L. D.; Ellman, J. A. *Journal of the American Chemical Society* **2013**, *135*, 7122–7125.

[220] Zheng, Q.-Z.; Feng, P.; Liang, Y.-F.; Jiao, N. *Organic Letters* **2013**, *15*, 4262–4265.

[221] Li, L.; Wang, H.; Yu, S.; Yang, X.; Li, X. *Organic Letters* **2016**, *18*, 3662–3665.

[222] Peng, J.; Xie, Z.; Chen, M.; Wang, J.; Zhu, Q. *Organic Letters* **2014**, *16*, 4702–4705.

[223] Shang, E.; Zhang, J.; Bai, J.; Wang, Z.; Li, X.; Zhu, B.; Lei, X. *Chemical Communications* **2016**, *52*, 7028–7031.

[224] Zhang, Z.; Huang, Y.; Huang, G.; Zhang, G.; Liu, Q. *Journal of Heterocyclic Chemistry* **2017**, *54*, 2426–2433.

[225] Gaikwad, D. D.; Chapolikar, A. D.; Devkate, C. G.; Warad, K. D.; Tayade, A. P.; Pawar, R. P.; Domb, A. J. *European Journal of Medicinal Chemistry* **2015**, *90*, 707–731.

[226] Yao, B.; Miao, T.; Li, P.; Wang, L. *Organic Letters* **2018**, *21*, 124–128.

[227] Subramanian, P.; Rudolf, G. C.; Kaliappan, K. P. *Chemistry - An Asian Journal* **2015**, *11*, 168–192.

[228] Lin, W.-C.; Yang, D.-Y. *Organic Letters* **2013**, *15*, 4862–4865.

[229] Han, S.; Shin, Y.; Sharma, S.; Mishra, N. K.; Park, J.; Kim, M.; Kim, M.; Jang, J.; Kim, I. S. *Organic Letters* **2014**, *16*, 2494–2497.

[230] Li, P.; Wu, C.; Zhao, J.; Rogness, D. C.; Shi, F. *The Journal of Organic Chemistry* **2012**, *77*, 3149–3158.

[231] Inamoto, K.; Saito, T.; Katsuno, M.; Sakamoto, T.; Hiroya, K. *Organic Letters* **2007**, *9*, 2931–2934.

[232] Zhang, T.; Bao, W. *The Journal of Organic Chemistry* **2013**, *78*, 1317–1322.

[233] Li, X.; He, L.; Chen, H.; Wu, W.; Jiang, H. *The Journal of Organic Chemistry* **2013**, *78*, 3636–3646.

[234] Jin, T.; Yamamoto, Y. *Angewandte Chemie International Edition* **2007**, *46*, 3323–3325.

[235] Markina, N. A.; Dubrovskiy, A. V.; Larock, R. C. *Organic & Biomolecular Chemistry* **2012**, *10*, 2409.

[236] Jeong, T.; Han, S. H.; Han, S.; Sharma, S.; Park, J.; Lee, J. S.; Kwak, J. H.; Jung, Y. H.; Kim, I. S. *Organic Letters* **2016**, *18*, 232–235.

[237] Long, Z.; Wang, Z.; Zhou, D.; Wan, D.; You, J. *Organic Letters* **2017**, *19*, 2777–2780.

[238] Geng, X.; Wang, C. *Organic Letters* **2015**, *17*, 2434–2437.

[239] Hummel, J. R.; Ellman, J. A. *Journal of the American Chemical Society* **2014**, *137*, 490–498.

[240] Xu, P.; Wang, G.; Wu, Z.; li, S.; Zhu, C. *Chemical Science* **2017**, *8*, 1303–1308.

[241] Liu, Z.; Wang, L.; Tan, H.; Zhou, S.; Fu, T.; Xia, Y.; Zhang, Y.; Wang, J. *Chem. Commun.* **2014**, *50*, 5061–5063.

[242] Counceller, C. M.; Eichman, C. C.; Wray, B. C.; Stambuli, J. P. *Organic Letters* **2008**, *10*, 1021–1023.

[243] yi Chen, C.; Tang, G.; He, F.; Wang, Z.; Jing, H.; Faessler, R. *Organic Letters* **2016**, *18*, 1690–1693.

[244] Tang, X.; Gao, H.; Yang, J.; Wu, W.; Jiang, H. *Org. Chem. Front.* **2014**, *1*, 1295–1298.

[245] Wang, Q.; Li, X. *Organic Letters* **2016**, *18*, 2102–2105.

[246] Wray, B. C.; Stambuli, J. P. *Organic Letters* **2010**, *12*, 4576–4579.

[247] Counceller, C. M.; Eichman, C. C.; Wray, B. C.; Stambuli, J. P. *Organic Letters* **2008**, *10*, 1021–1023.

[248] Stokes, B. J.; Vogel, C. V.; Urnezis, L. K.; Pan, M.; Driver, T. G. *Organic Letters* **2010**, *12*, 2884–2887.

[249] Hu, J.; Cheng, Y.; Yang, Y.; Rao, Y. *Chemical Communications* **2011**, *47*, 10133.

[250] Dai, G.; Yang, L.; Zhou, W. *Organic Chemistry Frontiers* **2017**, *4*, 229–231.

[251] Cenini, S.; Gallo, E.; Caselli, A.; Ragaini, F.; Fantauzzi, S.; Piangiolino, C. *Coordination Chemistry Reviews* **2006**, *250*, 1234–1253.

[252] Kim, S. H.; Park, S. H.; Choi, J. H.; Chang, S. *Chemistry - An Asian Journal* **2011**, *6*, 2618–2634.

[253] Yadav, M. R.; Rit, R. K.; Sahoo, A. K. *Organic Letters* **2013**, *15*, 1638–1641.

[254] Bhanuchandra, M.; Yadav, M. R.; Rit, R. K.; Kuram, M. R.; Sahoo, A. K. *Chemical Communications* **2013**, *49*, 5225.

[255] Zheng, Q.-Z.; Liang, Y.-F.; Qin, C.; Jiao, N. *Chemical Communications* **2013**, *49*, 5654.

[256] Yu, D.-G.; Suri, M.; Glorius, F. *Journal of the American Chemical Society* **2013**, *135*, 8802–8805.

[257] Yu, S.; Tang, G.; Li, Y.; Zhou, X.; Lan, Y.; Li, X. *Angewandte Chemie International Edition* **2016**, *55*, 8696–8700.

[258] Wang, N.; Liu, L.; Xu, W.; Zhang, M.; Huang, Z.; Shi, D.; Zhao, Y. *Organic Letters* **2019**, *21*, 365–368.

[259] Xu, S.; Huang, B.; Qiao, G.; Huang, Z.; Zhang, Z.; Li, Z.; Wang, P.; Zhang, Z. *Organic Letters* **2018**, *20*, 5578–5582.

[260] Park, Y.; Heo, J.; Baik, M.-H.; Chang, S. *Journal of the American Chemical Society* **2016**, *138*, 14020–14029.

[261] Park, S. H.; Kwak, J.; Shin, K.; Ryu, J.; Park, Y.; Chang, S. *Journal of the American Chemical Society* **2014**, *136*, 2492–2502.

[262] Maestre, L.; Dorel, R.; Pablo, Ó.; Escofet, I.; Sameera, W. M. C.; Álvarez, E.; Maseras, F.; Díaz-Requejo, M. M.; Echavarren, A. M.; Pérez, P. J. *Journal of the American Chemical Society* **2017**, *139*, 2216–2223.

[263] Kim, J. Y.; Park, S. H.; Ryu, J.; Cho, S. H.; Kim, S. H.; Chang, S. *Journal of the American Chemical Society* **2012**, *134*, 9110–9113.

[264] Ryu, J.; Kwak, J.; Shin, K.; Lee, D.; Chang, S. *Journal of the American Chemical Society* **2013**, *135*, 12861–12868.

[265] Das, S. K.; Roy, S.; Khatua, H.; Chattopadhyay, B. *Journal of the American Chemical Society* **2018**, *140*, 8429–8433.

[266] Zhang, Y.; Duan, D.; Zhong, Y.; Guo, X.-A.; Guo, J.; Gou, J.; Gao, Z.; Yu, B. *Organic Letters* **2019**, *21*, 4960–4965.

UNIVERSITAT ROVIRA I VIRGILI
THE ROLE OF COPPER IN HOMOGENEOUS CATALYSIS: SINGLE ELECTRON TRANSFER AND BEYOND.
Shaofei Ni

UNIVERSITAT
ROVIRA i VIRGILI